

THE USE OF MULTIMETRIC FRAMEWORK IN CALIBRATING
THE HBV MODEL

A THESIS SUBMITTED TO
THE GRADUATE SCHOOL OF NATURAL AND APPLIED SCIENCES
OF
THE MIDDLE EAST TECHNICAL UNIVERSITY

BY

SERDAR SÜRER

IN PARTIAL FULFILLMENT OF THE REQUIREMENTS
FOR
THE DEGREE OF DOCTOR OF PHILOSOPHY
IN
GEODETIC AND GEOGRAPHIC INFORMATION TECHNOLOGIES

FEBRUARY 2015

Approval of the thesis:

**THE USE OF MULTIMETRIC FRAMEWORK IN CALIBRATING
THE HBV MODEL**

submitted by **SERDAR SÜRER** in partial fulfillment of the requirements for the degree of **Doctor of Philosophy in Geodetic and Geographic Information Technologies, Middle East Technical University** by,

Prof. Dr. Gülbin Dural Ünver
Dean, Graduate School of **Natural and Applied Sciences** _____

Assoc. Prof. Dr. Uğur Murat Leloğlu
Head of Department, **Geodetic and Geographic Inf. Tech.** _____

Prof. Dr. Zuhal Akyürek
Supervisor, **Civil Engineering Dept., METU** _____

Assist. Prof. Dr. Koray K. Yılmaz
Co-Supervisor, **Geological Engineering Dept., METU** _____

Examining Committee Members:

Assoc. Prof. Dr. İsmail Yücel
Civil Eng. Dept., METU _____

Prof. Dr. Zuhal Akyürek
Civil Eng. Dept., METU _____

Prof. Dr. Burcu Altan Sakarya
Civil Eng. Dept., METU _____

Assoc. Prof. Dr. Nuri Merzi
Civil Eng. Dept., METU _____

Assoc. Prof. Dr. Yakup Darama
Civil Eng. Dept., Atılım University _____

Date: 06.02.2015

I hereby declare that all information in this document has been obtained and presented in accordance with academic rules and ethical conduct. I also declare that, as required by these rules and conduct, I have fully cited and referenced all material and results that are not original to this work.

Name, Last Name : Serdar Sürer

Signature

ABSTRACT

THE USE OF MULTIMETRIC FRAMEWORK IN CALIBRATING THE HBV MODEL

Sürer, Serdar

PhD, Geodetic and Geographic Information Technologies Department

Supervisor : Prof. Dr. Zuhal Akyürek

Co-supervisor: Assist. Prof. Dr. Koray K. Yılmaz

February 2015, 113 pages

In this study, the HBV model is applied on the upper Euphrates basin in Turkey. Individual sensitivity of the parameters is analyzed by calibrating the model using the Multi-Objective Shuffled Complex Evolution (MOSCEM) algorithm. The calibration is performed against snow cover area (SCA) in addition to runoff data for the water years 2009, 2010, 2011 and 2012. Detailed validation studies are also performed for the snow products namely snow recognition (H10) and snow water equivalent (H13) over Turkey and Austria. In this study signature metrics, which are based on the flow duration curve (FDC) are used to see the performance of the model for low flows. The sensitivity analysis of the parameters around the calibrated optimum points showed that parameters of the soil moisture and evapotranspiration have a strong effect in the total volume error of the model. The parameters from the response and transformation routines have a significant influence on the peak flows. It is observed that the parameters of snow routine have strong effect in high flows and total volume. Besides the Shuffled Complex Evaluation Method in the calibration of the model, multi-metric evaluation framework, which represent the different phases of the hydrograph precisely, is used. A stepwise evaluation is done

with commonly used statistical performance metrics (Nash-Sutcliffe, Percent Bias) and signature metrics, which are based on the flow duration curve. Validation of the model is performed for the water year 2013.

Keywords: Hydrological modeling, snow, calibration, HBV, EUMETSAT-HSAF

ÖZ

ÇOKLUMETRİK ÇERÇEVE İLE HBV MODELİNİN KALİBRASYONU

Sürer, Serdar

Doktora, Jeodezi ve Coğrafi Bilgi Teknolojileri

Tez Yöneticisi: Prof. Dr. Zuhâl Akyürek

Ortak Tez Yöneticisi: Y. Doç. Dr. Koray K. Yılmaz

Şubat 2015, 113 sayfa

Bu çalışmada HBV modeli yukarı Fırat Havzasında uygulanmıştır. MOSCEM (Multi-Objective Shuffled Complex Evolution) algoritması kullanılarak model parametrelerinin her birinin hassasiyet analizi yapılmıştır. Model kalibrasyon kar kaplı alan bilgisi ve yüzey akışına göre 2009, 2010, 2011 ve 2012 yılları için yapılmıştır. Kar kaplı alan (H10) ve kar su eşdeğeri (H13) ürünleri için Türkiye ve Avusturya üzerinde detaylı yersel doğrulama yapılmıştır. Düşük akımların tahmini için model performansını tespit etmek amacıyla debi süreklilik eğrilerinden elde edilen temel metrikler gözlenmiştir. Toprak nemi ve buharlaşma-terleme değişkenlerinin toplam su hacmine ilişkin hataya hassas oldukları kalibre edilmiş optimum değerler yakınında yapılan hassasiyet analizlerinde tespit edilmiştir. Tepki ve dönüşüm rutinlerine ilişkin parametrelerin pik akımlara önemli ölçüde etki ettiği gözlenmiştir. Model kalibrasyonunda Shuffled Complex metoduna ek olarak hidografin değişik fazlarını hassas şekilde temsil edebilen çoklometrik değerlendirme çerçevesi de kullanılmıştır. Debi süreklilik eğrileriyle ilintili olan bazı genel istatistiksel performans değerlendirme sabitleri (Nash-Sutcliffe, Percent Bias) kademeli olarak kullanılmıştır. Model doğrulaması 2013 su yılı için yapılmıştır.

Keywords: Hidrolojik modelleme, kar, kalibrasyon, HBV, EUMETSAT-HSAF

To Nicolaus Copernicus

ACKNOWLEDGEMENTS

My deepest thanks go to Dr. Zuhale Akyürek for her guidance throughout all years of studies. It has been a great pleasure to work with her for many different projects under various different responsibilities. She deserves the biggest credit for her endless support.

I would like to thank to Dr. K. Koray Yılmaz for his valuable comments and suggestions which significantly helped to improve this work.

Dr. Juraj Parajka deserves many credits for his very kind support and guiding during the preparation of this study.

I also wish to express my gratitude to my friend Kenan Bolat for his modesty and kind support.

Precious comments of members of the jury have significantly helped for improvement of the thesis. Thanks to Dr. Burcu Altan Sakarya, Dr. Nuri Merzi, Dr. İsmail Yücel, and Dr. Yakup Darama for their time and valuable comments.

My good friends Özgür Beşer and his wife Sibel Beşer have always been there for me during hard times.

Thanks to Orhan Gökdemir for his sincere support with an enduring knowledge.

Thanks to Çağrı Hasan Karaman for his kind support.

My sincere gratitude to Melih Çalamak for last minute boost on my fights with MS Word.

My family has always been my greatest supporter. Thank you for always being there.

TABLE OF CONTENTS

ABSTRACT.....	v
ÖZ.....	vii
ACKNOWLEDGEMENTS.....	ix
TABLE OF CONTENTS.....	x
LIST OF FIGURES	xii
LIST OF TABLES.....	xiv
LIST OF ABBREVIATIONS.....	xv
CHAPTERS	
1. INTRODUCTION.....	1
1.1 General.....	1
1.2 Objectives.....	5
1.3 Thesis Outline	5
2. METHODOLOGY AND DATA	7
2.1 Literature Review.....	7
2.2 Methodology	12
2.3 Study area and Data used	16
3. HSAF SNOW PRODUCTS AND THEIR VALIDATIONS.....	21
3.1. Snow Cover Area H10.....	22
3.2. Snow Water Equivalent H13	24
3.3. Validation of Snow Products	26
3.3.1. Validation of H10	27
3.3.2. Validation of H13	29
4. HYDROLOGICAL MODELING AND SENSITIVITY ANALYSIS	35
4.1 General.....	35
4.2 Sensitivity Analysis of the model parameters.....	36
4.3 Sensitivity analysis of the model thresholds	46
5. MODEL CALIBRATION AND DISCUSSION OF THE RESULTS	49
5.1 Model Calibration	49

5.2	Model Verification	61
5.3	Discussion of the Results	68
	CONCLUSIONS AND RECOMMENDATIONS	75
	REFERENCES.....	77
	APPENDICES	
	Appendix A: PUBLICATION-1	89
	Appendix B: PUBLICATION-2	101
	CURRICULUM VITAE.....	113

LIST OF FIGURES

FIGURES

Figure 2-1 The model structure.....	13
Figure 2-2 The flowchart of the HBV model.....	14
Figure 2-3 DEM of Karasu Basin with discharge measurement stations in the basin, meteorological stations in and around the basin.	17
Figure 2-4 Elevation zones and meteorological stations used in the study.	18
Figure 2-5 Monthly temperature distribution for each zone	19
Figure 2-6 Monthly precipitation distribution for each zone	20
Figure 3-1 HSAF domain and mountain mask boundaries.....	23
Figure 3-2 Example of a MSG-SEVIRI snow cover map for February, 21st, 2012.	24
Figure 3-3 Process flow chart of developed methodology (Beşer, 2011).....	25
Figure 3-4 A sample of H13 SWE product for March 7, 2013.....	26
Figure 3-5 Distribution of ground observations used in the validation studies.	28
Figure 3-6 The calculated mean SWE values obtained from H13 corresponding to measured SWE values for the period January, March for the years 2010, 2011, 2012 and 2013 (HSAF-PUM, 2013).....	31
Figure 3-7 Overall accuracy (k_A , %) of H13 product at 178 meteorological stations in the period April 2008-June 2012.	31
Figure 3-8 Seasonal frequency of H13 snow overestimation (k_O , left side) and underestimation (k_U , right side) errors that are summarized for stations at different elevations, and matching H13 pixel mean.	32
Figure 3-9 Comparison of pixel SWE estimate from H13 satellite product, and SWE estimated from snow depth observations at Brand station (Vorarlberg region). Station is located approximately at the mean pixel elevation of H13 product (1014 m).	33
Figure 3-10 Comparison of pixel SWE estimate from H13 satellite product, and SWE estimated from snow depth observations at Eisenstadt station (Burgenland region). Station is located approximately at the mean pixel elevation of H13 product (184 m).....	33
Figure 4-1 Sensitivity plots of parameters L_{SUZ} , C_{PERC} , K_0 , K_1 , K_2 with reference to PBIAS, RMSE, NSE and Cor. Coeff.....	40
Figure 4-2 Sensitivity plots of parameters L_{PRAT} , FC , $BETA$, B_{MAX} , C_{ROUTE} with reference to PBIAS, RMSE, NSE and Cor. Coeff.....	41
Figure 4-3 Sensitivity plots of parameters CSF , DDF , T_{rain} , T_s and T_{melt} with reference to PBIAS, RMSE, NSE and Cor Coeff.....	42
Figure 4-4 FDCs for the simulations where one parameter was changed between the specified limits and the rest 14 parameters were kept at their optimum values.	44
Figure 4-5 RMSE of the FDCs for the simulations where one parameter was changed between the specified limits and other 14 parameters were kept at their	

optimum values. (Blue: RMSE_Q5, Red:RMSe_Q20, Green:RMSE_midflow, Orange:RMSE_Q70 and Yellow:RMSE_Q95).	45
Figure 4-6 Available number of dates used related with cloud cover percentage	46
Figure 4-7 Change of SCA from H10 product for different cloud thresholds	47
Figure 4-8 Snow overestimation error to different thresholds ζ_{SWE}	48
Figure 5-1 Discharge simulation with respect to calibrations to runoff only.....	52
Figure 5-2 Discharge simulation with respect to calibrations to runoff and H10.....	53
Figure 5-3 Discharge simulation with respect to calibrations to H10 only.....	54
Figure 5-4 Sensitivity of the runoff model efficiency (normalized ME, red dashed line) and snow cover error (normalized SE, blue line) to the weight w_s	56
Figure 5-5 Flow segments on FDC	56
Figure 5-6 Stepwise evaluation of discharge calibration results.....	58
Figure 5-7 Observed (blue) and simulated (gray) discharge for 8 best runs, and calibration with SCE- UA (dashed black).....	60
Figure 5-8 FDC of observed discharge (black), and the selected best calibration runs (gray).....	61
Figure 5-9 Runoff simulation for the verification period for runoff only, and runoff and H10	63
Figure 5-10 Eight best runs vs. runoff simulation for the verification period	64
Figure 5-11 Simulated SWE, and SCA (from H10) for elevation zones A, B, C.....	65
Figure 5-12 Simulated SWE, and SCA (from H10) for elevation zones D, E.....	66
Figure 5-13 Temperature distribution for elevation zones A, B, C, D, E for water year 2013 (red lines indicate the border where the temperatures are lower than 0 °C.	67

LIST OF TABLES

TABLES

Table 2-1 The area of the elevation zones.....	18
Table 3-1 Snow products from some of the snow products (Surer et al. 2014).....	22
Table 3-2 The frequencies of the bands for AMSR-E and SSMI/S sensors	25
Table 3-3 Description of contingency matrix	27
Table 3-4 Validation metrics calculation	27
Table 3-5 Overall accuracy results of H10 for flat and mountain areas in Turkey...	28
Table 3-6 Validation results of H13 product over Turkey	30
Table 4-1 Model parameters	37
Table 4-2 Model performance for different cloud thresholds.	47
Table 4-3 Underestimation error with respect to different threshold ζ_{SCA}	48
Table 5-1 Statistical measures obtained from model run by two different calibrations and the calibrated model parameters.....	50
Table 5-2 Final selection of best calibration runs	57
Table 5-3 Model parameters obtained from best calibration results, and the statistical measures for the calibration	59
Table 5-4 Statistical measures for the validation period	62

LIST OF ABBREVIATIONS

AMSRE	: Advanced Microwave Scanning Radiometer
AVHRR	: Advanced Very High Resolution Radiometer
EUMETSAT	: European Organization for the Exploitation of Meteorological Satellites
FDC	: Flow Duration Curve
HBV	: Hydrologiska Byråns Vattenbalansavdelning
HSAF	: Satellite Application Facility on Support to Operational Hydrology and Water Management
MERIS	: Medium Resolution Imaging Spectrometer
MODIS	: Moderate Resolution Imaging Spectroradiometer
NASA	: National Aeronautics and Space Administration
NDSI	: Normalized Difference Snow Index
NOAA	: National Oceanic and Atmospheric Administration
NOHRSC	: National Operational Hydrologic Remote Sensing Center
NSE	: Nash Sutcliffe Efficiency
NSIDC	: National Snow and Ice Data Center
RMSE	: Root Mean Square Error
SCA	: Snow Cover Area
SCE-UA	: Shuffled Complex Evolution, University of Arizona
SEVIRI	: Spinning Enhanced Visible and Infrared Imager
SSMIS	: Special Sensor Microwave Imager/Sounder
SWE	: Snow Water Equivalent
VE	: Volume Error
VZA	: View Zenith Angle

CHAPTER 1

INTRODUCTION

1.1 General

Snow has a significant importance in water cycle as being a vital and crucial component of it. Substantial amount of effort is required in order to accurately monitor and report the amount and coverage of the snow by relevant scientists and experts. Since snow has high reflectivity, it also plays an important role for energy budget of the Earth by the effect of large areas that are mostly or completely covered by snow.

Precise monitoring of the snow for acquiring more accurate information about its coverage has to be handled delicately. This monitoring should aim to find out both the temporal and spatial distribution of the snow covered area to be available for use in hydrological sciences. Since the snow will turn into water when it gets melted, it means a potential reservoir to be monitored and calculated carefully. The melting of the snow may cause flooding events, or can be used as a source to electricity production in hydro power plants. Thus, in order to better predict discharges in melt seasons the monitoring of the snow parameters is important.

The observed snow height values are available on vast areas but these measurements are very dependent on the local weather and topographical conditions. Especially for mountainous areas the scarcity of the field observations and the representativeness of the stations for the areal extent due to the complexity of the terrain make the use of ground observations in snow monitoring and simulation difficult and insufficient. For mountainous regions, satellite imagery is the most convenient way for keeping

track of snow cover extent considering the inaccessibility due to the difficulties of rough terrain and high elevations.

Remote sensing data have been used for better comprehension of information on snow cover extent (Painter et al. 2003, Cline et al. 1998). Several satellite sensors have been used for snow cover mapping such as: AVHRR, MODIS, and MERIS (Harrison & Lucas 1989, Hall et al. 2002, Tampellini et al. 2003). MODIS has a good temporal and spatial resolutions for snow cover monitoring, therefore it has been utilized in numerous studies (Parajka and Blöschl, 2012). There are several studies discussing the accuracy and providing information about MODIS snow cover products. Most of these studies depicts that under clear sky conditions, there is an accuracy of around 94% according to the measurements made on the ground stations (Hall and Riggs, 2007; Parajka and Blöschl, 2006; Parajka and Blöschl, 2012).

Satellite driven snow cover information gains more importance by the developments in space sciences due to getting easier to use for many scientific studies including hydrological sciences (Andreadis and Lettenmaier, 2006; Rodell and Houser, 2004; Zaitchik et al., 2008; Bavera and De Michele, 2009).

Snow satellite observations can be found in two forms: Snow Water Equivalent (SWE) or Snow Cover Area (SCA). However the quality of SWE data are often not good enough to be used in hydrological studies. Still the studies indicate large errors in microwave estimates compared with ground measurements (Pullianinen and Hallikainen, 2001). It is not possible to make accurate SWE determinations with current satellite measurement technologies especially over mountainous terrain due to highly changing topography unless the snow depth is between 20cm-80cm values. A high underestimation of SWE value determination is observed for the snow depths higher than 150cm. There is also a significant overestimation for shallow snow depths of lower than 15 cm (Beşer, 2011). On the contraray, the data on SCA gets more available for large regions with higher temporal resolutions (Parajka and Blöschl, 2006). The detection of cloud covered areas is the most important and most challenging step to be taken into account during snow covered area detection by using satellite images that are measuring in the optical span of the spectrum. Parajka and Blöschl (2008) presented an evaluation of simple mapping methods in order to

reduce the amount of cloud obscured parts using spatial and temporal filtering. Tekeli and Tekeli (2011) performed a similar approach for improving MODIS standard snow cover products for snow cover monitoring over Eastern part of Turkey. A study by Ault et al. (2006) presented results from a validation of MODIS snow product and cloud mask in the Lower Great Lake region. They have also observed that any existence of cloud coverage may cause misinterpretation of snow covered area with cloud coverage.

Within the framework of Satellite Application Facility on Support to Operational Hydrology and Water Management (HSAF) Project, several snow products have been developed in support of European Organisation for the Exploitation of Meteorological Satellites (EUMETSAT). Turkey has a role in the development of two of the snow products which are namely snow cover recognition (H10), and snow water equivalent (H13). All the snow products will be operational in the next phase of the project (2012-2017). Meteosat Second Generation satellite Spinning Enhanced Visible and Infrared Imager (MSG-SEVIRI) data are used in snow recognition, METOP-AVHRR data are used for fractional snow cover and AMSR-E, SSMI/S data are used for snow water equivalent product generation. The validation studies for three products have been performed since 2008. Average values of 80% of probability of detection for snow recognition product, 60% of overall accuracy for the fractional snow cover product and 45 mm RMSE for the snow water equivalent product have been obtained from the validation studies and all scores fulfill the product requirements.

SEVIRI instrument provides imagery with 3-km resolution at nadir observing with 12 spectral channels from visible to infrared regions of the electromagnetic spectrum, and covers the whole hemisphere. Most importantly, SEVIRI has a very high temporal resolution of 15 minutes, and this makes the H10 product highly compatible on cloud reduction ability. A comparison on cloud percentages and ground validation of H10 product with MODIS snow cover product (MOD10A1) for mountainous parts of Eastern Turkey was presented by Surer and Akyurek (2012), where they have obtained 37% more cloud reduction by H10 (uses 32 consecutive images per day) than MODIS snow cover product (a single image per day). The high cloud reduction possibility with H10 product makes it appealing for end-users like

hydrological modelers. High temporal resolution (15 min) and wide aerial coverage of SEVIRI imagery make it a good choice to use it for observing rapidly changing phenomena like fog monitoring, tracking cloud movements or snow cover mapping (Bertrand et al., 2008; Cermak and Bendix, 2008).

Several studies have presented the potential of using satellite data for calibration and the validation of hydrological models (Rodell and Houser, 2004; Tekeli et al., 2005; Andreadis and Lettenmaier, 2006). The outcomes of these studies mostly reflect that to integrate MODIS snow cover data into hydrological models did not significantly improve the performance of the model regarding the capability to predict runoff values. In a study of Udnaes et al. (2007), they have calibrated the HBV model by using SCA information and runoff values together in order to observe an improvement at the prediction of potential flood events. They have observed that this integration only improved the SCA simulations of the HBV model, but not the prediction of runoff values. Andreadis and Lettenmaier (2006) made an assimilation of the MODIS snow cover information into a hydrologic model and observed the efficiency of the assimilation compared with the ground observations on snow. They presented that the snow coverage simulations of the model have been improved when compared with using ground snow measurements.

Remotely sensed snow cover information can be either used as direct input into a hydrological model such as Snowmelt Runoff Model (SRM) which is a lumped temperature-index model (Martinec, 1975; Georgievsky, 2009; Tekeli et al., 2005). Another method can be the comparison of the simulated snow water equivalent values by modeling with the snow data indirectly (Parajka and Blösch, 2008).

Hydrological complexity is reflected in different phases within the discharge time series. The challenging part in hydrological modelling is to represent all phases with the same model parameters. In order to reproduce the hydrological processes, hydrological models have to be calibrated to the conditions of the study catchments. Generally hydrological models are calibrated to the measured discharge time series. The most suitable parameters are selected with a sensitivity analysis. During the calibration processes well known statistical measures namely Root Mean Square Error (RMSE), Nash-Sutcliffe Efficiency (NSE), percent bias are used to present the

volume error, timing error and the error in simulating the high flows. It is known that NSE is sensitive to differences in the observed and simulated means and variances; hence it is more sensitive to extreme values. The RMSE overemphasizes flood peaks and leads to a bad calibration of low flow periods. It is stated that one single performance measure is insufficient to take into account the representation of all relevant processes (Gupta et al., 1998; Wagener and Gupta, 2005; Gupta et al., 2008). Using the statistical and hydrological metrics into the calibration process can lead to make better representing the complex hydrological processes.

1.2 Objectives

The purpose of this work is to present the usefulness of satellite snow cover information namely MSG-SEVIRI in hydrological modelling. Among the several objectives, the most important motivations of this study are listed below:

- To assess the performance of using HSAF snow products on simulations of a hydrologic model on a catchment in Turkey.
- To apply multi-objective calibration with snow information and runoff information.
- To illustrate the incorporation of H10 into a conceptual hydrological model with assimilation at calibration stage.
- Including the hydrological measures into the calibration of HBV model and making comparison of the multimetric calibration with the calibration by an optimization method using statistical measures only.
- To perform snow water equivalent simulations comparison with values from hydrologic model, and H10 product.
- To evaluate the performance of H10 snow cover and H13 products by using the in-situ observations.

1.3 Thesis Outline

The subjects described in the following chapters are given below:

In Chapter 2, the related literature survey about the use of remote sensing in snow cover mapping, snowmelt runoff modeling, and model calibration is presented. The methodology and the data used in the study are discussed.

In Chapter 3, the description of snow cover products depicted from satellite imagery are given. The two different types of satellite snow products, which are from optical and microwave bands of the spectrum, are presented. The capability of these products to be used in hydrological modeling is discussed.

In Chapter 4, the sensitivity of HBV model parameters are given. The sensitivity of thresholds in the models is also presented.

Chapter 5 presents the calibration of the model using statistical and hydrological measures and verification of the model. It includes the main results of the study and discusses the use of snow cover maps in hydrological modelling in multi objective calibration and the equifinality concept.

Finally, Chapter 6 presents the conclusions of the study and gives some related recommendations.

CHAPTER 2

METHODOLOGY AND DATA

2.1 Literature Review

Snow is an important component of the water cycle and of the climate evolution. It is vital to accurately monitor the amount and coverage of the snow for many purposes such as: flood forecasting, energy production forecast and planning, better allocation of water from melting of the snow. Thus, in order to better predict discharges in melt seasons the monitoring of the snow parameters is important.

Even though it is possible to derive snow depth measurements over large areas from ground stations, these data very much depend on the local conditions. Especially for mountainous areas the scarcity of the field observations and the representativeness of the stations for the areal extent due to the complexity of the terrain make the use of ground observations in snow monitoring difficult and insufficient. For mountainous regions, satellite imagery is the most convenient way for keeping track of snow cover extent considering the inaccessibility due to the difficulties of rough terrain and high elevations.

Remote sensing data have been used for better comprehension of information on snow cover extent (Painter et al., 2003, Cline et al., 1998). Several satellite sensors have been used for snow cover mapping such as: AVHRR, MODIS, and MERIS (Harrison and Lucas 1989, Hall et al., 2002, Tampellini et al., 2003). AVHRR sensor that got operational in 1979 from aboard a polar orbiting satellite has been providing images until then. AVHRR has a high spatial resolution of 1 km, and a temporal makes it appealing to use for operation snow cover estimation (Carroll et al., 2001) On the other hand this 1 km resolution can be rather low for making snow mapping in small size watersheds (Schmugge et al., 2002). MODIS has good temporal and

spatial resolutions for snow cover monitoring, therefore it has been utilized in numerous studies (Parajka and Blöschl, 2012).

Snow products that have varying spatial and temporal resolutions are available from operational satellites on near-real time. The spatial resolution of such products differs from 500 m to 5 km. Under low cloud appearance days, these operational snow products derived from satellite measurements can provide from 70% to 95% accurate snow cover information controlled with ground measurements in winter season. The cloud coverage causes the main problem in using these satellite driven snow cover products. Different approaches have been utilized for reducing cloud contamination including a space time filtering method (Parajka and Blöschl, 2008; Gafurov and Bárdossy, 2009). López-Burgos et al. (2013) applied a regression method which is locally weighted and uses relationships between the spatial and topographic attributes of pixels surrounding a cloudy pixel to estimate the “probability of snow occurrence”. They also applied Terra/Aqua combination, time interpolation and nearest neighbor spatial interpolation methods in order to compare the performance of these methods to reduce the cloud obscuration of MODIS snow cover area products. They concluded that sequential combination of these algorithms provides synergistic effect. They also recommended eliminating the spatial interpolation methods from the sequence, since the spatial interpolation method has very little overall impact on the results.

Merging satellite images can be counted as an alternative to space time filtering method. Images obtained every 15 minutes by the SEVIRI sensor of MSG satellite can provide information on snow cover by measuring in very high temporal resolution on the whole hemisphere. The first assessments have shown that the merging of 32 satellite images in a day significantly improves cloud reduction by even 37% when it is compared to MODIS snow cover product (Surer and Akyurek, 2012).

Surer et al. (2014) evaluated the mapping accuracy of the H10 product over Austria. Their results show that the high temporal resolution of SEVIRI sensor helps to make a significant level of cloud reduction by making measurements every 15 minutes. During cloud clear days, the accuracy of H10 is around 89%, while it was 94% for

MODIS snow cover product. Frequent cloud coverage is another problem in snow mapping through remote sensing.

The satellite snow observations are being used in the field of hydrology (Andreadis and Lettenmaier, 2006; Rodell and Houser, 2004; Su et al, 2008; Zaitchik et al., 2008; Bavera and De Michele, 2009; Tekeli et al., 2005). Remotely sensed snow covered area information has been used successfully in snowmelt and runoff models (e.g. Yang et al., 2003, Clark et al., 2006, Dressler et al., 2006, Kolberg and Gottschalk, 2006, Kolberg et al., 2006, Andreadis and Lettenmaier, 2006, Parajka and Blöschl, 2008). Remotely sensed snow water equivalent has also been used in some studies (e.g. Derksen et al. 2003, Andreadis and Lettenmaier 2006, Pulliainen, 2006). Remotely sensed snow cover information can be either used as direct input into a hydrological model (Tekeli et al., 2005) or the simulated snow water equivalent values can be compared with the snow cover data indirectly (Parajka and Blöschl, 2008).

Using reliable observed data is also important for performing real-time flood forecasts. Thirel et al. (2012) made an assessment of a real-time snow cover area daily product at 250 m-resolution (the EURAC MODIS SCA product, which is based on the MODIS sensor) by comparing it directly or indirectly to the classical NASA MODIS SCA daily product and to the simulated snow cover area of the distributed hydrological model, LISFLOOD. The Shuffled Complex Evolution, University of Arizona (SCE-UA) algorithm was used for carrying out the calibration of the model. In their work both satellite products overestimated the SCA, during the whole year for the EURAC SCA, and at the beginning of the winter for the NASA SCA, compared to hydrological model simulations. The reason of the overestimation is stated as the misclassification of cloud pixels as snow.

Franz and Karsten (2013) used MODIS SCA observations in calibrating the SNOW17 model in North Fork Basin, USA. They used single objective function by only utilizing MODIS SCA information within a multi-step approach.

There are different assimilation methods that have been applied to land surface models in order to update the snow information. Recently, some of those methods have been utilized in hydrological modelling studies as well. Among these methods,

variants of Kalman Filter technique are the most preferred ones. It is the method of adjusting uncertain variables and parameters in order to obtain the best fit to the values from observations (Houser et al., 1998). Direct insertion method is another option to update and assimilate snow information in hydrological models as Liston et al. (1999) has successfully applied in a regional climate model for snow association and Rodell et al. (2004) used this method to assimilate MODIS data into a global land surface model. Statistical interpolation technique is sort of an improvement for direct insertion which is applied by Brasnett (1999) to assimilate snow depth observations from synoptic stations. Thirel et al. (2011) compared Ensemble Kalman filter and particle filter assimilation techniques to improve the runoff simulation with a spatially distributed hydrological model. Their results and discussion to that paper indicate that there is still more research needed for better understanding on how to robustly assimilate satellite snow cover data into hydrologic models.

Another important application is the simulation mode where the snow cover data are used in the calibration of hydrological models together with other data sources. Parajka et al. (2006) assimilated the scatterometer data into the hydrological model during the calibration phase. They stated that the rationale of combining two sources of information on soil moisture, hydrological models and satellite data, is that even though both sources have clear limitations and are associated with significant uncertainty it is their combination that should help reduce the uncertainty of the integrated estimates. Knowing that the estimates come from completely different instruments, ground based instruments and spaceborne sensors, the expected errors of these sources are completely different. Their results indicate that assimilating the scatterometer data into the hydrologic model during the calibration phase improves the relationship between the two soil moisture estimates without any significant decrease in runoff model efficiency. Several studies that have presented satellite-based snow cover information utilization for calibrating parameters of a snow model (Udnes et al., 2007; Parajka and Blöschl, 2008; Şorman et al., 2009; Konz et al., 2010).

Beven and Freer (2001), reports that the optimization problem is mostly ill-posed in hydrological modeling if it is purely based on the comparison of simulated and observed discharge. It is because the data on discharge may have lack of information

which is required to identify all of the parameters of the model properly. This finding is also valid for snow models, since these models are mostly calibrated by using the observed discharge values.

The use of satellite based snow cover information can reduce the need of relying on a single variable at the basin outlet, during calibration stage of hydrological modeling. Model states can be updated using either snow water equivalent or SCA data from MODIS as presented in several studies (Rodell and Houser, 2004; Andreadis and Leetennmair, 2006; Nagler et al., 2008; Tang and Lettenmaier, 2010). The information of SCA maps produced from MODIS maps can be used as model inputs for hydrological models simulating snow melt (Tekeli et al., 2005).

HBV (Bergström, 1976) is a semi distributed conceptual hydrological model which is used extensively in operational inflow forecasting and water balance studies. There are several studies using HBV concept in the literature Skaugen and Onof (2014) developed a new model where the HBV soil moisture concept was modified by a new soil moisture routine, which estimates saturated and unsaturated volumes of subsurface water and with only one parameter to calibrate is included in the new model. The number of parameters to be calibrated in the module concerning soil moisture and runoff dynamics is reduced from seven in the HBV model to one in the new model. Rientjes et al. (2013) used streamflow (Q_s) and satellite-based actual evapotranspiration (ETA) in a multi-variable calibration framework to reproduce the catchment water balance. The application is for the HBV rainfall-runoff model at daily time-step for the Karkheh River Basin (51,000km²) in Iran. Tian et al. (2013) used HBV model besides GR4J and Xinanjiang models to study the extreme high flows in Jinhua River basin under the impact of climate change for the near future 2011-2040. Mayr et al. (2013) modified HBV-ETH model to develop a partially distributed hydrological model that was able to simulate runoff in a highly glacierised basin. Driessen et al. (2010) used the HBV model (version HBV Light 2.0) to find the effect of the projected changes in precipitation characteristics due to climate change on the hydrological regime of the river Meuse. The hydrological model is forced with three high-resolution (0.088°) regional climate scenarios, each based on one of the three different IPCC CO₂ emission scenarios for the period of

2002-2040 and 2062-2100. Their results indicate a decrease in summer discharge, because of the decrease in snow pack, and an increased discharge in winter.

2.2 Methodology

A semi-distributed and conceptual rainfall runoff model is used following the structure of HBV (Bergström, 1976). Lindström (1997) improved the HBV model performance by improving its potential for making use of spatially distributed data and they made it more physically sound. The model uses elevation zones and runs on daily bases. It has several routines for snow, soil moisture, and flow routing (Figure 2.1). As most of the conceptual models, this one is also a degree-day method working model which accumulates and melts the snow accordingly with temperature values based on certain threshold values. Related with the mean daily air temperature, model splits the precipitation into two forms as rain (P_r) and snow (P_s). T_r and T_s are the lower and upper threshold temperatures, respectively. A snow correction factor (CSF) corrects the precipitation during snowfall. Below a temperature called melting air temperature (T_m), the falling snow starts to accumulate. SWE is defined as the water stored in a pack of snow. Depending on the semi-distributed structure of HBV model, individual SWE simulations are produced for each elevation zone. The melting of the snow is proportional to a degree day factor (DDF), and the difference of air temperature (T_a) from T_m . The soil moisture routine of the model is consists of runoff generation and soil moisture state change of the catchment. There parameters of the model define soil moisture related processes: maximum soil moisture storage as FC, soil moisture state above which evaporation is at its potential rate (LP), and the other parameter that relates runoff generation to state of soil moisture (B). The routing of the runoff on the hillslopes is incorporated by a lower and upper soil reservoir. The upper zone collects the rainfall that is excess, and this accumulated rain leaves this upper zone reservoir in three different ways. The fast storage from the reservoir is shown with K_1 , percolation with a constant percolation rate (C_p) to the lower zone, and in case a threshold of short state (L_{SUZ}) gets exceeded, it leaves through an additional outlet based on a very fast

storage coefficient (K_0). Water is flown from lower zone reservoir with a slow storage coefficient (KZ).

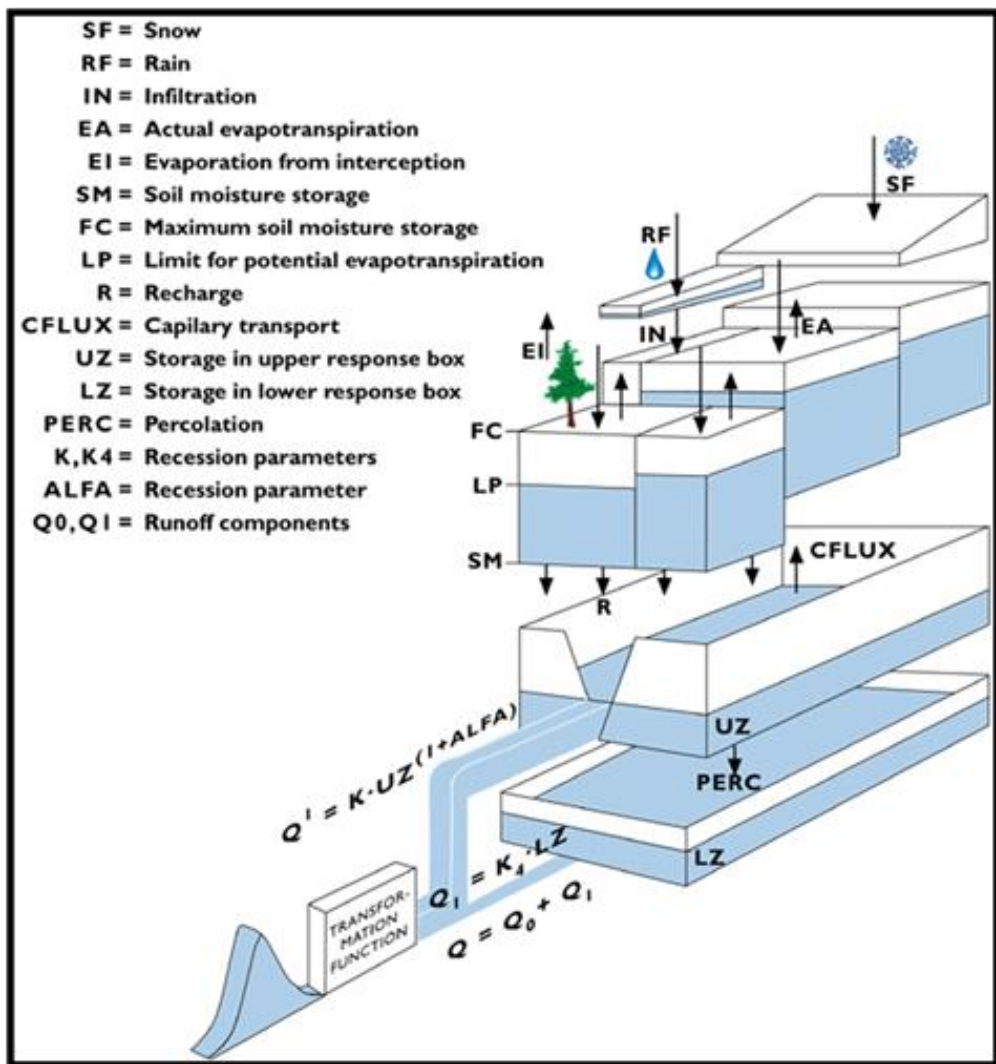


Figure 2-1 The model structure

The flowchart of the model is presented in Figure 2.2. There are 15 parameters in the model and through the analysis of sensitivity of the model parameters that is described in Chapter 4, among these 15 parameters, 4 parameters were fixed ($T_i=2^0C$, $T_s=-2^0C$, $B_{MAX}=10$, $C_{ROUTE}=26.5$) considering the possible values of these parameters are available in the literature. 11 parameters were estimated by automatic model calibration using the discharge and snow cover area information and calibration by using low flow signature metrics.

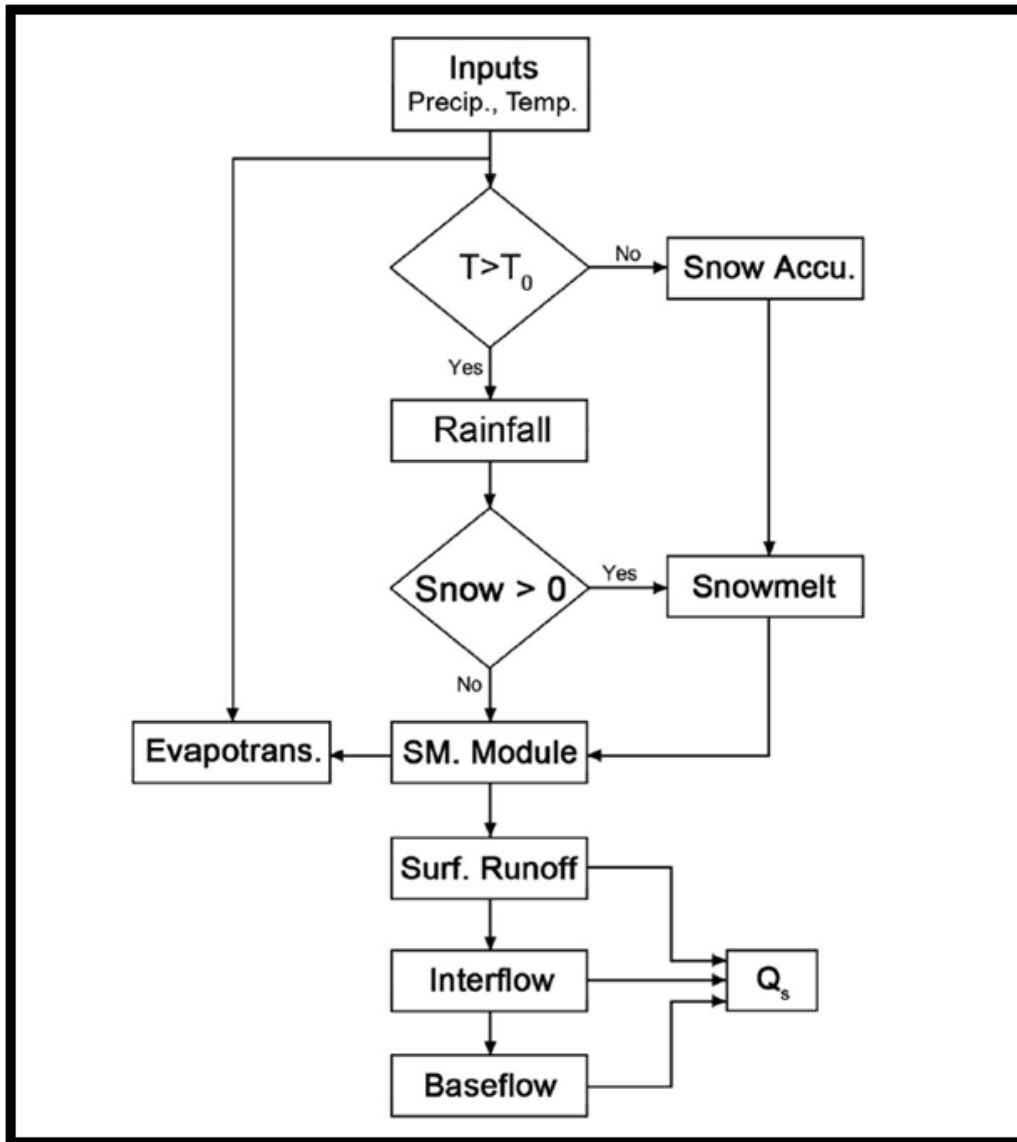


Figure 2-2 The flowchart of the HBV model

Using the SCE-UA method, the individual sensitivity of the model parameters is analyzed, and further Monte-Carlo based identifiability analysis was performed. Besides four objective function measures (PBIAS, RMSE, NSE, and correlation coefficient), RMSE of the flow duration curves are used to analyze the performance of the model parameters controlling volume errors from runoff and high flow and low-flow series.

The model calibration is performed in two different ways. In the first approach it is performed by using the SCE-UA method (Duan et al., 1992, Duan et al., 1994). This method is based on a synthesis of the best features from several existing methods, including genetic algorithm, and introduces the concept of complex shuffling. In the second approach the calibration is performed by a multi-metric evaluation framework to identify calibration runs, which represent the different phases of the hydrograph precisely.

Several efficiency measures and error measures are used in evaluating the model during calibration and validation periods. For runoff, the NSE has been used in two variants, M_E and M_E^{\log} , for high and low flows, respectively:

$$M_E = 1 - \frac{\sum_{i=1}^n (Q_{obs,i} - Q_{sim,i})^2}{\sum_{i=1}^n (Q_{obs,i} - Q_{obs})^2} \quad (2.1)$$

$$M_E^{\log} = 1 - \frac{\sum_{i=1}^n (\log(Q_{obs,i}) - \log(Q_{sim,i}))^2}{\sum_{i=1}^n (\log(Q_{obs,i}) - \log(Q_{obs}))^2} \quad (2.2)$$

where $Q_{sim,i}$ represents runoff simulation on the day “i”. $Q_{obs,i}$ is the observed runoff, Q_{obs} is the average of the observed runoff over the calibration (or verification) period of n days. Also a relative volume error (VE) of runoff has been used:

$$VE = \frac{\sum_{i=1}^n Q_{sim,i} - \sum_{i=1}^n Q_{obs,i}}{\sum_{i=1}^n Q_{obs,i}} \quad (2.3)$$

Root Mean Square Error, percent bias (PBIAS) and correlation coefficient are the other statistical measures used in the analyses:

$$RMSE = \sqrt{\frac{\sum_{i=1}^n (Q_{obs,i} - Q_{sim,i})^2}{n}} \quad (2.4)$$

$$pBias = \frac{\sum_{i=1}^n (Q_{obs,i} - Q_{sim,i}) \cdot 100}{\sum_{i=1}^n (Q_{obs,i})} \quad (2.5)$$

$$R = \frac{n \sum_{i=1}^n (Q_{obs,i}) \cdot (Q_{sim,i}) - \sum_{i=1}^n (Q_{obs,i}) \cdot \sum_{i=1}^n (Q_{sim,i})}{\sqrt{(n \sum_{i=1}^n (Q_{obs,i})^2 - \sum_{i=1}^n (Q_{obs,i})^2) \cdot (n \sum_{i=1}^n (Q_{sim,i})^2 - \sum_{i=1}^n (Q_{sim,i})^2)}} \quad (2.6)$$

H10 product is compared indirectly with the model simulated SWE values. While the model simulated SWE represents melted snow, H10 product can only provide the information about the pixel if it is snow covered, or not. To compare model simulated SWE and H10 products, two error metrics are used. The overestimation error that is depicted in Eq. 2.7 gives the count of the days, m_o , in case SWE from model simulation is higher than a threshold value but H10 product finds no snow. SWE is the simulated value in a specific zone and SCA is the H10 SCA within this zone, m is the number of days where H10 images are available (with cloud cover less than a threshold ζ_c), l is the number of zones in the basin and ζ_{SWE} is a threshold that determines when a zone can be essentially considered snow free in terms of simulations.

$$S_E^O = \frac{1}{m.l} \sum_{j=1}^l m_o \cap (SWE > \zeta_{SWE}) \cap (SCA = 0) \quad (2.7)$$

The underestimation error (S_E^U) presented in Eq. 2.8, gives the count of the days, m_U , while the hydrologic model finds no snow simulated in the represented zone but H10 shows that there is snow cover over a certain threshold value. ζ_{SCA} is the limit value which decides if a zone should be accepted as snow free in terms of the H10 data.

$$S_E^U = \frac{1}{m.l} \sum_{j=1}^l m_U \cap (SWE = 0) \cap (SCA > \zeta_{SCA}) \quad (2.8)$$

The accuracy of satellite driven SCA mostly depends on the existence and spatial extent of clouds. In order for having more accurate information, the days when cloud coverage is less than a threshold value ζ_c were utilized. The threshold values ζ_{SWE} , ζ_{SCA} and ζ_c are decided after detailed sensitivity analysis.

2.3 Study area and Data used

Karasu Basin which is the most upstream of Euphrates River is used in most of the analysis made in Turkey (Figure 2.3). The basin has an area of approximately 10,250 km² with an altitude range of 1125 m to 3500 m. The change of elevation along the basin is shown in Figure 2.4. Land cover is mostly pasture, cultivated, and bare land.

According to long term measurements and modeling studies, around 65% of the total amount of annual water is sourced from melting of snow (Tekeli, 2005).

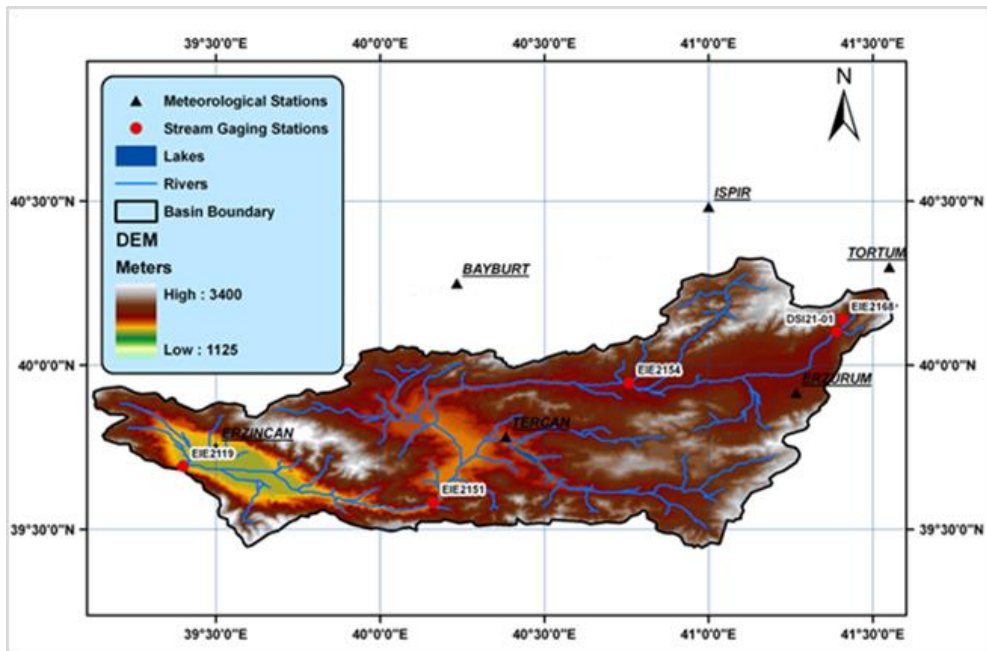


Figure 2-3 DEM of Karasu Basin with discharge measurement stations in the basin, meteorological stations in and around the basin.

The study basin was divided into five elevation zones. The hydrometeorological data used in this study includes daily precipitation and temperature at 21 stations, and runoff data observed at the outlet of the basin. The precipitation and the temperature data were spatially interpolated by geographically weighted regression method. Elevation was taken as an auxiliary data in the interpolation. The elevation zones and the meteorological stations, from which precipitation and temperature were obtained, are depicted in Figure 2.4.

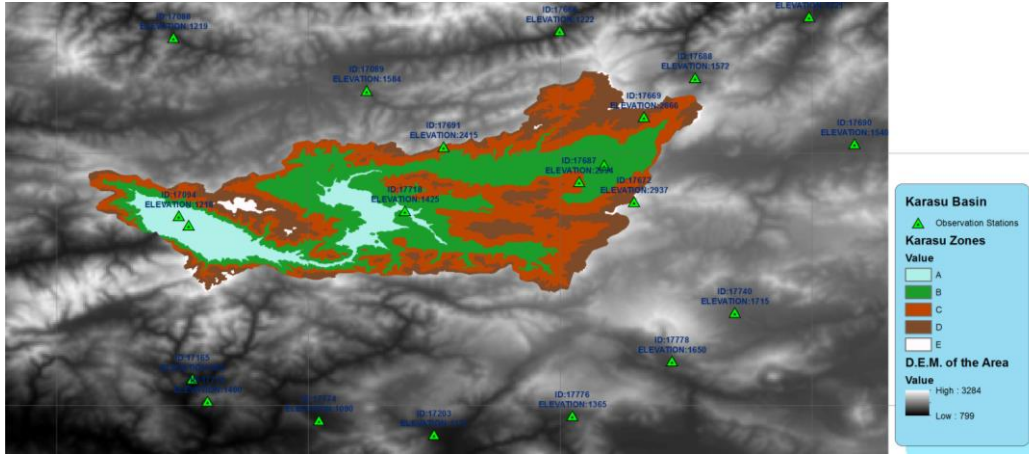


Figure 2-4 Elevation zones and meteorological stations used in the study.

The area of the elevation zones are also presented in Table 2.1 below.

Table 2-1 The area of the elevation zones

Zone	Elevation (m)	Area (km ²)	Area (%)
A	1100-1500	1158	11.43
B	1500-1900	3467	34.23
C	1900-2300	3427	33.83
D	2300-2900	2012	19.86
E	2900-3400	65	0.64

Spatially distributed temperature and precipitation values for each zone on a monthly basis is given in Figure 2.5 and Figure 2.6, respectively. The evapotranspiration values were calculated from daily temperature values by using Blaney Criddle method (Blaney and Criddle, 1962). Blaney Criddle method is selected because of being relatively simplistic method for calculating evapotranspiration and it only needs air temperature data.

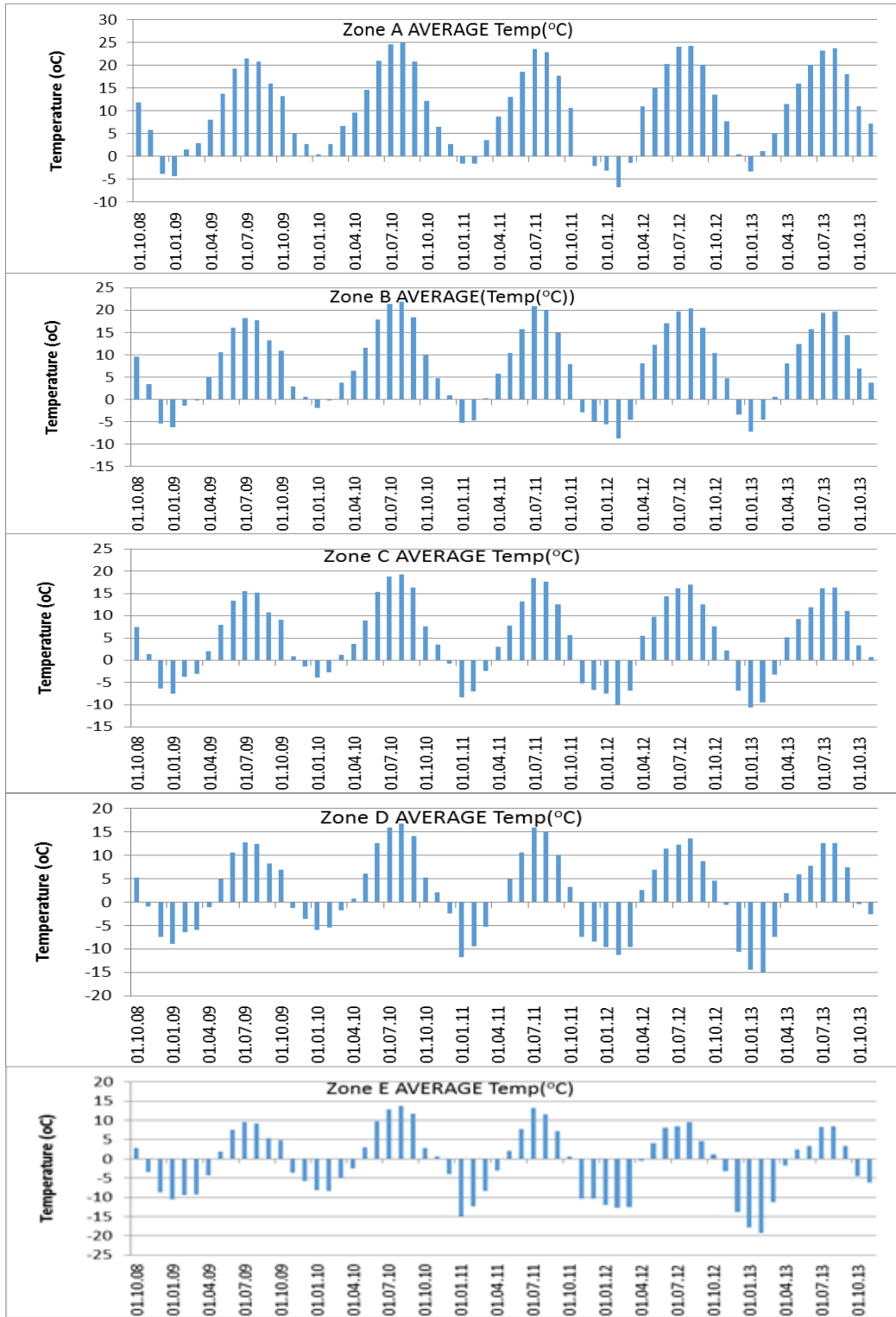


Figure 2-5 Monthly temperature distribution for each zone

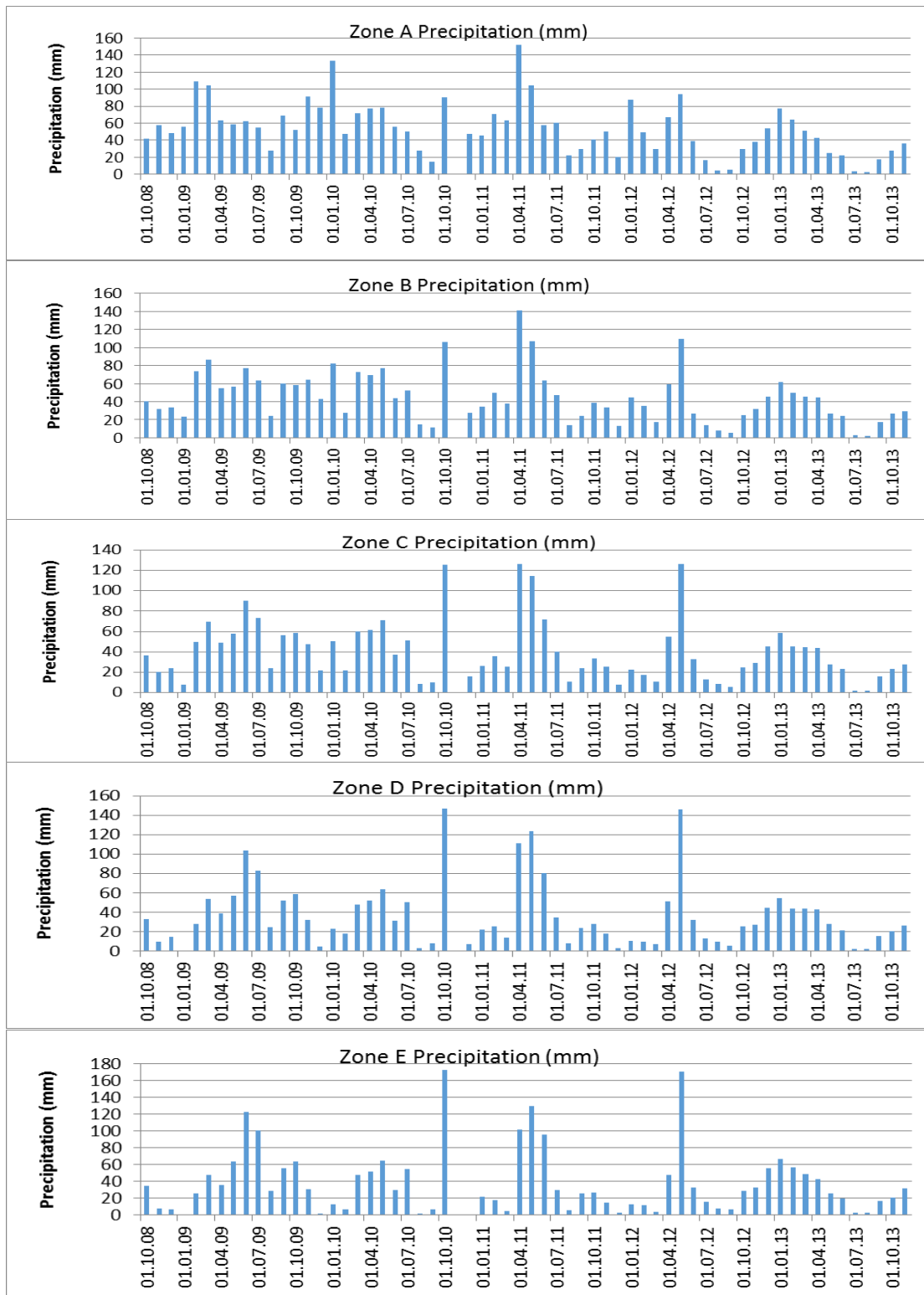


Figure 2-6 Monthly precipitation distribution for each zone

CHAPTER 3

HSAF SNOW PRODUCTS AND THEIR VALIDATIONS

The accurate monitoring and modelling of the amount and extent of snow cover is vital for hydrological executions such as forecasting of snowmelt and assessment of water resources by different approaches (Blöschl and Kirnbauer, 1991; Blöschl et al., 1991; Nester et al., 2012). It is difficult to monitor snow covering vast spatial areas with sparsely distributed ground observation stations. The high elevation difference makes it even harder to access reliable information for mountain environments. Thus, use of satellite driven imagery is a potential alternative since its availability and resolution does not depend on the characteristics of the terrain and basin (Parajka and Blöschl, 2008).

Nowadays, the snow cover information with different spatial and temporal resolutions is available from operational satellite products (Table 3.1). This table depicts that the operational snow cover information from satellites vary in spatial resolution from 500 m to 5 km.

The following parts of the thesis in this chapter will provide information about the two snow products which are snow cover area maps as H10, and snow water equivalent maps as H13. After the elaboration of the full production cycles of these products, the validation studies over Turkey and Austria will be provided in the proceeding parts.

Table 3-1 Snow products from some of the snow products (Surer et al. 2014).

Snow cover product	Sensor	Available since	Spatial resolution	Temporal resolution	Mapping accuracy
NOHRSC	NOAA/AVHRR+GOES	1986	Daily	1km	76%
NOAA/NESDIS (IMS)	GOES+SMS/I	1998	Daily/weekly	4km	85%
MOD10A1, MYD10A1, MOD10A2, MYD10A2, MOD10C1, MYD10C1	MODIS-Terra/Aqua	2000/2002	Daily, 8-day, monthly	500 m, 0.05°	94% (Hall and Riggs, 2007; Parajka, and Blöschl, 2012)
HSAF (EUMETSAT)	MSG-SEVIRI	2008	Daily	5 km	80% (Siljamo & Hyvärinen, 2011) 69-81% (Surer, and Akyurek, 2012)

3.1. Snow Cover Area H10

SEVIRI instrument is an optical sensor which scans the Earth on board the MSG satellite that is operated by EUMETSAT. The SEVIRI sensor scans Earth every 15 minutes in 12 spectral channels. It has approximately 3 km resolution over sub-satellite point, and becomes around 5 km over Europe latitudes (Aminou, 2002). The algorithm of H10 to define snow covered area is mainly based on use of different spectral information from multiple channel measurements. It is basically the exploitation of the high reflectivity of snow in the visible part of the spectrum, and low reflectivity at shorter wavelengths. The algorithm of H10 is different over flat and mountainous areas of working domain. The algorithm for flat areas uses radiance of top of atmosphere in 6 SEVIRI channels, and brightness temperature values from three different channels as the details can be found in Siljamo and Hyvärinen (2011). The cloud recognition of flat regions algorithm depends on cloud discrimination products generated in NWCSAF Project (NWCSAF, 2007).

The algorithm designated to detect snow cover over mountainous regions utilizes snow index (SI) that relates two different channels of SEVIRI instrument. The cloud detection part of mountainous regions also depends on cloud products of NWCSAF Project (Surer, 2008). In order to discard low illuminated areas from imagery a sun zenith angle barrier is used by both of the algorithms. Also another filter for covering pixels that are below freezing point is used (Romanov et al., 2003).

To define the mountain regions and separate the working area into two parts as flat, and mountain, another algorithm mainly depending on the elevation values is used. It is based on the mean elevation and standard deviation of slope values for each of the 5 km x 5 km (Lahtinen et al., 2009). The defined mountain mask is shown in Figure 3.1.

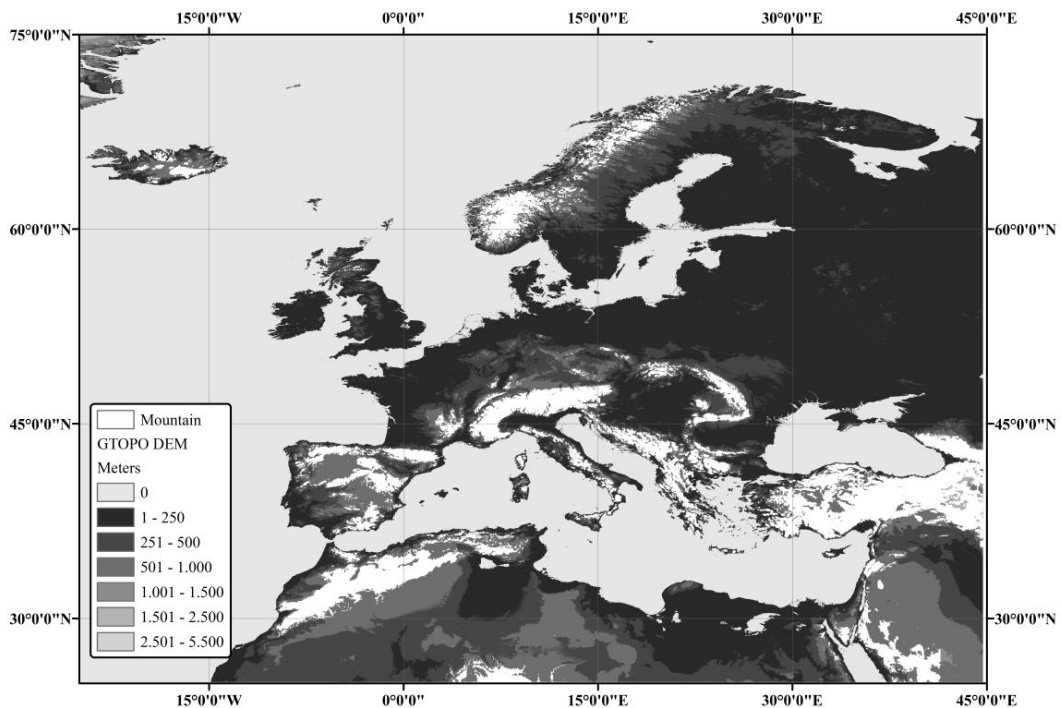


Figure 3-1 HSAF domain and mountain mask boundaries.

The H10 snow cover maps are produced by using 32 images from 08:00-16:00. To mark a pixel as snow, at least 4 hits is expected to be counted within the 32 images. The merged product from flat and mountain regions are produced on near real-time at Finnish Meteorological Institute. A sample merged product is shown in Figure 3.2.

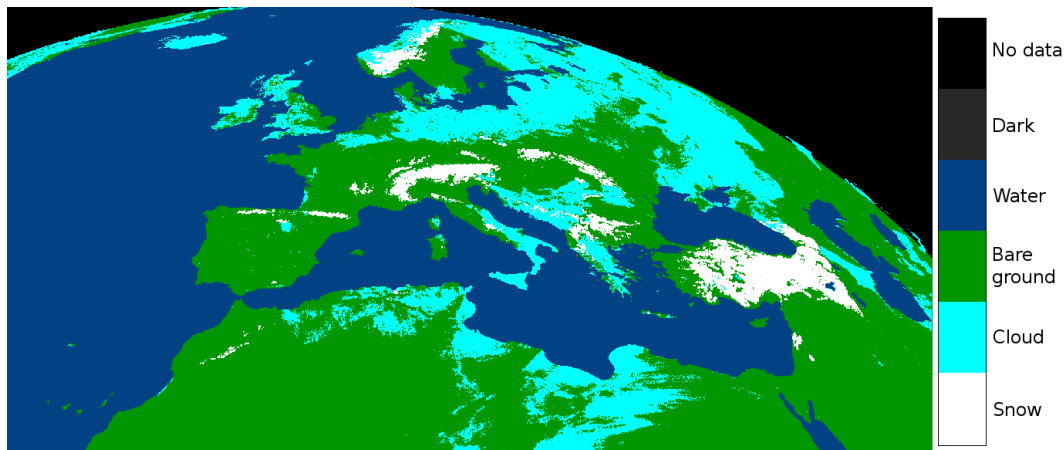


Figure 3-2 Example of a MSG-SEVIRI snow cover map for February, 21st, 2012.

3.2. Snow Water Equivalent H13

The daily snow water equivalent (SWE) maps named as H13 are produced by an assimilation technique utilizing modified Helsinki University of Technology (HUT) snow emission model. The data from AMSR-E ease gridded descending brightness temperature are downloaded from National Snow and Ice Data Centre (NSIDC) ftp site. The gridded brightness temperature values are produced by NSIDC and available in EASE-Grid projections at 25 km spatial resolution. The spatial coverage of these products is global that covers nearly the entire Earth sphere and the temporal resolution is daily. AMSR-E on NASA's EOS Aqua spacecraft stopped rotating on Oct 4, 2011. Therefore the H13 snow product was started to be produced using SSMI/S data on real time on April 10, 2012 and the archived data was produced from April 1, 2009 till April 10, 2012. The related wavebands which are used in the snow product (H13) development and available in both sensors are given in Table 3.2.

Table 3-2 The frequencies of the bands for AMSR-E and SSMI/S sensors

AMSR-E sensor		SSMI/S sensor	
Channel number	Frequency (GHz)	Channel number	Frequency
12	18.7H	12	19.35H
13	18.7V	13	19.35V
14	23.8V	14	22.235V
15	36.5H	15	37.0H
16	36.5V	16	37.0V

Developed SWE retrieval methodology is shown with Figure 3.3.

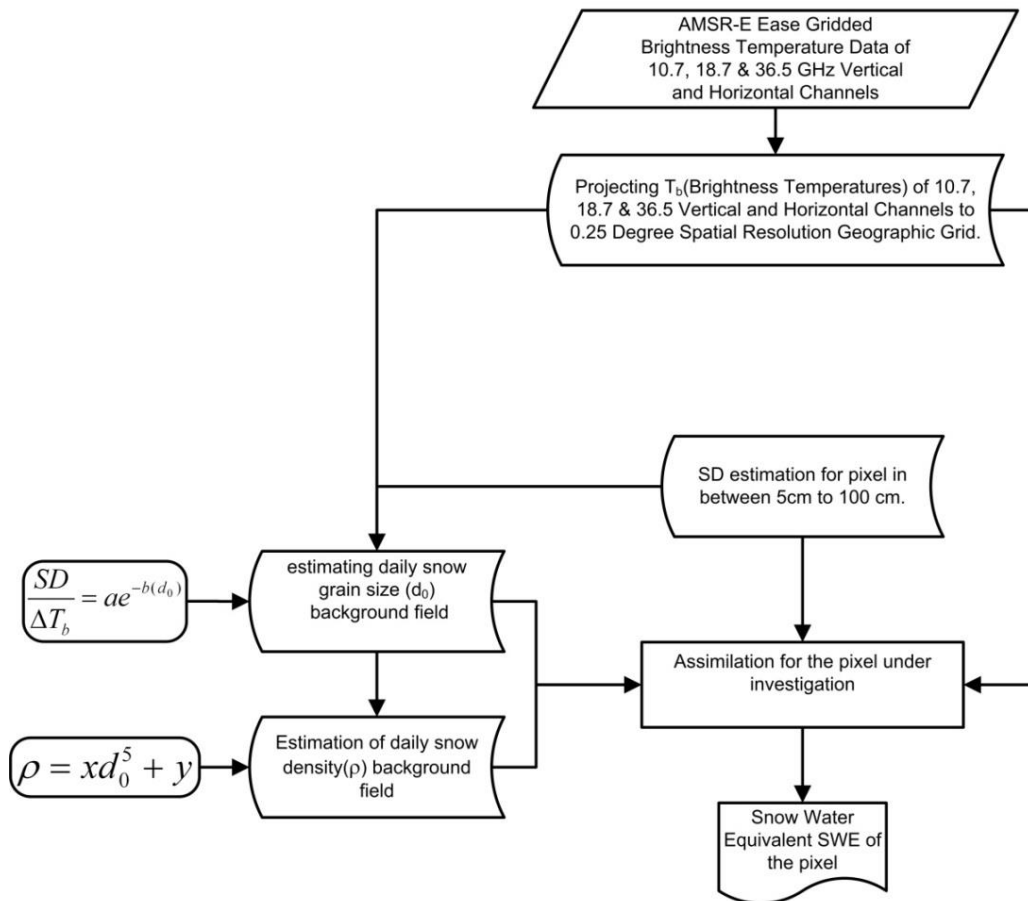


Figure 3-3 Process flow chart of developed methodology (Beşer, 2011)

The HUT model is executed for every pixel falling inside the HSAF domain by dividing the snow depth from 0.05 m to 1.00 m into 20 equal intervals of 5cm in order to minimize sum of measured and modelled brightness temperature differences at 18.7 GHz, and 36.5 GHz vertical channels. The snow grain size is calculated dynamically in order to derive a dynamic density for each interval. Following these calculations, a SWE value is assigned for each pixel. An example SWE map for March 7, 2013 is depicted below in Figure 3.4. The full details of the algorithm is presented in a study by Beşer (2011).

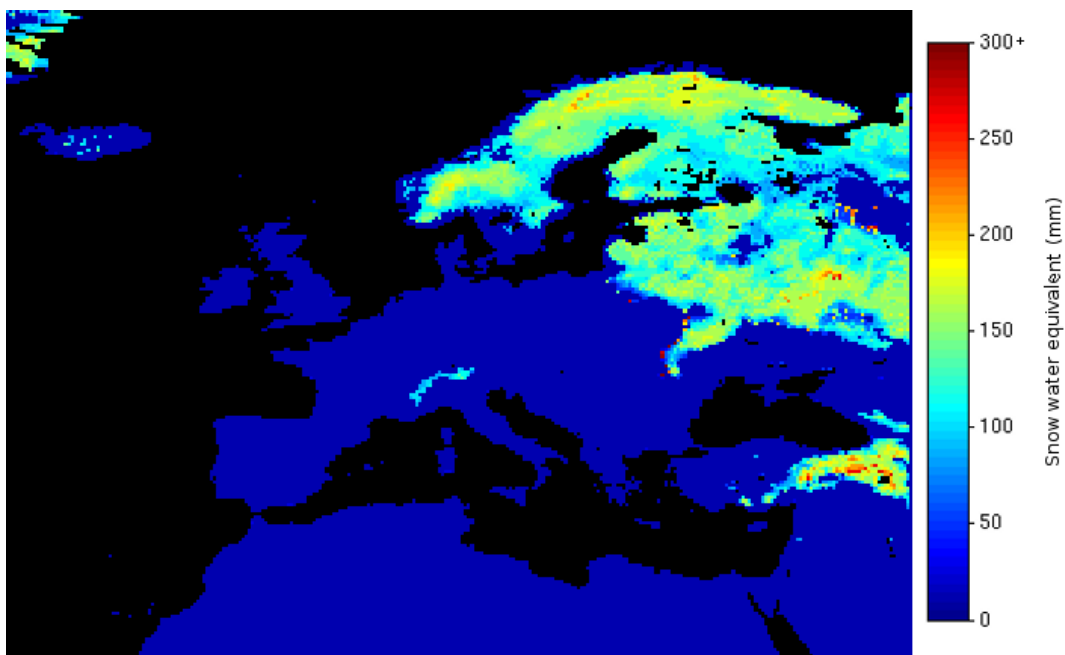


Figure 3-4 A sample of H13 SWE product for March 7, 2013

3.3. Validation of Snow Products

The accuracy of the two different snow products is evaluated differently depending on the properties and differences of these snow products; H10 and H13. The main source of truth for validation is derived from ground station measurements for both of the products. The exceedance limit of snow depth is chosen as 1 cm for accepting the area as snow covered.

Different approaches are used for the validation processes over Turkey and Austria depending on the availability and the density of the ground observations.

3.3.1. Validation of H10

In order to test the performance and accuracy of the H10 product, it is compared with ground measurements from Turkey and Austria. Due to the fact that the two data sets from these countries are different the validation method is also slightly differs by the utilized metrics. The daily ground measurements (snow or no snow) were compared to the collocated pixel information in the snow cover map by making contingency tables (snow, no snow) as in Table 3.3. For the validation, the most common forecasting metrics, such as probability of detection (POD), hit rate (HR), omission error (snow missing rate, SMR) and commission error (false alarm rate, FAR) were used. These were calculated using the metric values described in Table 3.4.

Table 3-3 Description of contingency matrix

		Ground Measurements	
		Snow Existence	None
Snow Cover Product	Snow Existence	<i>a</i>	<i>b</i>
	None	<i>c</i>	<i>d</i>

Table 3-4 Validation metrics calculation

POD	FAR	HR	SMR
$\frac{a}{(a+c)}$	$\frac{b}{(a+b)}$	$\frac{(a+d)}{(a+b+c+d)}$	$\frac{c}{(a+b+c+d)}$

3.3.1.1 Validation over Turkey

Snow depth measurements from synoptic weather observation stations and climatic stations were used for the validation of the H10 product. The data from those meteorological observation stations are mainly composed of periodically-measured snow depth information reported on a daily basis. The validation analyses using the ground observations were performed for different snow seasons. The elevation of the stations ranges between 808 m and 2500 m. The ground observations were obtained from TSMS synoptic observation stations and the distribution of the observations is given in Figure 3.5.

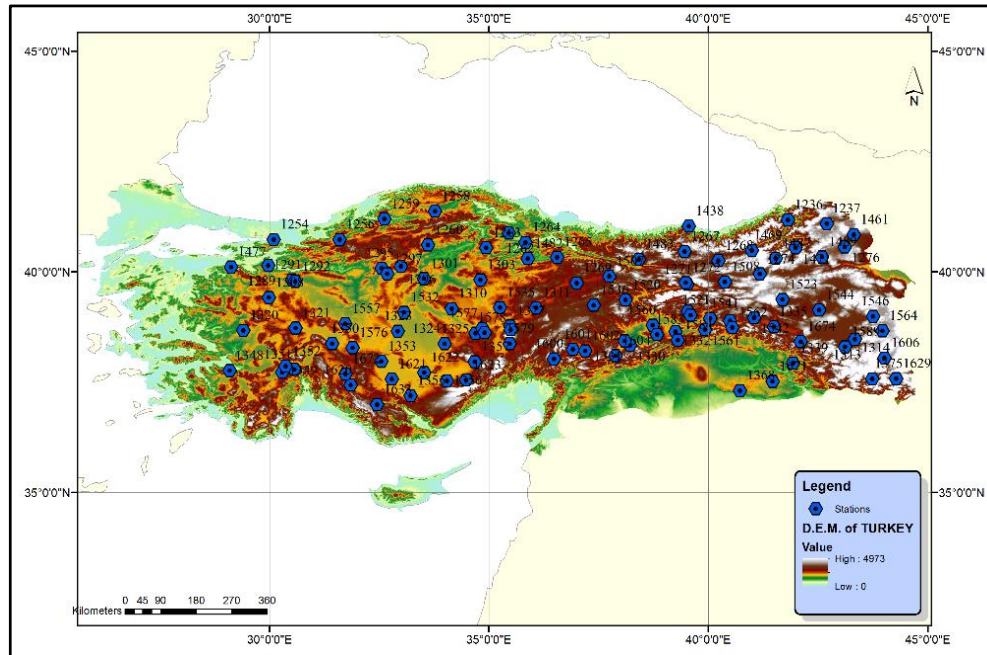


Figure 3-5 Distribution of ground observations used in the validation studies.

The validation studies have been continuously done since 2008 and the overall scores are given in Table 3.5. The results are presented with the requirements and the final accuracy values. A detailed validation study of H10 product over mountainous areas of Turkey is published by Surer and Akyurek (2012) and presented in Appendix A.

Table 3-5 Overall accuracy results of H10 for flat and mountain areas in Turkey

	Threshold		Target		Optimal		Acc.	Acc.
	Flat	Mount.	Flat	Mount.	Flat	Mount.	Flat	Mount.
POD	0.80	0.60	0.85	0.70	0.99	0.99	0.92	0.67
FAR	0.20	0.30	0.15	0.20	0.05	0.05	0.33	0.13

3.3.1.2 Validation of H10 over Austria

This section of the thesis investigates the validity of H10 product over Austria from 2008 to 2012 by making comparison of ground measurements of snow. Austria is an ideal region to test the accuracy of the H10 product since it gives chance to observe

the behaviour of H10 in different elevation zones, and also different land uses. Being close to some parts of the Alp Mountains, significant amount of precipitation in the form of snow is seen throughout the year. In addition to the ground measurement, a comparison of the product over Austria with combined MODIS snow products is also presented. The details of the validation procedure is provided in a paper published by Surer et al. (2014), and given in Appendix B.

3.3.2. Validation of H13

The validation of SWE (H13) product against ground snow depth measurements has two parts. The first part shows the ability of H13 to indicate if the region (pixel) is covered by snow. In the second part, the H13 estimates of SWE are compared with SWE derived from snow depth observations at meteorological stations.

3.3.2.1. Validation of H13 over Turkey

The validation of the H13 product is being carried out using Synoptic station observations and values measured during individual snow courses. In-situ measurements are compared individually with the corresponding 25 x 25 km² H13 snow product grid.

It should be kept in mind that SWE product is developed for dry snow conditions. Therefore for any pixel, if snow status has been detected as wet, no SWE calculation was done and SWE value was set as 0.0 mm. Hall et al. (2002) describe a simple algorithm to detect snow status. First snow depth (SD) is determined by:

$$SD = 15.9 (Tb18.7H - Tb36.5H) \quad (3.1)$$

where Tb is brightness temperature and subindices denote the channels. If the conditions in equation (3.2) are met the data is classified as dry snow.

$$SD > 80 \text{ and } Tb36.5V < 250K \text{ and } Tb36.5H < 240K \quad (3.2)$$

Snow status can also be checked for the snow state of pixel in which validation measurement exists. If the snow state of station is stated as wet then that station is excluded from validation studies. RMSE is used as the statistical metric to present the accuracy. Developed algorithm for SWE is valid for snow depths in between 20 cm and 100 cm. Snow depths out of this range cannot be modelled because of capabilities of the sensor. Thus, during validation studies measured snow depths out of this range are neglected.

If there exists only snow depth measurements, these values are multiplied with average snow densities that range in between 0.25 g/cm^3 to 0.30 g/cm^3 in order to obtain SWE values. The validation results obtained since 2010 are given in Table 3.7. The calculated mean snow water equivalent values obtained from H13 corresponding to measured snow water equivalent values for the period January, March for the years 2010, 2011, 2012 and 2013 are given in Figure 3.7.

Table 3-6 Validation results of H13 product over Turkey

Year	2010	2011	2012	2013
RMSE (mm)	46.14	45.24	45.54	39.62

3.3.2.2. Validation of H13 over Austria

The assessment of the overall snow cover accuracy (k_A) of H13 is presented in Figure 3.8. The k_A varies between 24.4% at the Sonnblick (3109 m) in the Eastern Alps (Carinthia) and 99.6% in Seibersdorf (185 m) near Vienna. Similarly as for H10, the H13 the accuracy in the flatland is higher than mountain regions such that the median of k_A is 88.8% for flatland, and 80.3% for mountain regions. The results indicate that in the Alps, the snow cover accuracy of H13 tends to be lower than H10 while in the flatland region (with shorter snow cover occurrence) is the H13 accuracy similar to H10.

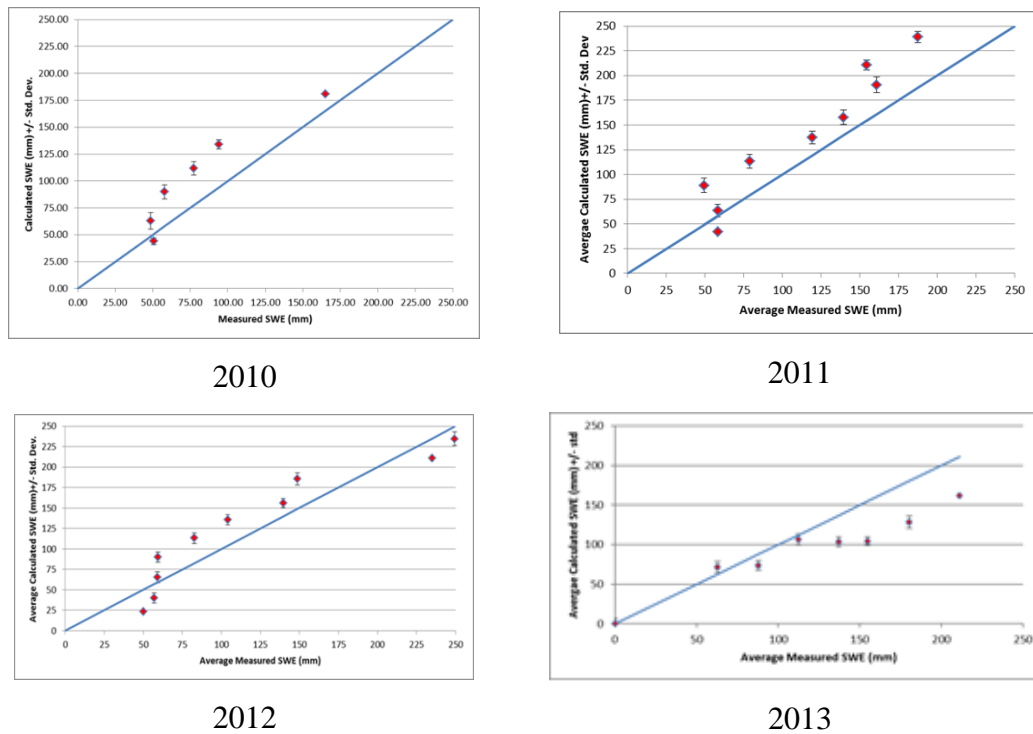


Figure 3-6 The calculated mean SWE values obtained from H13 corresponding to measured SWE values for the period January, March for the years 2010, 2011, 2012 and 2013 (HSAF-PUM, 2013).

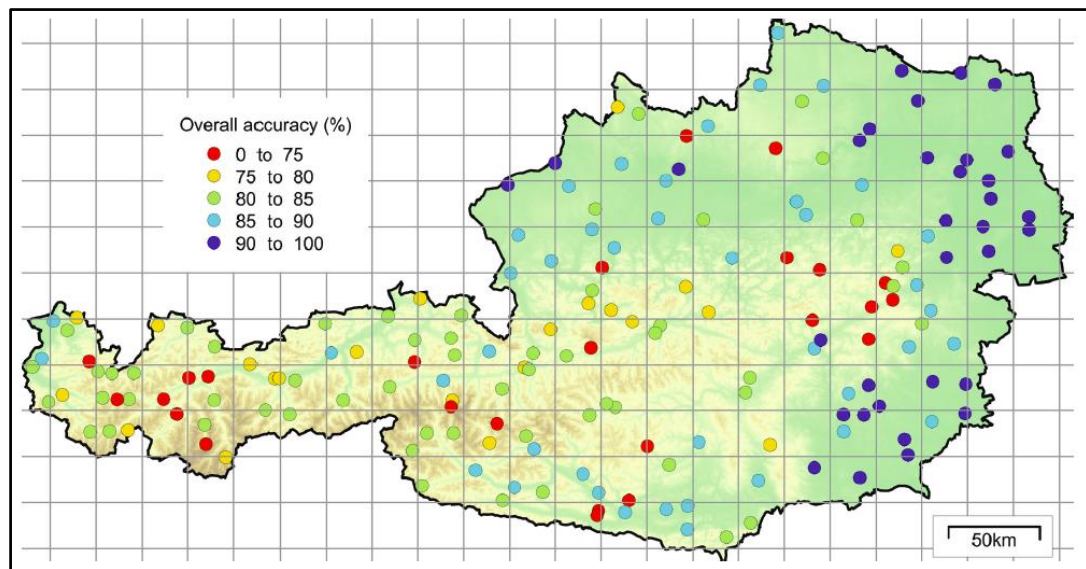


Figure 3-7 Overall accuracy (k_A , %) of H13 product at 178 meteorological stations in the period April 2008-June 2012.

The seasonal frequency of H13 snow cover mapping errors is presented in Figure 3.9. The left and right panels show the frequency of H13 over (k_o) and under (k_u) estimation errors, respectively. From this assessment, it is clear that the microwave

H13 product significantly underestimate the snow cover at meteorological stations, particularly at locations, which are situated above the H13 pixel mean. The mapping errors are obviously the largest in winter and exceed 50% even for stations, which are located below the mean pixel elevation. The largest k_U errors exceed 80% at stations situated more than 500m above mean pixel elevation in April and December. The snow cover over-estimation errors are very small, the largest k_O errors exceed 20% only at locations significantly (more than 500m) below the mean pixel elevation in February and March.

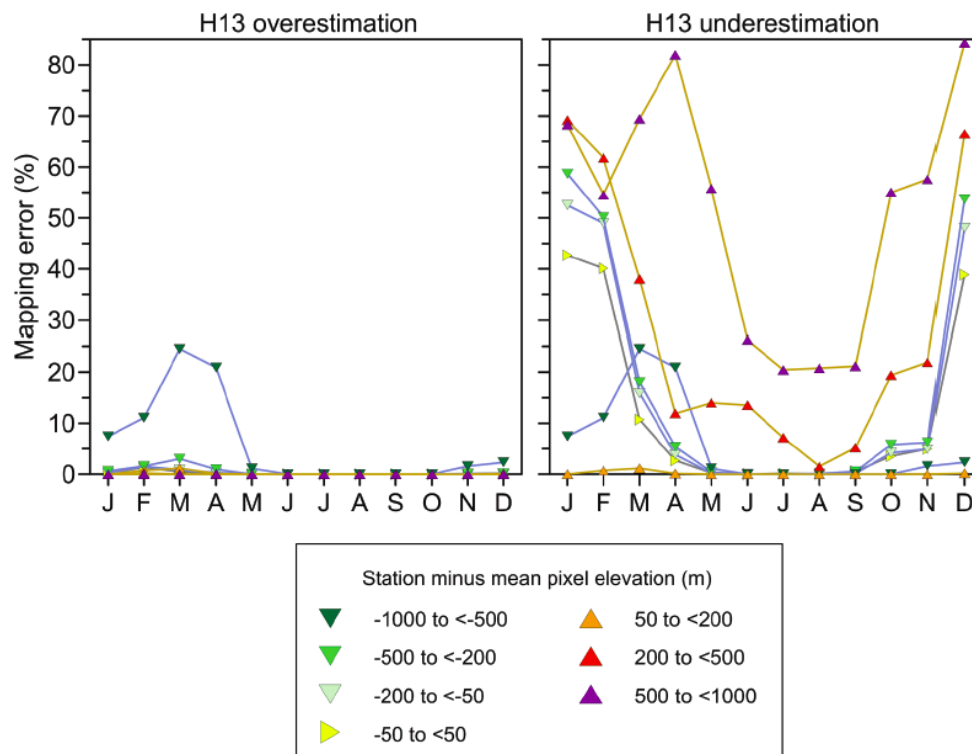


Figure 3-8 Seasonal frequency of H13 snow overestimation (k_O , left side) and underestimation (k_U , right side) errors that are summarized for stations at different elevations, and matching H13 pixel mean.

A clear underestimation of snow is documented also in Figures 3.10 and 3.11, which compares H13 microwave estimates of SWE with SWE derived from daily snow depth observations at two meteorological stations in the mountains (Figure 3.10) and flatland (Figure 3.11) regions. The station SWE is plotted as a range of SWE values by using two different snow densities (0.150 and 0.300kg/m³) in the derivation of SWE from the snow depth values. Even if the snow density is not measured on daily

time scale, the range of values used in the assessment shows a probable variability during the snow seasons. The results indicate that the maximum SWE values from the H13 product are around 100mm, which is significantly lower than derived from the observed snow depth measurements. The snow depth measurements at Brand station (Figure 3.10) exceed in some days 5m, which is clearly not captured by the H13 product. Also the snow depth observations at the beginning of winter seasons are not estimated from the microwave observations. Similar underestimation of SWE is observed in the flatland region (Figure 3.11), where there is no snow estimated for shorter snow events in the 2010 and 2011 winter seasons and only a small overestimation of SWE observed for 3 days in February 2010.

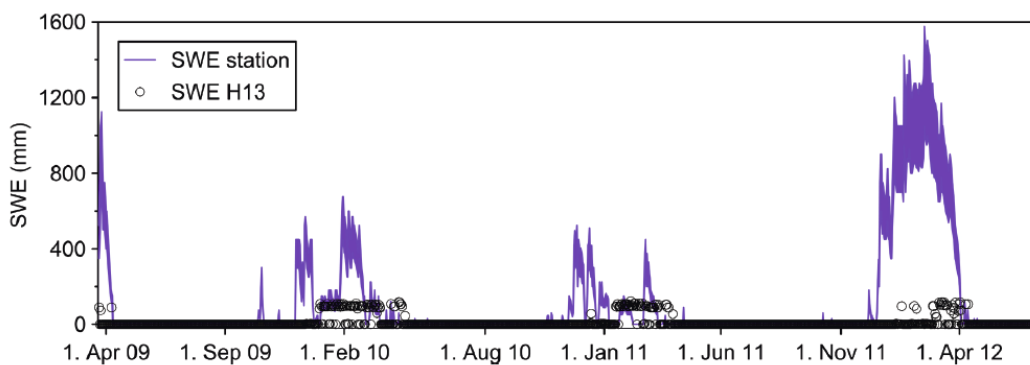


Figure 3-9 Comparison of pixel SWE estimate from H13 satellite product, and SWE estimated from snow depth observations at Brand station (Vorarlberg region). Station is located approximately at the mean pixel elevation of H13 product (1014 m).

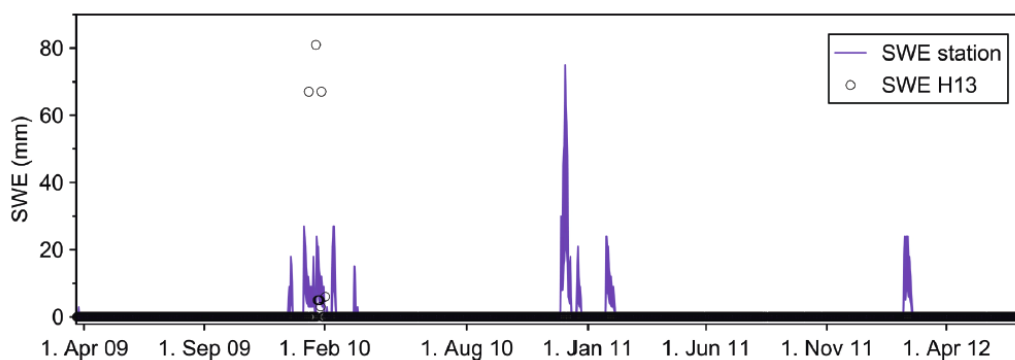


Figure 3-10 Comparison of pixel SWE estimate from H13 satellite product, and SWE estimated from snow depth observations at Eisenstadt station (Burgenland region). Station is located approximately at the mean pixel elevation of H13 product (184 m).

CHAPTER 4

HYDROLOGICAL MODELING AND SENSITIVITY ANALYSIS

4.1 General

Model parameters should be accepted as important part of the structure of the model which can be used in order to fine tune the model output. These parameters can be estimated by use of different approaches such as using an initial estimate considering the catchment physical characteristics, and look-up tables, manually and/or automatic calibration using optimization algorithms, and using transfer functions in between similar basins (Abebe et al., 2010, Yilmaz et al., 2010). In modelling, the main idea is to estimate the model parameters through calibration of the model by matching simulated outputs with the observed ones. Various reasons may result in uncertainties in modeling effort which in turn can adversely affect model predictions. In order to reduce the level of uncertainty, the detailed analysis of behaviors and sensitivities of parameters should be performed. Therefore sensitivity analysis is an important research topic in hydrological modelling. The common approach is to assume constant model parameters in certain time, while the characteristics of the test basin remain constant. In model calibration the optimum values of the parameters describing the model structure is aimed to be identified. Identifiability is described as the level of how well a parameter is defined in model structure. The length and content level of the data used for calibration may affect the optimum values of a parameter (Wriedt and Rode, 2006). There is an increasing number of studies in hydrological literature stating that rather than optimality, “equifinality” must be sought in the parameter estimation. Equifinality indicates the ability of systems to reach the same state from different starting conditions (Bertalanffy, 1950). This concept has also been applied by Beven and Freer (2001) in hydrology, they grouped the parameter sets as behavioral and non-behavioral. They stated that

behavioral parameter sets allow models to simulate the observed variables to a higher degree, as measured by objective functions and they found no unique solution to the calibration of hydrological models. This approach of creating a set of variables for observing their behaviors in a margin of specified thresholds has been proposed by Hornberger and Spear (1981) in their well-known Generalized Sensitivity Analysis framework.

4.2 Sensitivity Analysis of the model parameters

Sensitivity analysis of the model parameters is considered in order to depict the most sensitive parameters. The HBV model is firstly calibrated via SCE-UA method (Duan et al., 1992, Duan et al., 1994) with the data from October 1, 2008 through September 30, 2013. The ranges of the model parameters used in the automatic calibration are given in Table 4.1; these values were determined by using the initial levels applied by Parajka & Blöschl (2008).

i- Calibration with runoff only

The calibration of model was performed by using a single objective function where the model parameters were obtained using measured runoff only. The runoff objective function is defined as;

$$Z_Q = w_Q(1 - M_E) + (1 - w_Q)(1 - M_E^{\log}) \quad (4.1)$$

where the weight w_Q is set to 0.5 and both the high (M_E) and low flows (M_E^{\log}) are combined in the optimization.

ii- Calibration to both runoff and H10 snow product

The calibration of the model is performed by using a single-objective function where both runoff and H10 snow cover data were combined through a weighting scheme. The compound objective function Z_M , which involves two parts Z_Q and Z_S that are related to the runoff and the snow cover respectively, is minimized to obtain the model parameters.

$$Z_M = w_S Z_S + (1 - w_S) Z_Q \quad (4.2)$$

The coefficients are obtained through a sensitivity analysis. The snow part of the objective function represents the sum of the over and underestimation snow errors:

$$Z_S = w_1 S_{E^o+} + w_2 S_{E^u} \quad (4.3)$$

where w_1 and w_2 equal to 1, and the over and underestimation errors are set equally weighted.

Table 4-1 Model parameters

Model parameter		Model component	Lower	Upper
Snow correction factor(-)	CSF	Snow	0	1.5
Degree Day factor(mm/°Cday)	DDF	Snow	0	5.0
Rain air temp. Thresold (°C)	T _{rain}	Snow	2	2
Snow air temperature threshold (°C)	T _{snow}	Snow	-2	-2
Melting air temperature threshold (°C)	T _{melt}	Snow	-2.0	2.0
Soil moisture state/maximum soil moisture storage (-)	LP/FC	Soil	0	1.0
Maximum soil moisture storage (mm)	FC	Soil	0	600
Runoff generation to the soil moisture state (-)	BETA	Soil	0	20
Very Fast storage coefficient (days)	K ₀	Runoff	0	2.0
Fast storage coefficient (days)	K ₁	Runoff	2.0	30
Low storage coefficient (days)	K ₂	Runoff	30	250
Threshold of storage state exceedence (mm)	LSUZ	Runoff	1.0	100
Percolation rate (mm/day)	C _{PERC}	Runoff	0	1.0
	B _{MAX}	Runoff	10	10
Routing parameter	C _{ROUTE}	Runoff	26.5	26.5

During the sensitivity analysis calibration is performed by using a single objective function, where the model parameters are obtained using measured runoff only. During calibration NSE measure is used. PBIAS, RMSE and correlation coefficient are the other statistical measures used in the sensitivity analysis.

A parameter set that is accepted as most representative is obtained by calibrating the model. Following the calibration, feasible range of each parameter is divided into 20 equal increments and their behavior is observed while the other remaining parameters are fixed during new runs. Figure 4.1 shows that the response parameters L_{SUZ} , C_{PERC} , K_0 , K_1 , and K_2 are insensitive to the PBIAS. L_{SUZ} and K_1 appear to be sensitive to RMSE and correlation coefficient indicating that they have an effect on high flow series and timing of the discharge. C_{PERC} is sensitive to RMSE and correlation coefficient. None of the response parameters has an optimum value in the statistical measures as the parameter varies. It has been observed that parameters L_{SUZ} , C_{PERC} , K_0 , and K_1 play roles in the response and transformation routines. They influence the high flow series more than the volume balance. L_{SUZ} , K_0 , and K_1 are parameters that control the overland runoff and the quick interflow. Their influence on the catchment response is through changing the shape of the outflow hydrograph at the outlet of the catchment and hence they have negligible effect when it comes to the overall volume. On the other hand, K_2 is the parameter controlling the baseflow from deep groundwater and is expected to have an effect on total volume, for this basin it is found insensitive within the given range. C_{PERC} and K_2 work together. A higher value of C_{PERC} allows high flow of water from the upper to the lower reservoir and indicates more storage in the lower zone. K_2 determines the baseflow. It is the main parameter that controls the low flow series. C_{PERC} controls the volume of flow in the first tank.

Figure 4.2 shows the soil parameters (L_{PRAT} , FC , $BETA$) and routing parameters (B_{MAX} and C_{ROUTE}) sensitivity with reference to PBIAS, RMSE, NSE, and Correlation Coefficient. L_{PRAT} and $BETA$ show sensitivity to PBIAS, RMSE, and correlation coefficient indicating their effect on total volume, high flow series and timing of the flows. FC is sensitive to RMSE and correlation coefficient and also shows sensitivity to PBIAS. FC is the parameter that divides the precipitation into soil moisture and surface runoff. If the FC is lower, then it means also the water

holding capacity of the soil is very low. It also indicates the amount of surface runoff. L_{PRAT} is the ratio between the soil moisture state and the maximum soil moisture storage. It calculates the actual evapotranspiration in relation with the currently available soil moisture. In this semi-arid catchment BETA was found as the most dominant parameter of the model controlling the volume error. B_{MAX} and C_{ROUTE} are insensitive to all the statistical measures used.

Figure 4.3 shows the sensitivity of snow parameters (CSF , DDF , T_{rain} , T_s and T_{melt}) with reference to PBIAS, RMSE, NSE and Correlation Coefficient. T_{rain} and T_s are found insensitive to all the statistical measures. T_{melt} appears to be sensitive to correlation coefficient, indicating that it controls the high flow series. Degree Day Factor (DDF) is sensitive to PBIAS, RMSE and correlation coefficient. Within 10% change in the range of DDF , the volume balance changes. DDF affects the amount of water due to melting of snow. It also controls the high flow series and timing of the flows. Snow Correction Factor (CSF) also controls the volume error, high flow series and timing of the flows.

None of the used statistical measures indicate the sensitivity of parameters to low flow series. Therefore in addition to the performed sensitivity analysis signature measure is used to find out the parameter sensitivity to low flow series. Signature measures are defined as hydrologic response characteristics that provide insights into the hydrologic functioning of the catchments (Sawicz et al., 2011). Flow duration curves can be used to diagnose model performance for different characteristics of the catchment. Dividing the flow duration curve into segments leads to a process-based calibration for the dominant processes within the catchment, which are reflected by the different parts of the hydrograph. It is well-known that FDC does not include information on accurate flow timing. Yilmaz et al. (2008) used FDC to derive the signature measures to quantify the performance of a distributed hydrological model. They used four divisions in FDC and investigated the applicability of the FDC segments, especially for high flow events with a range of flow exceedance probability between 0- 0.02%.

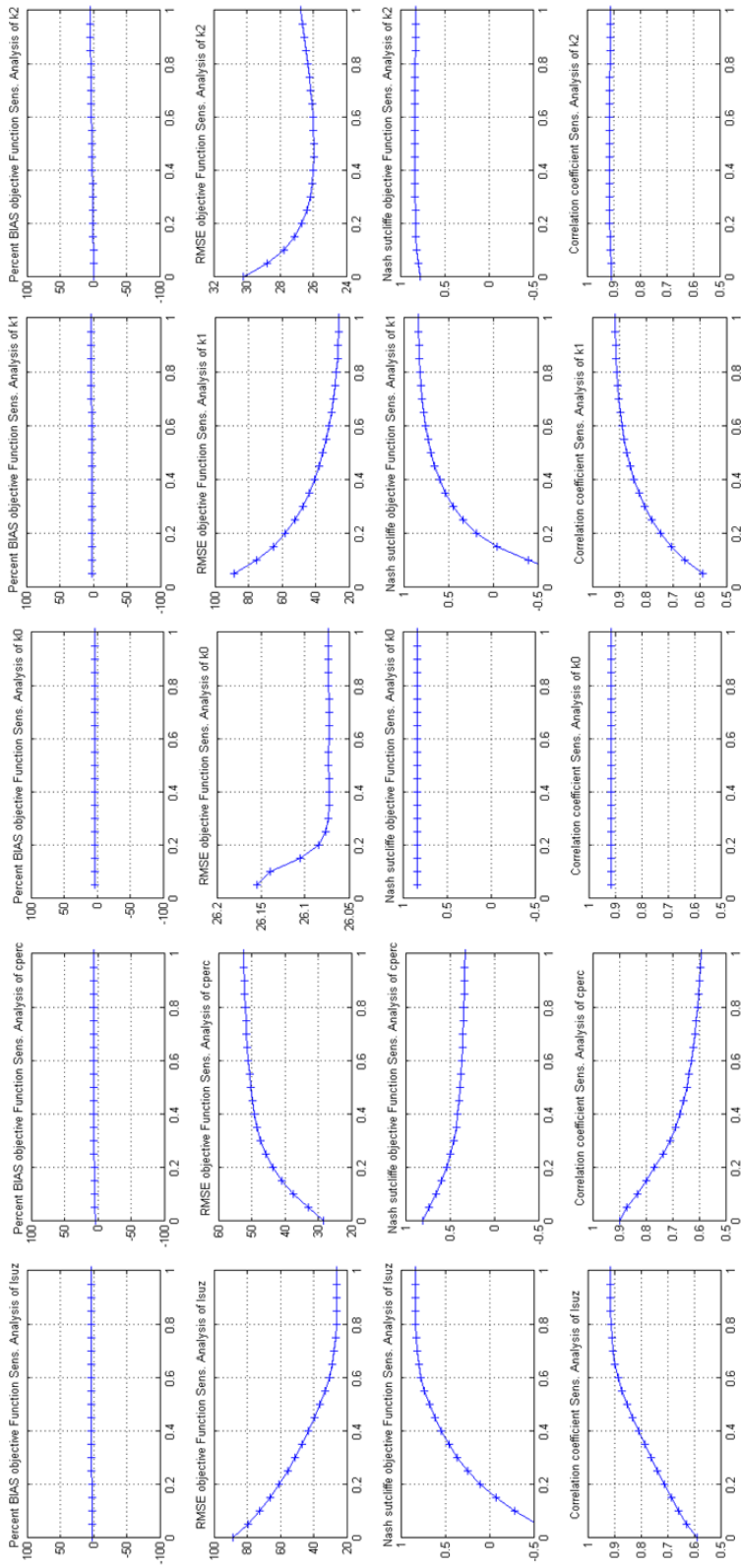


Figure 4-1 Sensitivity plots of parameters L_{SUZ}, C_{PERC}, K₀, K₁, K₂ with reference to PBIAS, RMSE, NSE and Cor. Coeff.

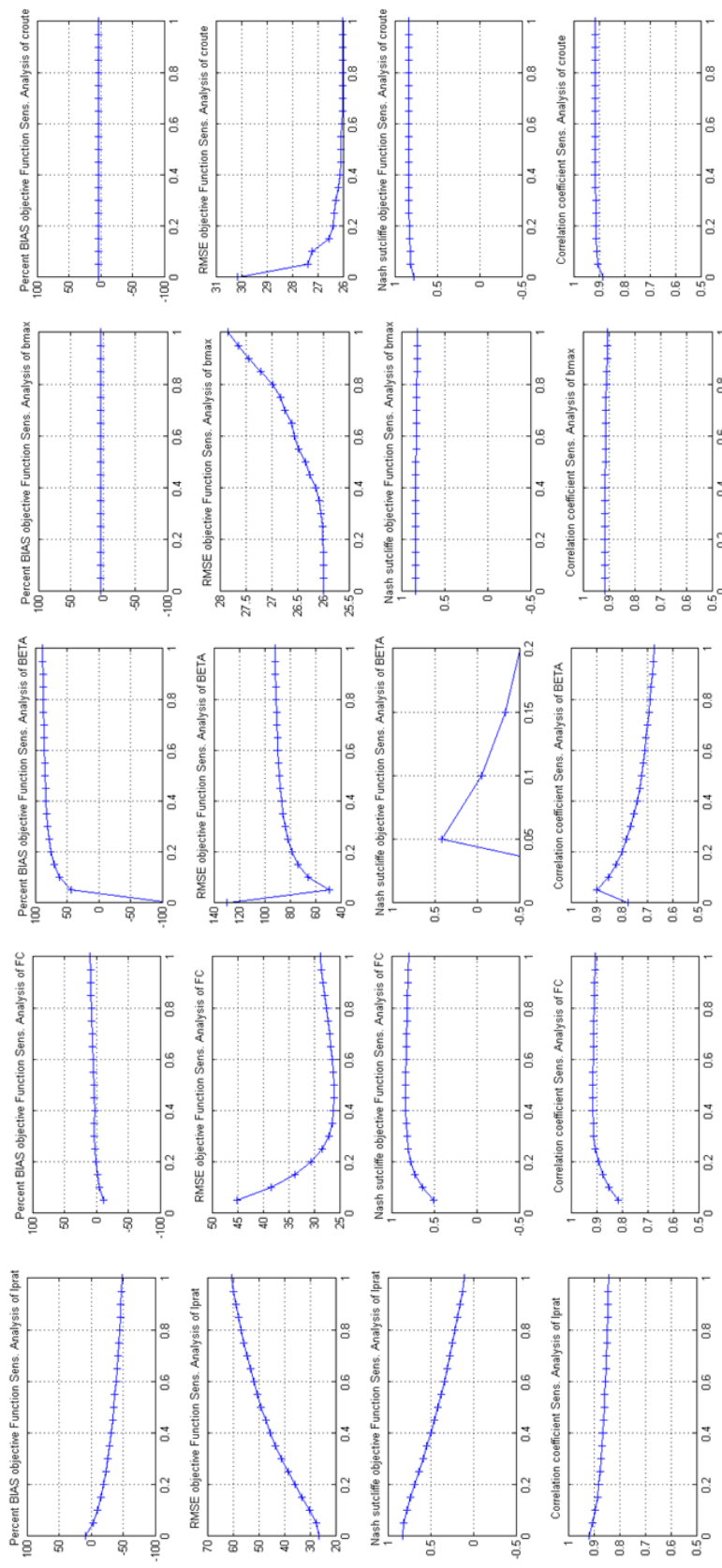


Figure 4-2 Sensitivity plots of parameters L_{pratt}, FC, BETA, BMAX, CROUTE with reference to PBIAS, RMSE, NSE and Cor. Coeff.

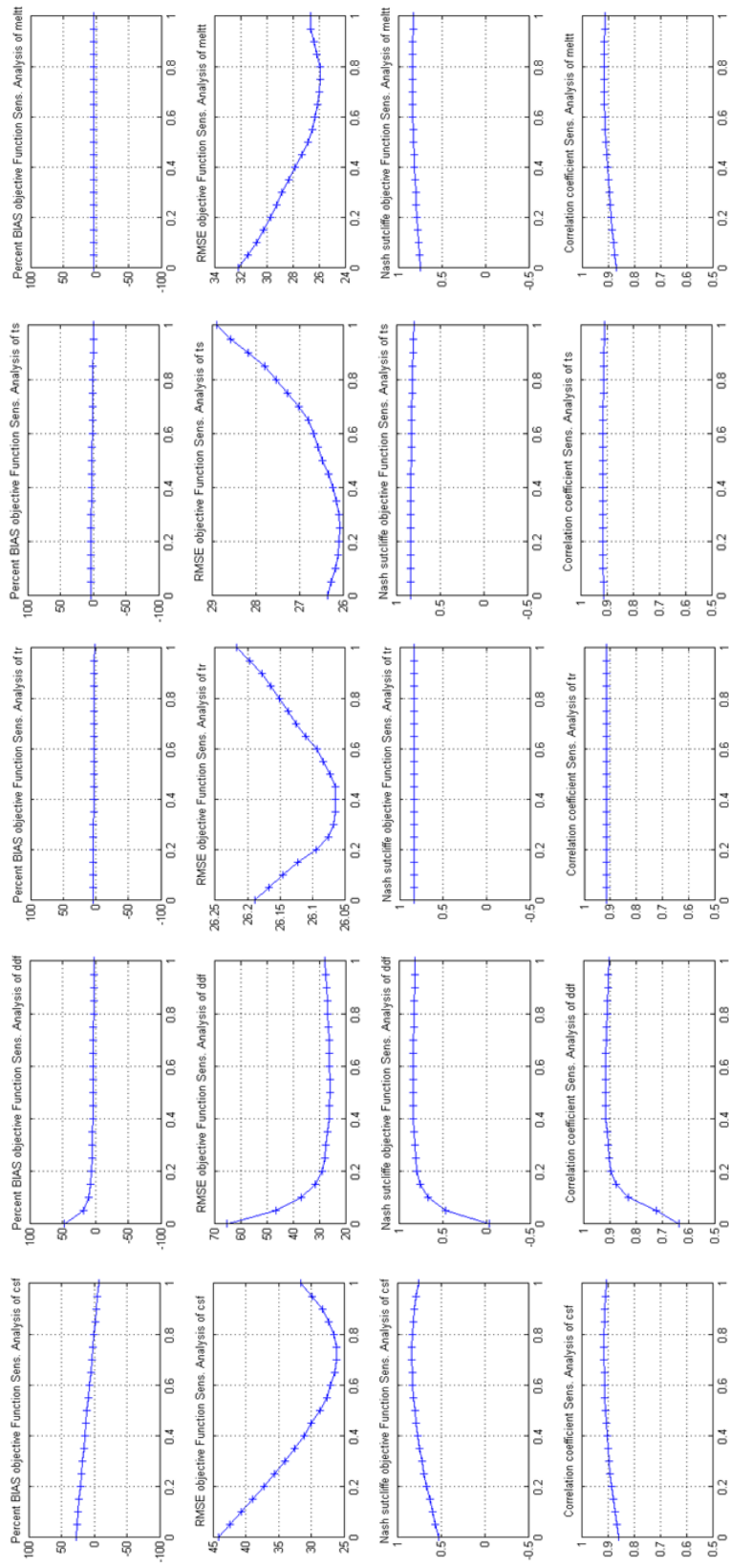


Figure 4-3 Sensitivity plots of parameters CSF, DDF, T_{train}, T_s and T_{melt} with reference to PBIAS, RMSE, NSE and Cor Coeff.

The low flows are considered within the range of flow exceedance probability between 70% and 100% with logarithmic discharge volumes without further subdivision. Pfannerstill et al. 2014, designed additional segmentation of the FDC. They used 5 segments in the FDC and with this segmentation very low and very high flows are segmented in the flow duration curve in equal ranges. The very high flow range was defined below Q5, high flow range was defined between Q5 and Q20, middle flow range was defined between Q20 and Q70, low flow range was defined between Q70 and Q95 and very low flow range was defined between Q95 and Q100. In this study 5 segments were used and the parameter sensitivities were analyzed for different parts of the FDC. Figure 4.4 presents the FDC of the simulations where one parameter changes and the rest 14 were kept at their optimum value. RMSE was used as the statistical measure to make the comparison of different parts of the FDC and the results are presented in Figure 4.5. It is observed that BETA, B_{MAX}, C_{ROUTE}, T_{SNOW} do not show any sensitivity to the flow partitions in FDC. C_{PERC}, L_{PRAT} and T_{MELT} are the parameters found as insensitive to very low flows. L_{SUZ}, K₀, K₁, K₂, and FC are found as sensitive to very low flows. It is expected for the snow parameters CSF and DDF control the volume error, it is observed that CSF, DDF and Train show sensitivity to very low flows too. This can be due to the existence of parameter interaction.

In general L_{PRAT}, FC and BETA as soil parameters and DDF and CSF as snow parameter control the volume error, L_{SUZ}, K₀, K₁ directly and C_{PERC} and K₂ indirectly control the high flow series and timing of the flow, T_{MELT} controls the maximum flow series. L_{SUZ}, K₀, K₁, K₂ and FC control very low flows. B_{MAX}, C_{ROUTE}, T_{RAIN}, T_{SNOW} are found as insensitive for this catchment. The sensitivity analysis has shown that model calibration should be made multi-objective in order to better reflect catchment responses on different modes, since NSE and RMSE mostly emphasizes only the high flow series (Gupta et al., 2008).

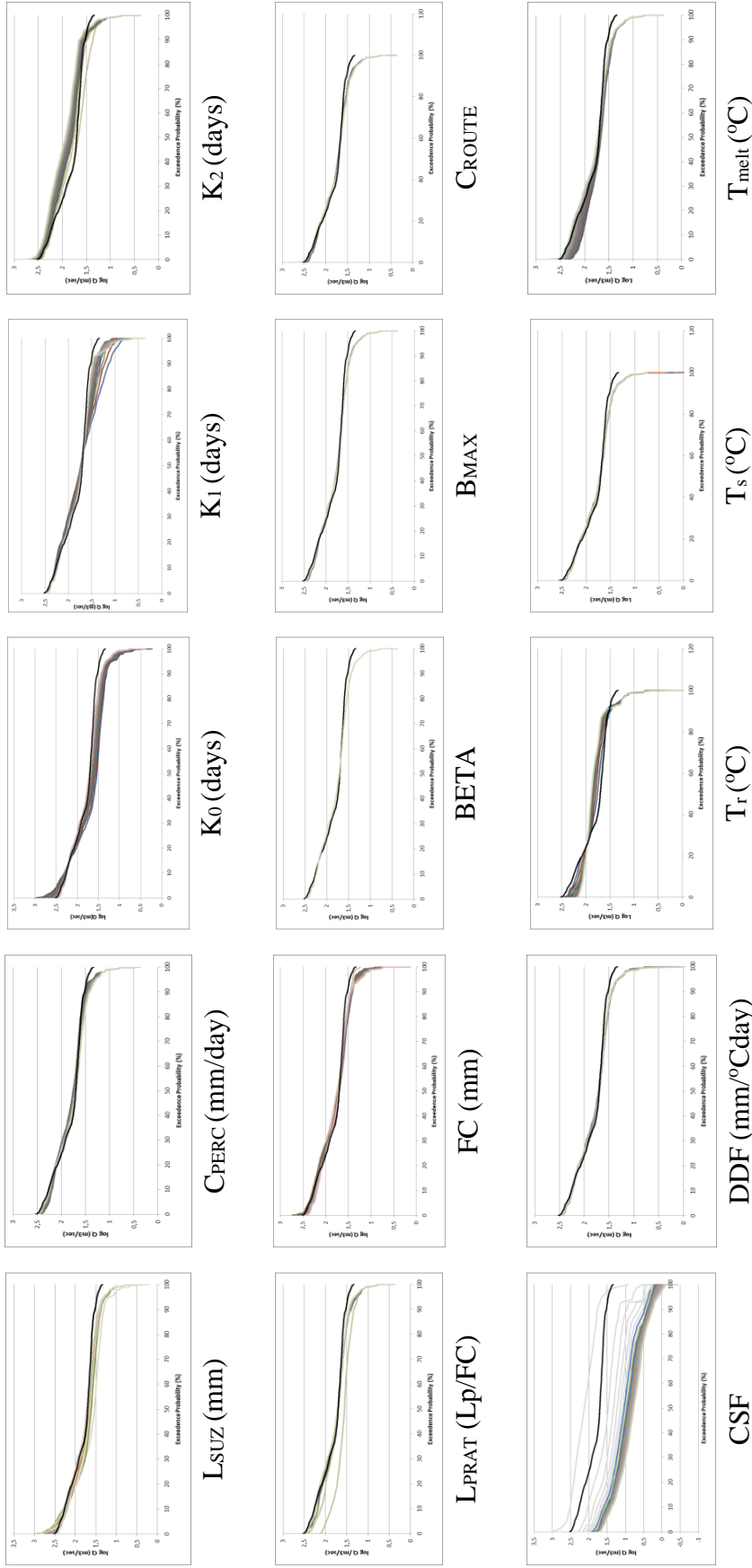


Figure 4-4 FDCs for the simulations where one parameter was changed between the specified limits and the rest 14 parameters were kept at their optimum values.

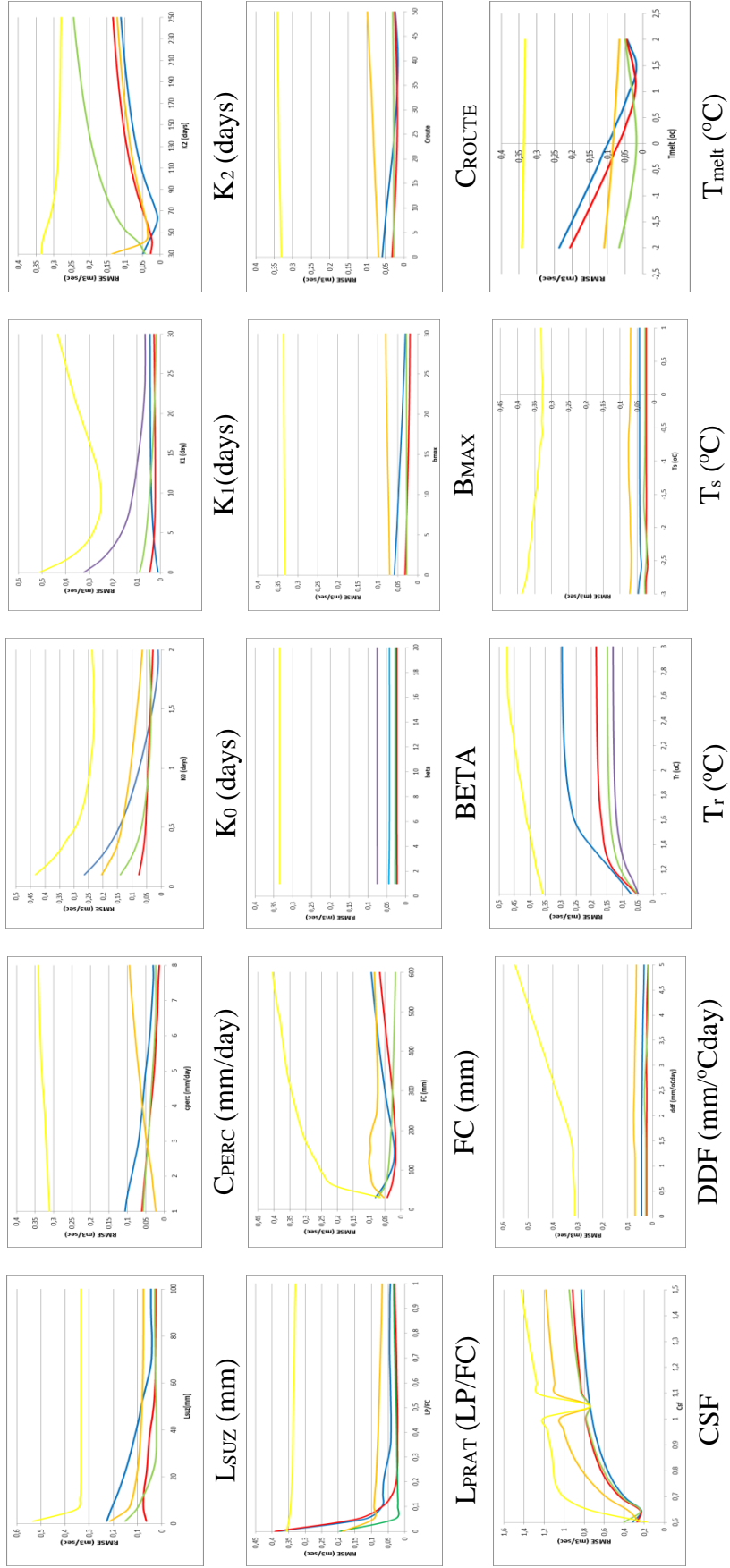


Figure 4-5 RMSE of the FDCs for the simulations where one parameter was changed between the specified limits and other 14 parameters were kept at their optimum values. (Blue: RMSE_Q5, Red:RMSe_Q20, Green:RMSE_midflow, Orange:RMSE_Q70 and Yellow:RMSE_Q95).

4.3 Sensitivity analysis of the model thresholds

The cloud coverage is an important factor in snow mapping. The reliability of the snow cover data depends on the cloud coverage. Number of days available for calculating SCA from H10 for different cloud thresholds ζ_c ranging from 0.10 to 0.80 were obtained (Figure 4.6). Days are expressed as the frequency relative to the total number of days in the period 2011-2012. The magnitude of the threshold ζ_c affects the number of days for which H10 images are available. A threshold of $\zeta_c < 20\%$, SCA images are available on at least 42% of the days in the catchment. The good temporal resolution of H10 snow product provides more images having less cloud coverage. The SCA was estimated for different H10 snow products, only using images with less than 10%, 20% and 60% cloud cover (Figure 4.7). During most of the season, they are very similar. The exception is SCA gets scattered for the days $\zeta_c < 60\%$. The larger scatter may be related to the more frequent snow melt and rain-on-snow events. In previous hydrological modeling satellite images having cloud cover $< 25\%$ were used (Tekeli et al., 2005). The model is run using different cloud thresholds (Table 4.2). According to the results cloud coverage threshold $\zeta_c < 60\%$ gives the lowest volume error and maximum NSE results.

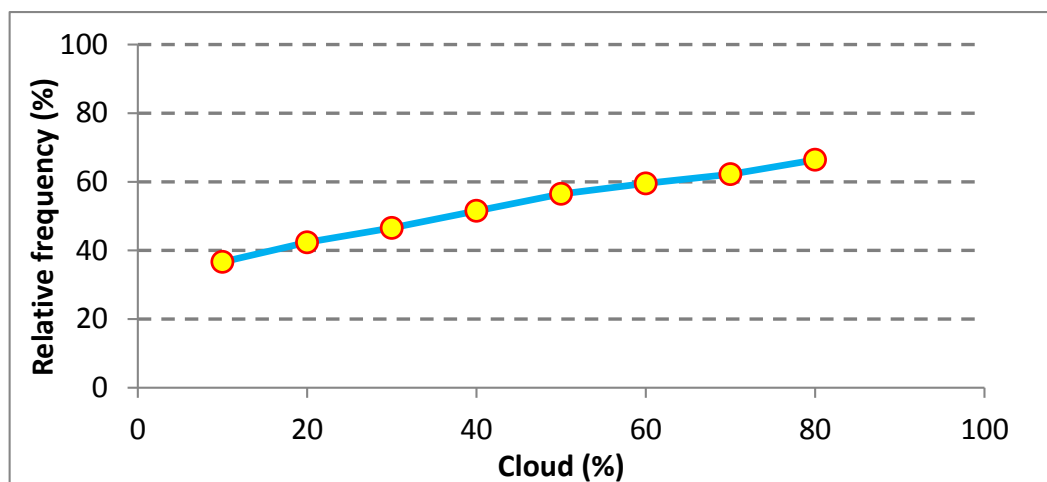


Figure 4-6 Available number of dates used related with cloud cover percentage

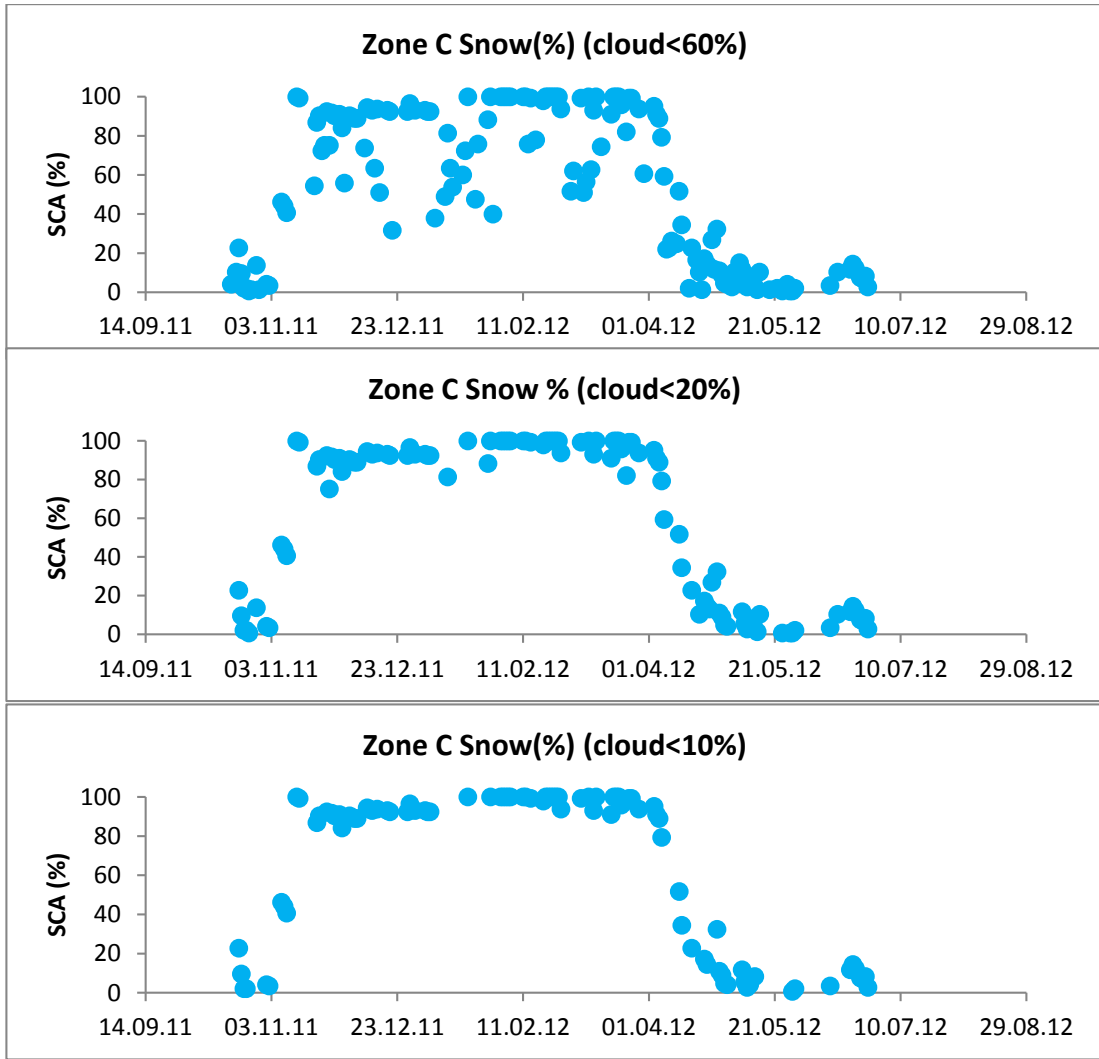


Figure 4-7 Change of SCA from H10 product for different cloud thresholds

Table 4-2 Model performance for different cloud thresholds.

	Cloud <10%	Cloud <20%	Cloud < 40%	Cloud <60%	Cloud < 80%
Volume error	0.0149	-0.0335	-0.0028	-0.0049	0.0022
M_E	0.7941	0.7914	0.7704	0.86	0.8021
logM_E	0.7204	0.7002	0.7236	0.83	0.7909

In the comparison of the model simulations and the H10 snow cover observations, thresholds ζ_{SCA} and ζ_{SWE} are used to define over and underestimation errors. It is obtained that snow overestimation error is sensitive to threshold ζ_{SWE} . As ζ_{SWE}

increases from 0 to 10mm the snow overestimation error is decreasing from 11 days to 4 days (Figure 4.8). The underestimation errors are largest for $\zeta_{SCA}=0$ and as SCA value increases, the underestimation days are decreased and get the value of 0 (Table 4.3). During the sensitivity analysis of thresholds ζ_{SCA} and ζ_{SWE} single-objective calibration to only observed runoff has been used. $\zeta_{SCA} = 25\%$ and $\zeta_{SWE} = 0$ were selected for the rest of the study.

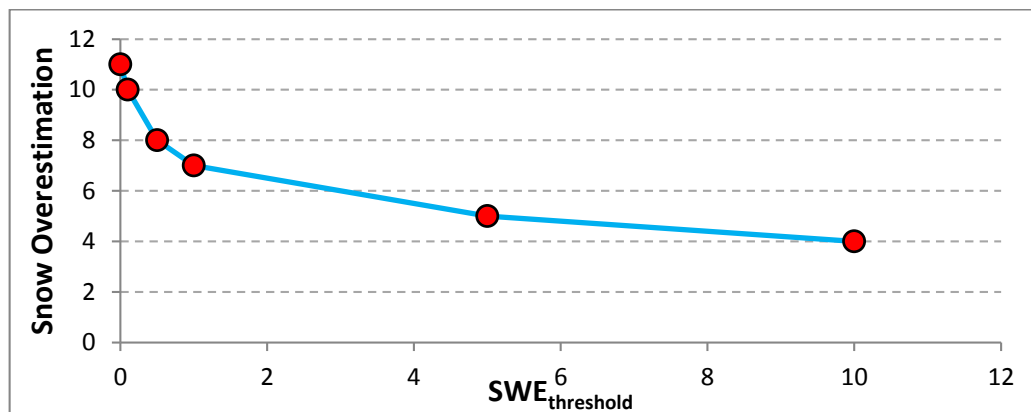


Figure 4-8 Snow overestimation error to different thresholds ζ_{SWE}

Table 4-3 Underestimation error with respect to different threshold ζ_{SCA}

ζ_{SCA}	0	1	5	10	15	25	30
S_E^U	620	0	0	0	0	0	0

CHAPTER 5

MODEL CALIBRATION AND DISCUSSION OF THE RESULTS

5.1 Model Calibration

Hydrological models have to be calibrated accurately to provide reasonable model results. Generally model parameters representing specific catchment characteristics are calibrated to the measured discharge time series. The most suitable parameters are selected with a sensitivity analysis (van Griensven et al., 2006). A challenge of hydrological models is to adequately represent all phases with the same model parameter set (Madsen et al., 2000). Generally, model simulations are evaluated by performance metrics, which can be divided into statistical metrics and signature metrics. In this study HBV modelling concept is modified by considering a multi-metric framework evaluation in model parameter calibration in addition to classical calibration approach by using observed discharge series.

i- Calibration by using statistical metrics:

Two different model calibrations were performed by using SCE-UA. NSE, and VE are used as performance metrics to quantify the accuracy of high flow events and their timing. To emphasize the low flow periods, logarithmic transformation of discharge are used with NSE. The model was calibrated to runoff only and then it was calibrated to both runoff and H10 snow cover. Table 5.1 presents the statistical evaluation of the runoff model efficiencies (M_E , M_E^{\log}), runoff volume error and the snow model errors (S_E^U and S_E^O) obtained by single-objective calibration to measured runoff only. The simulated runoff and the observed runoff with the precipitation distribution are depicted in Figure 5.1.

In the second calibration, the model was calibrated to both runoff and the H10 snow cover data. In the calibration a runoff component and a snow component that are weighted by w_s are used. When only snow component is used in the objective function, w_s gets the limiting factor which is 1, and when $w_s = 0$ it indicates the calibration is performed to runoff only. A sensitivity analysis was performed to understand the effect of w_s (Figure 5.4). It is observed that M_E does not change significantly for the whole interval of w_s variation. When w_s exceeds 0.90, M_E starts dropping so small for the calibration using runoff only. Similarly snow model error (the sum of over and under estimation error) does not show big changes for w_s between 0.9 and 1.0. When w_s drops below 0.9, S_E begins to increase since not much information on the H10 is used in the calibration.

Table 5-1 Statistical measures obtained from model run by two different calibrations and the calibrated model parameters.

Statistical Measures	CALIBRATION (2009-2012)		
	Runoff only	Runoff+H10	H10 only
Volume Error	0.0012	0.0094	-0.1688
Snow overestimation	18	0	0
Snow Underestimation	0	0	0
M_E	0.8421	0.7611	-0.7098
$\log M_E$	0.7621	0.6994	-0.1356
Model Parameters			
CSF	1.4864	1.4119	0.7001
DDF	1.0986	3.6389	4.7343
T_r	2	2	2
T_s	-2	-2	-2
T_{melt}	-1.9296	-1.9942	0.0101
LP/FC	0.0179	0.0196	0.5996
FC	230.7042	225.0944	223.1497
BETA	0.3009	0.2861	11.8676
K_0	0.8114	1.7933	1.3591
K_1	29.4026	28.6689	12.9841
K_2	109.6936	54.4516	168.8469
LSUZ	97.841	38.1338	73.7456
C_{PERC}	0.9826	7.8167	4.947
B_{MAX}	10	10	10
C_{ROUTE}	26.5	26.5	26.5

The model was calibrated by using H10 snow cover data only. The model parameters are presented in Table 5.1 and the simulated runoff hydrograph is given in Figure 5.1, 5.2, and 5.3. In calibrating the model to H10 snow cover data, parameters were obtained different from the ones obtained by using runoff only and runoff and H10 together. The most different parameters are DDF, and T_m , which are part of snow routine of HBV model. The results of calibration by using only runoff values, and integrating H10 were completely different. This makes it possible to refer that these data are independent but can be used in a complementary way. The w_s parameter, which is a representative trade-off between the runoff and snow objectives, was selected as 0.9.

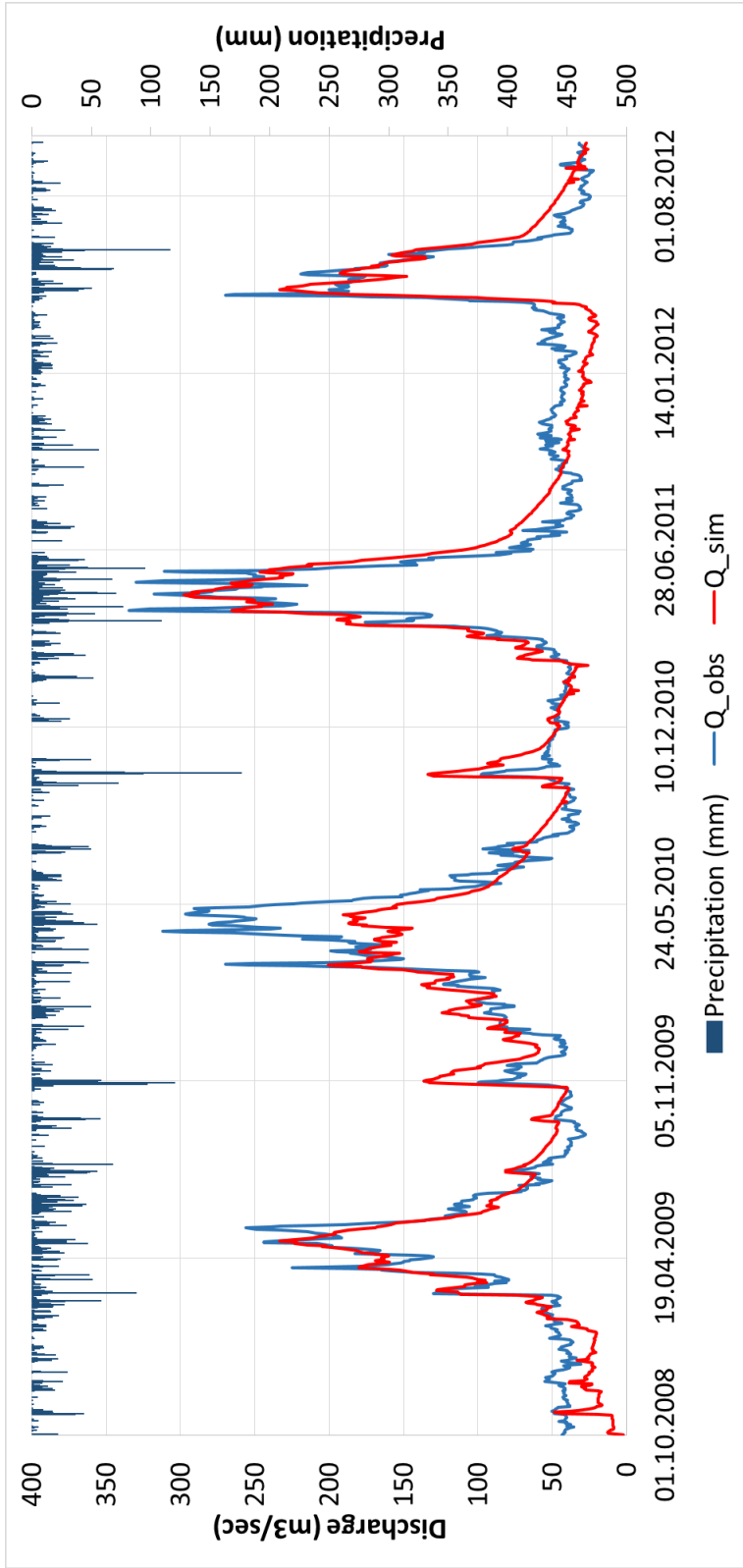


Figure 5-1 Discharge simulation with respect to calibrations to runoff only.

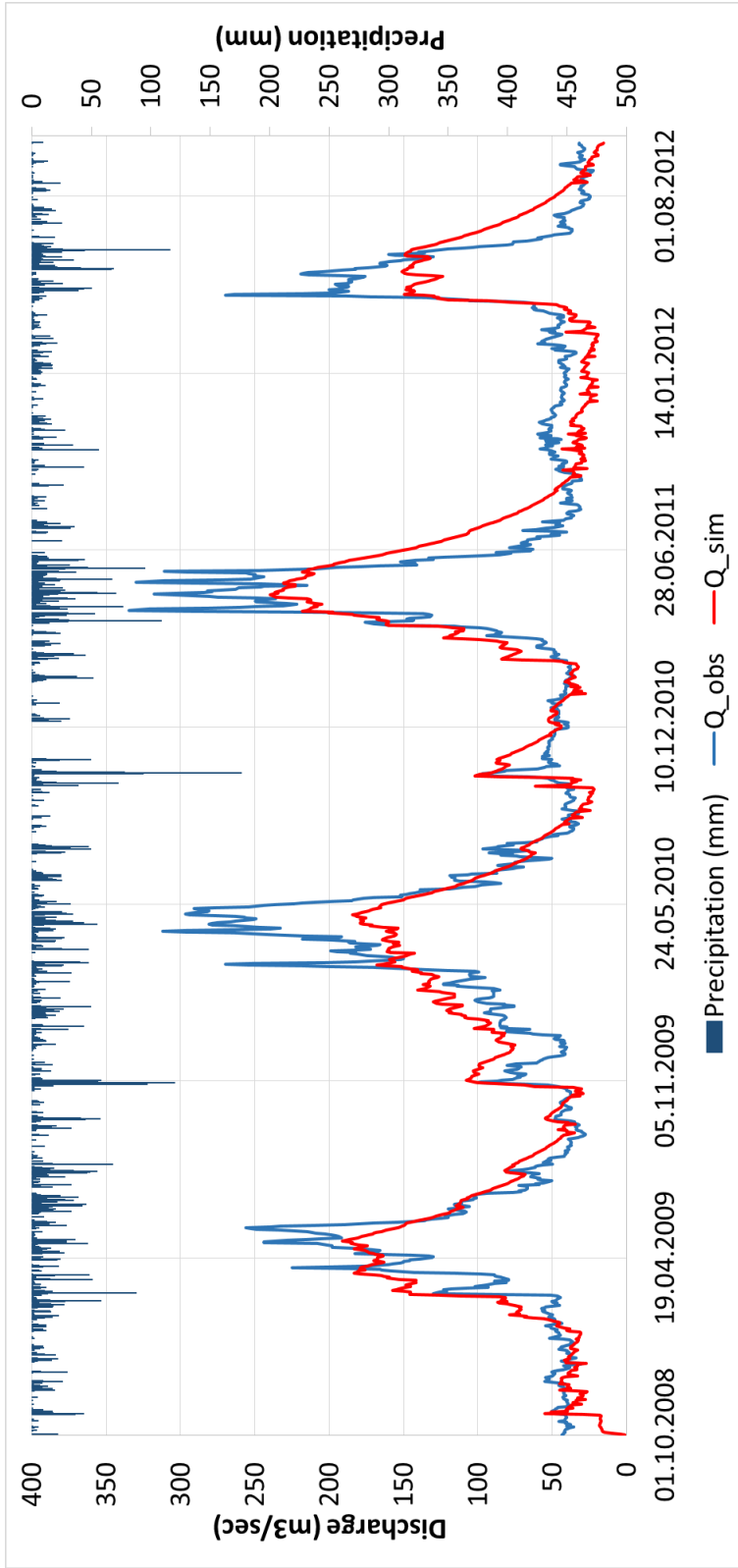


Figure 5-2 Discharge simulation with respect to calibrations to runoff and H10

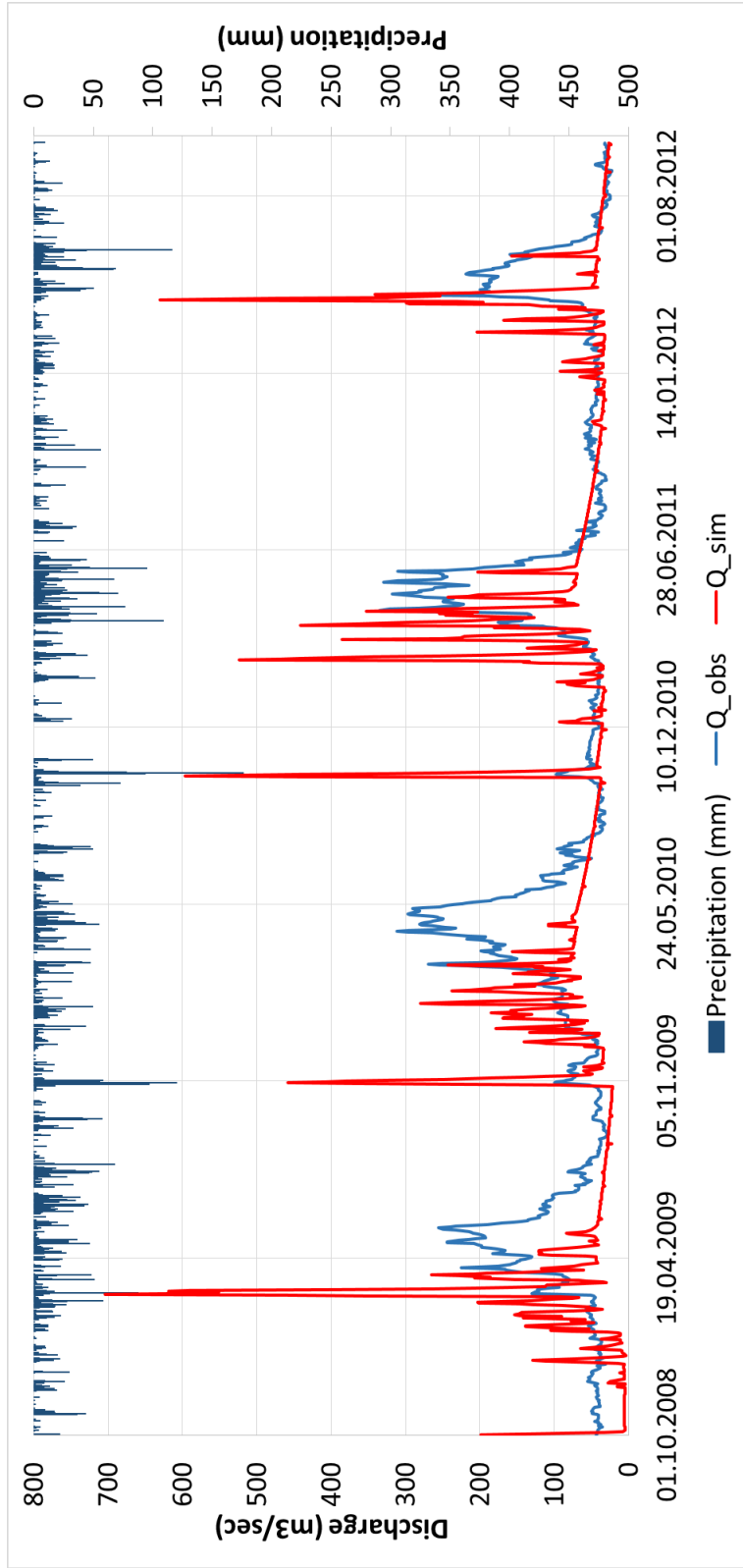


Figure 5-3 Discharge simulation with respect to calibrations to H10 only

ii- Calibration with low flow signature metrics

In order to present the model performance for different flow periods, flow duration curve (FDC) is used as a signature metric. In several studies FDC was segmented into different parts as fast flow, which is controlled by large precipitation events and a mild flow segment, which is controlled by moderate size precipitation events and slow flow segment which considers retention due to catchment storages segment and it is controlled by catchment parameters (Yılmaz., 2008; Pfannerstill et al., 2014). 5 segments were used in this study. To account for the very high flow range, FDC was defined for the flow exceedance probability of 5% (Q5), for high flows between Q5 and Q20, for mid. flows between Q20 and Q70, for low flows between Q70 and Q95 and for very low flows the flow exceedance probability of 95% (Q95) were used. This segmentation was used by Pfannerstill et al., (2014). Figure 5.5 presents the flow segments on a FDC.

In performing the calibration runs Monte Carlo simulation was implemented. Among 15 parameters, 4 parameters set as constant values as they were found insensitive in the sensitivity analysis as described in Section 4.2. The other 11 parameters were changed randomly. 25 000 runs were performed and in the first step, a ranking from best performance metric to worst performance metric value was calculated for the NSE, RMSE_Q5, RMSE_Q20, RMSE_mid, RMSE_Q70, and RMSE_Q95. The best performance for the NSE is 1 and for all RMSE the best performance is 0. In the second step, a value above the threshold defined by the %20 of the best model runs was applied to select the best simulation runs for each performance metric independently. These selections were plotted with the NSE against PBIAS for every performance metric. Afterwards, these selections were intersected with each other to identify the simulation runs with the best combination, where all performance metrics have a value above the threshold as determined by the 20% of best simulation runs. All calibration runs with NSE lower than 0 were excluded from the data set.

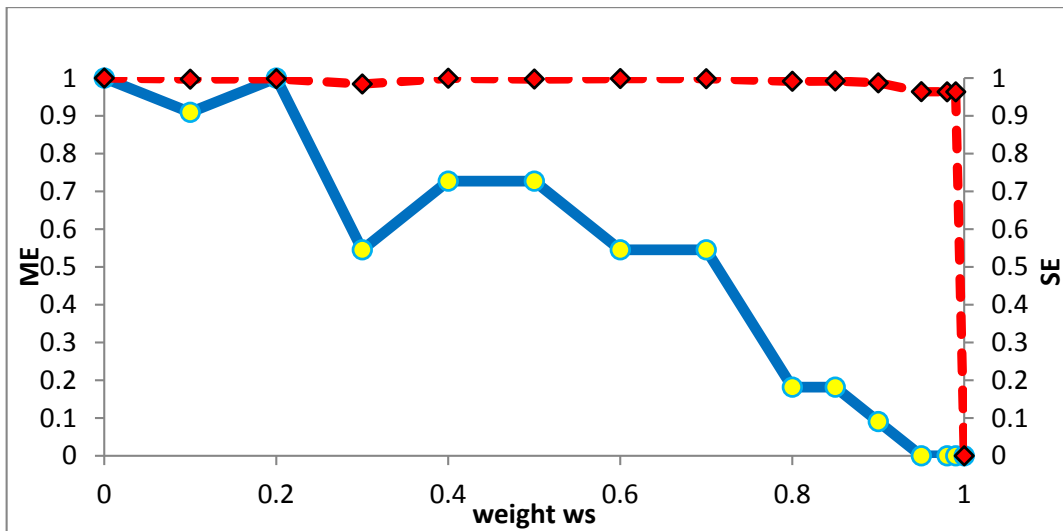


Figure 5-4 Sensitivity of the runoff model efficiency (normalized ME, red dashed line) and snow cover error (normalized SE, blue line) to the weight w_s .

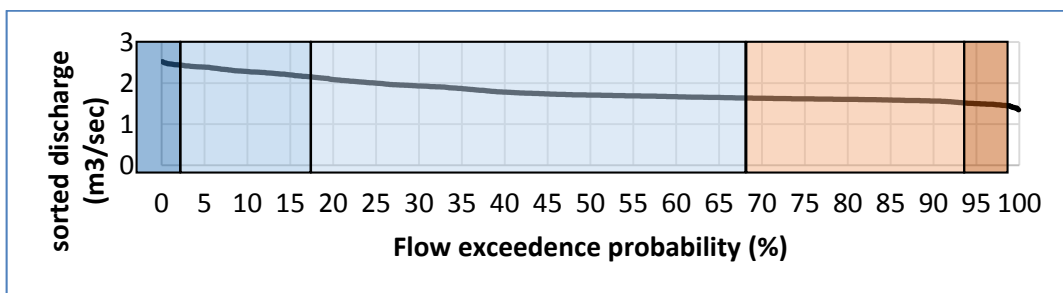


Figure 5-5 Flow segments on FDC

In the third step, different ranking values of the performance metrics for each calibration were summed up to obtain a joined ranking. The optimum values for all performance metrics were obtained by intersecting the final ranking with the one having NSE greater than 0.6 (Figure 5.6).

The stepwise intersection of the best selection runs resulted in a small group of best calibration runs (Table 5.2). The NSE, PBIAS and RMSE for all the flow parts are depicted. The NSE values are very similar and the PBIAS are between 0.741% and 2.143%. Among the flow parts in the FDC, the highest RMSE values were obtained for the very low flow parts. The minimum RMSE were obtained for the mid-flow part of the FDC. The very high flow simulations are also comparatively good. These results are matching up with the findings of Pfannerstill et al. (2014). The model

parameters obtained for these best runs are given in Table 5.3. The calibrated model parameters with the SCE-UA algorithm are also given in this table. CSF, L_{PRAT} , BETA, K_0 , K_1 , L_{SUZ} , and C_{PERC} do not show too much variation among these best run values, but DDF, T_{melt} , FC, K_2 show variation. When the best run values are compared with the ones obtained by SCE-UA, the values are close to the values obtained by SCE-UA, only DDF, T_{melt} and K_2 values show some variation. The precision of the parameters obtained by SCE-UA is higher than the precision of the parameters obtained through joint ranking method.

Table 5-2 Final selection of best calibration runs

Calibration run	NSE	PBIAS	RMSE				
			Q95	Q70	Mid	Q20	Q5
538	0.887	2.143	0.739	0.217	0.083	0.122	0.145
1524	0.874	1.547	0.756	0.230	0.102	0.131	0.174
1686	0.875	1.818	0.786	0.228	0.084	0.116	0.144
1860	0.893	0.741	0.744	0.172	0.103	0.120	0.141
2346	0.875	1.802	0.773	0.221	0.097	0.128	0.160
2706	0.890	0.965	0.802	0.168	0.084	0.094	0.111
2824	0.899	1.315	0.643	0.199	0.114	0.131	0.162
3183	0.890	2.013	0.681	0.208	0.104	0.148	0.195

For visualizing the general performance of the best calibration runs, the simulated discharges were compared with the observed discharges (Figure 5.7). The overlay of the selected calibration runs resulted in small discharge band, because all the simulated discharges are similar. All simulation runs tend to over predict high peak events of the hydrograph which occurs due to rainfall only. The low flow and recession events are predicted satisfactorily for recession in 2011 and 2012. The hydrograph simulation using SCE-UA overlays with the best run hydrograph simulation result as well. The early peaks due to snow melting of the hydrograph are simulated better for the best run simulations for the years 2010, 2011 and 2012.

The FDCs for the best runs are presented in Figure 5.8. The very low flow discharge shows an underestimation, the very high flow and high flow discharge show slight underestimation, the mid flow segment of the flow duration curve shows an overestimation in the part of lower than 50% exceedance probability.

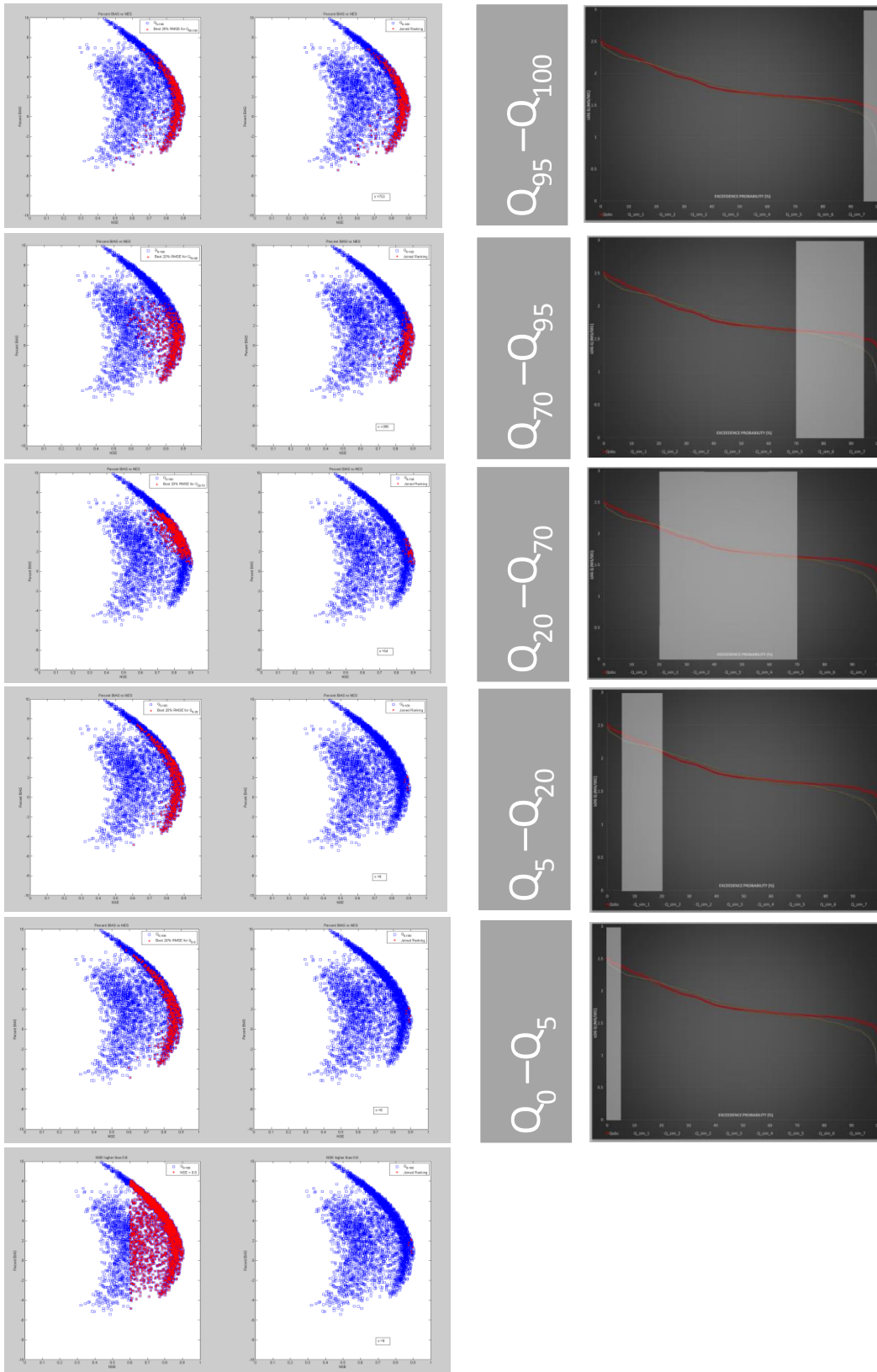


Figure 5-6 Stepwise evaluation of discharge calibration results.

Table 5-3 Model parameters obtained from best calibration results, and the statistical measures for the calibration

Cal. Run	CSF	DDF	Tr	Ts	Tmelt	L _{PRAT}	FC	BETA	K ₀	K ₁	K ₂	L _{SUZ}	C _{PERC}	B _{MAX}	C _{ROUTE}	VE	SOE	SUE	ME	Log ME
538	1.02	2.62	2	-2	0.42	0.0121	219	0.156	1.51	30	189	84.2	0.631	10	26.5	-0.051	3	0	0.744	0.72
1524	1.03	3.5	2	-2	0.92	0.0166	309	0.201	1.54	30	154	83.3	0.621	10	26.5	-0.037	3	0	0.799	0.74
1686	1.04	2.84	2	-2	0.92	0.0176	254	0.191	1.76	30	172	89.9	0.651	10	26.5	-0.0383	4	0	0.803	0.75
1860	1.04	3.18	2	-2	1.23	0.0251	144	0.191	1.63	30	167	85.7	0.871	10	26.5	-0.0205	7	0	0.775	0.745
2346	1.05	3.06	2	-2	0.42	0.0256	189	0.226	1.63	30	172	87.2	0.621	10	26.5	-0.0394	3	0	0.789	0.752
2706	1.06	2.74	2	-2	1.23	0.0156	204	0.156	1.7	30	192	89.3	0.771	10	26.5	-0.0134	9	0	0.785	0.74
2824	1.06	3	2	-2	-0.17	0.0261	154	0.211	1.98	30	151	88.7	0.651	10	26.5	-0.0273	2	0	0.752	0.74
3183	1.07	2.74	2	-2	-0.77	0.0146	209	0.181	1.55	29	171	90.5	0.601	10	26.5	-0.055	2	0	0.721	0.72
SCE	1.48	1.09	2	-2	-1.92	0.0179	230	0.300	0.81	29	109	97.84	0.982	10	26.5	0.001	18	0	0.842	0.76

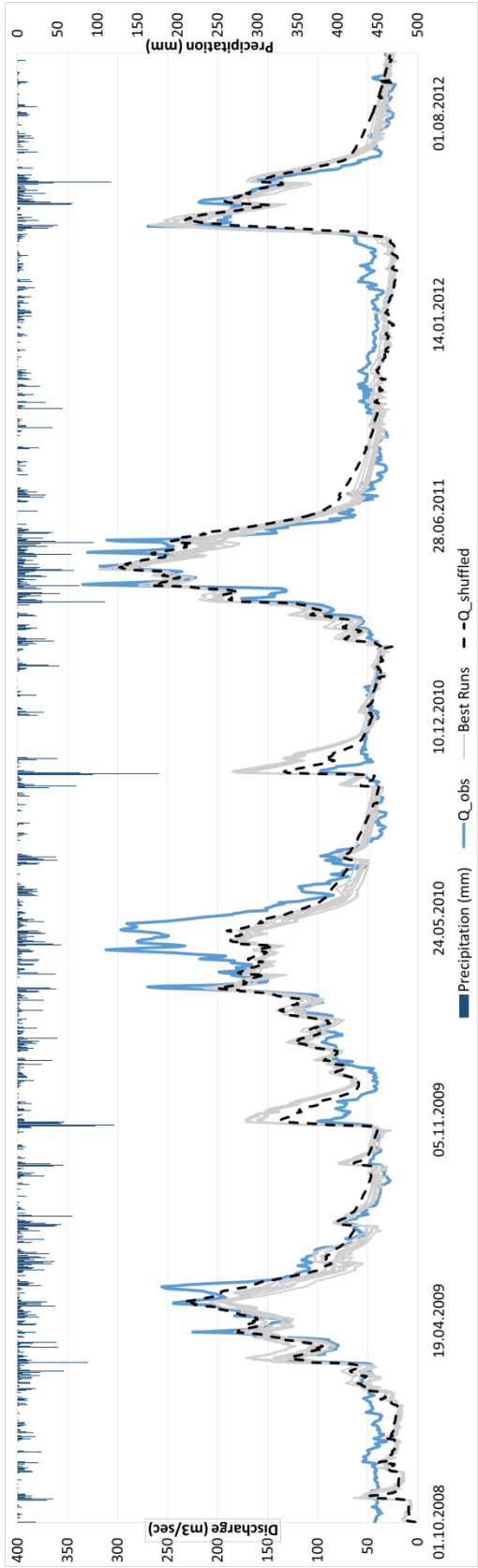


Figure 5-7 Observed (blue) and simulated (gray) discharge for 8 best runs, and calibration with SCE-UA (dashed black)

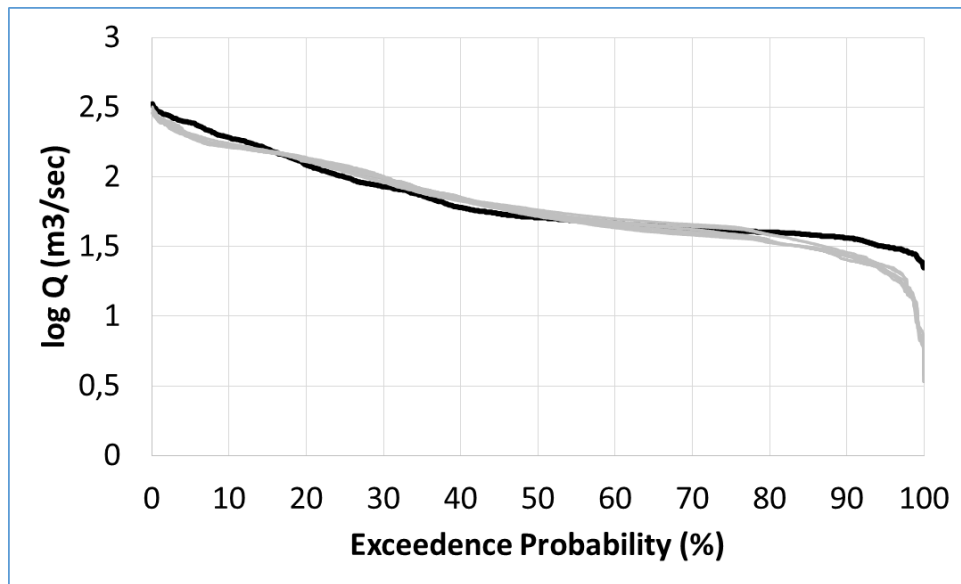


Figure 5-8 FDC of observed discharge (black), and the selected best calibration runs (gray)

5.2 Model Verification

The model parameters obtained from the calibration were used in the model verification. The validation was performed for the water year 2013. The results are presented in Table 5.4. The simulated runoff for the verification period is given in Figure 5.9. The best eight runs are shown in Figure 5.10. The simulated SWE values obtained from the model were compared with the snow cover area derived from H10 snow cover data in Figure 5.11, and Figure 5.12. The more scattering in SCA is seen for zone A. This zone has the lowest elevation and smallest area compared to the zones B, C and D. Due to the coarse spatial resolution of H10 snow product, SCA percentages show variations much in this zone. The melting time coincides with model simulated SWE and H10 SCA observations. In zone A melting starts at the end of January whereas usually it starts in February, in zone B the first melting occurs at the end of January due to the temperature rise above 0 °C on 27th January 2013, and then second melting starts at the end of February, in zone C and D at the end of March, in zone E at the end of April. Temperatures were increased quickly after 29th March 2013 in zone D, and the melting occurs very fast. In all the basins melting occurs in 7 or 10 days due to temperature increases where the change of temperature for verification period is given in Figure 5.13.

Table 5-4 Statistical measures for the validation period

	Runoff only	Runoff+H10
Volume error	0.144	0.187
ME	0.665	0.652
logME	0.615	0.40
Snow over estimation	1	0
Snow under estimation	0	0

Contributing the snow cover in calibration does not provide too much improvement in runoff simulations. The most noticeable differences between the multiple-objective and single-objective snow model performance are the decrease in the snow overestimation errors.

H13 SWE data were also used to make a comparison between the model simulated SWE and SWE retrieved from satellite data. The comparisons indicate that H13 product overestimate the SWE compared to model simulated SWE values. This results supports the findings in the literature (Pulliainen and Hallikainen., 2001).

The quality of SWE data is often not good enough for use in hydrology, large errors are found in microwave estimates compared with measurements. In zone A maximum SWE obtained from H13 is 159 mm and it is occurred on March 6, 2013 whereas model gives maximum SWE as 58 mm on January 15, 2013. In zone B maximum SWE obtained from H13 is 183 mm and it is occurred on March 8, 2013 whereas model gives maximum SWE as 56 mm on January 22, 2013. In zone C maximum SWE obtained from H13 is 183 mm and it is occurred on March 8, 2013 whereas model gives maximum SWE as 87 mm on March 8, 2013. In zone D maximum SWE obtained from H13 is 176 mm and it is occurred on March 8, 2013 whereas model gives maximum SWE as 165 mm on March 26, 2013. In zone E maximum SWE obtained from H13 is 151 mm and it is occurred on March 10, 2013 whereas model gives max SWE as 253 mm on March 30, 2013.

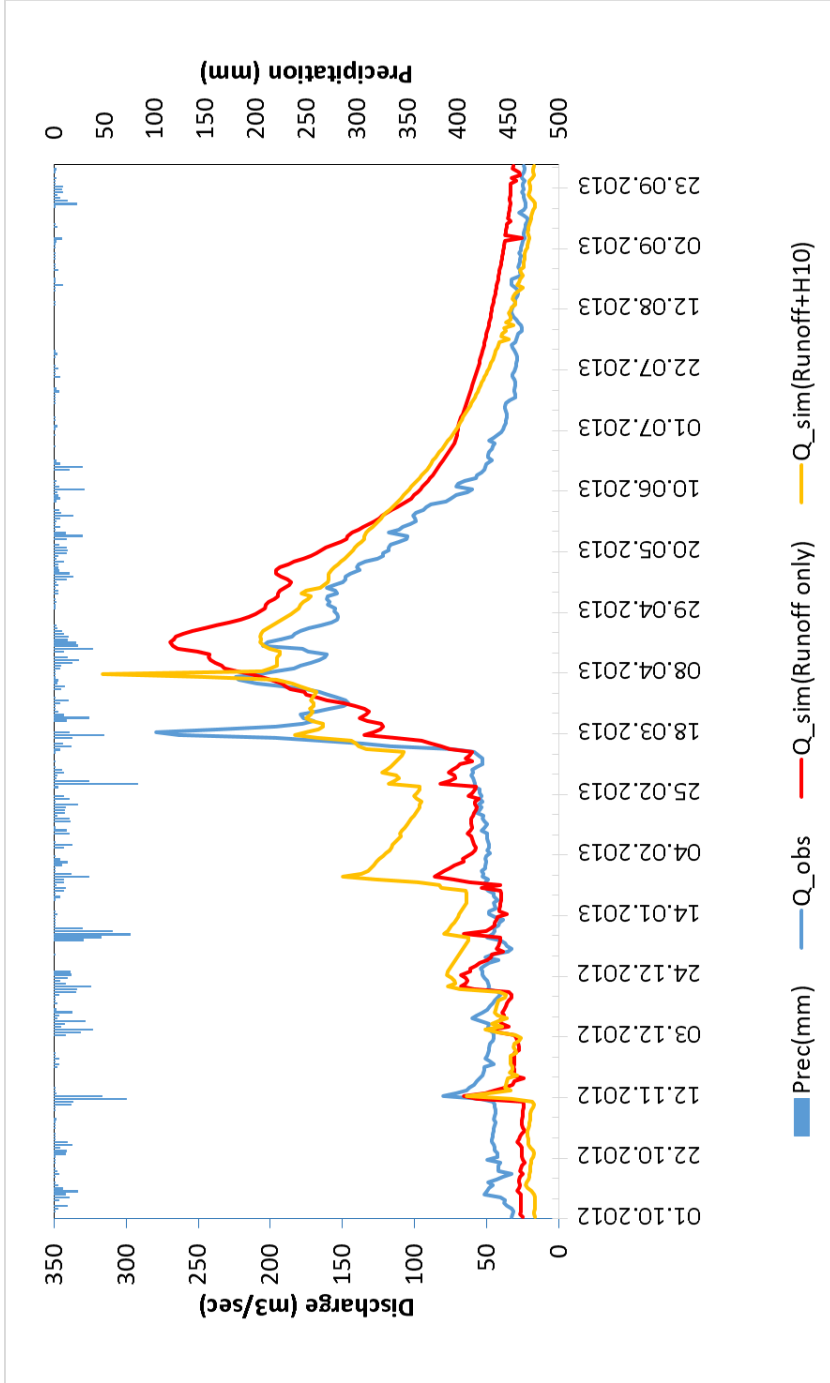


Figure 5-9 Runoff simulation for the verification period for runoff only, and runoff and H10

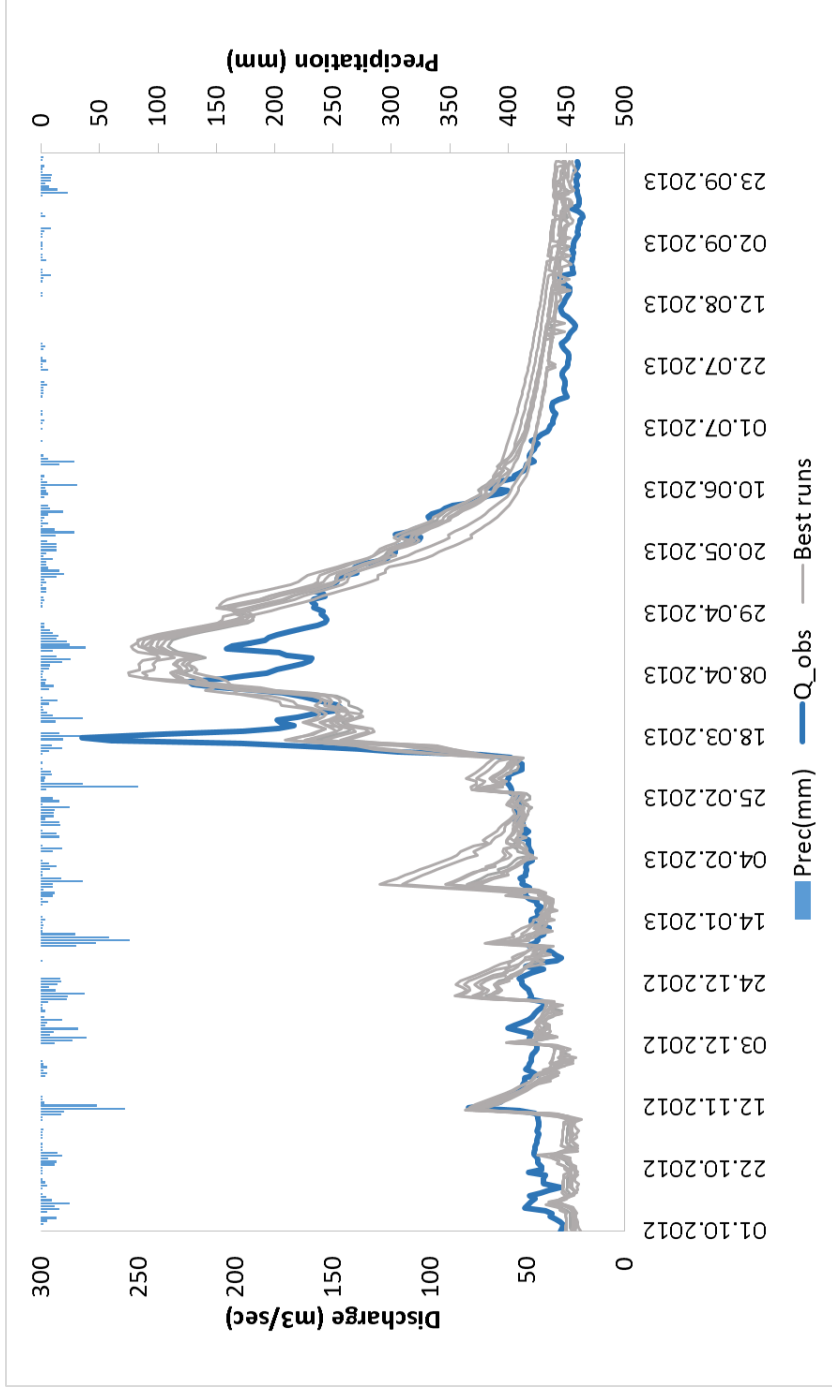


Figure 5-10 Eight best runs vs. runoff simulation for the verification period

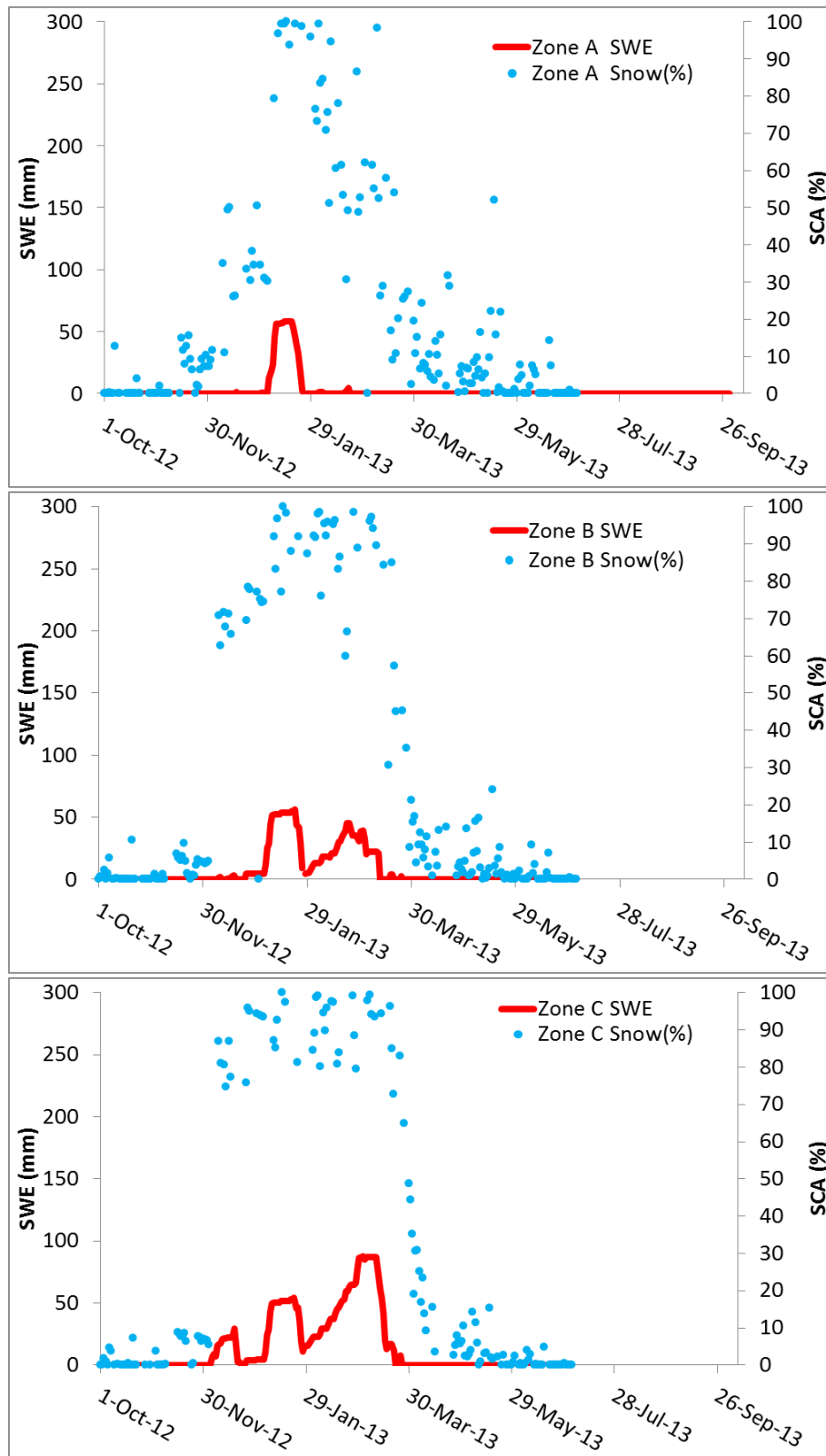


Figure 5-11 Simulated SWE, and SCA (from H10) for elevation zones A, B, C

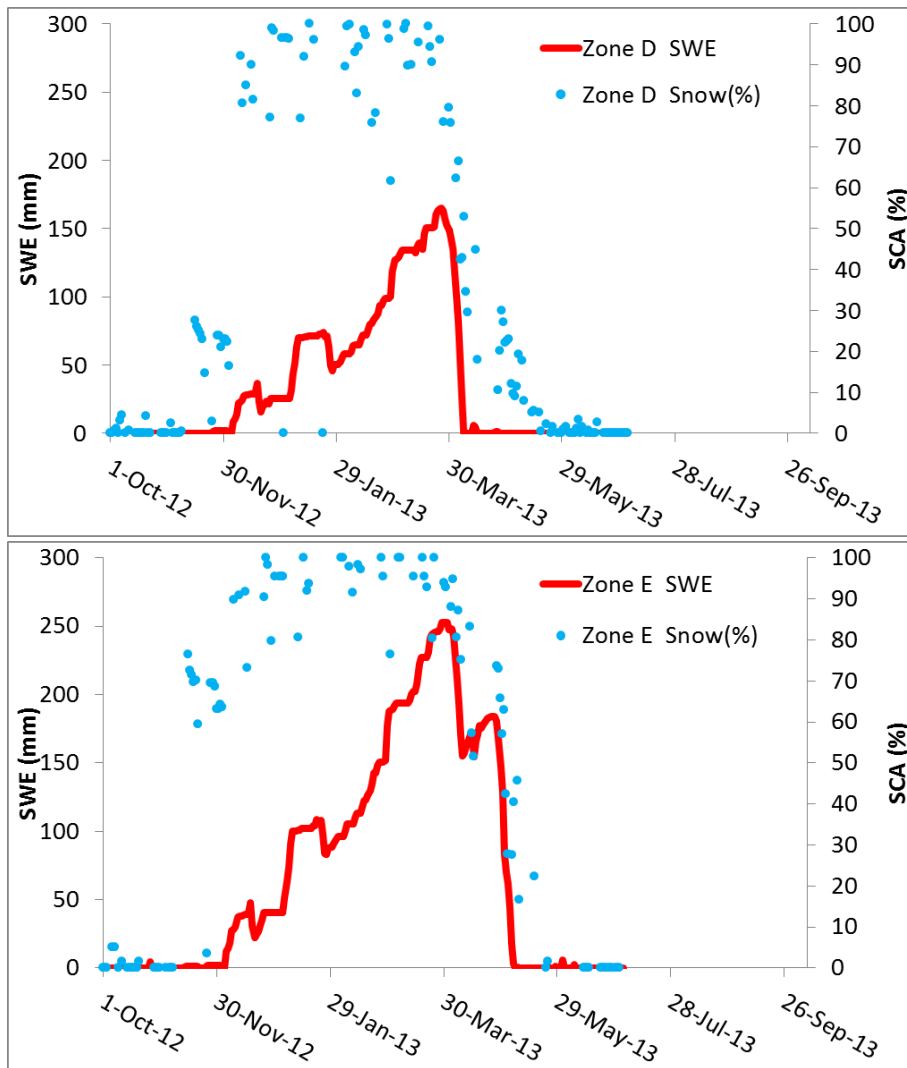


Figure 5-12 Simulated SWE, and SCA (from H10) for elevation zones D, E

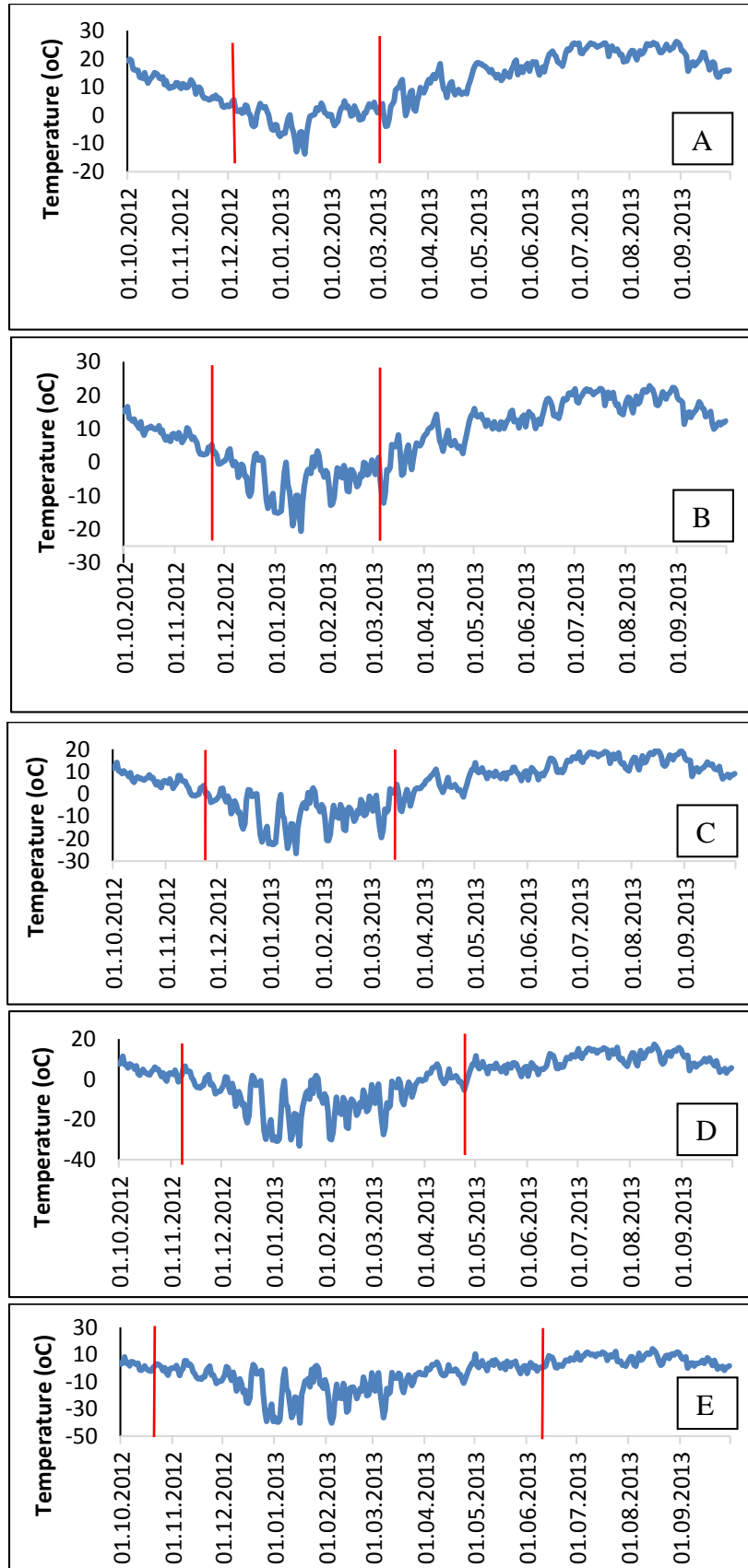


Figure 5-13 Temperature distribution for elevation zones A, B, C, D, E for water year 2013 (red lines indicate the border where the temperatures are lower than 0 °C).

5.3 Discussion of the Results

The accuracy of H10 product is evaluated in Chapter 3. This product is created by using 32 consecutive images per day from SEVIRI sensor of MSG satellite. The use of multiple images per day in optical spectrum enhances the chance of reducing quick moving phenomena such as cloud contamination before stepping towards snow mapping. This type of merging satellite imagery provided to make significant cloud reduction over Austria, and Turkey. Mean annual ratio of cloud coverage is around 30% for H10 product, which is more than 20% lower than snow products that are generated using MODIS data. A disadvantage of H10 product can be its rather low spatial resolution as 5 km over European domain. Despite the coarser spatial resolution of H10, the overall mapping accuracy is moderately higher. The average accuracy for cloud-free days is 89 %, which is 5% lower than obtained by the MODIS-combined product, but similar to that obtained by land-surface (JULES) model simulations driven by a regional climate model HadRM3-P (Parajka et al., 2010). The overall accuracy also relates well with the hit rate measure of Surer and Akyurek (2012), which is in between 68 and 81% in winter. The accuracy with respect to all weather conditions (in all weather conditions assessments the pixels with clouds are considered as mapping errors) is, however, about 3–4% better than the one which is obtained by MODIS product. The higher frequency of information about SCA, even for lower spatial resolution, indicates the potential of H10 for using in operational assimilation into hydrologic models.

The mapping error analysis shows that H10 has a tendency to underestimate SCA, especially in flat regions. High mapping errors are observed over Alpine territory due to high elevation variation and quick changes in SCA. The highest errors are observed to be resulted from the stations that are located at an elevation which has high altitude difference between the mean elevations of the H10 pixel. This type of mapping errors also indicates the need to find a better way of validating such satellite products having lower spatial resolution, instead of using ground measurements having low representativeness of the matching pixel.

In order to tackle with this kind of scaling problems between pixel size of the satellite product and ground measurement, different threshold values to accept

ground as snow covered has been utilized (Blöschl et al., 1991; Blöschl, 1999; Skøien et al., 2006). Simic et al. (2004) studied the sensitivity of the mapping accuracy to the reference threshold of 1 cm, and 3 cm. They found that the difference is small, ranging approximately between -2 and 4 %. In this study, a 1 cm threshold is used in order to be consistent and comparable with other studies performed in Austria.

The snow detection algorithms for H10 and MODIS snow products show resemblance in many ways. The metrics used as NDSI, and SI shows a close relationship (Surer and Akyurek, 2012). The selected SI threshold value of 0.6 for the snow-cover area retrieval corresponds to 0.2 for the NDSI value. For the MODIS products the NDSI value for 50% snow-covered areas is taken as 0.4 (Dozier, 1989; Hall et al., 2002). The aim of selecting SI as 0.6 is to include the partial snow-covered areas in the retrieval of H10 product. This small difference is resulting from lower spatial resolution of H10.

The outcomes of this work presents the importance of using satellite imagery driven snow information in hydrological and climatological studies by relating spatial and temporal resolution criteria. The H10 and MODIS products generally show a good agreement on overall comparison. H10 product has higher under and overestimation errors when compared to MODIS product. Especially, over mountainous regions these errors increase mainly due to high elevation variation and hardness to reflect the changes in rather coarse spatial resolution. Spring and summer periods are the ones that higher errors are observed for both of the products.

Besides the spatial resolution affecting the snow mapping accuracy, the difference in the viewing geometries of two sensors may have an effect on the snow mapping. The influence of the changing MODIS view zenith angles on snow mapping algorithm must be investigated in detail, since this factor can be one of the sources of error in snow mapping. As view zenith angle increases, it is known that NDSI decreases (Xin et al., 2012). Since MODIS observes the surfaces at a much smaller view zenith angle (VZA) than the H10, it may detect more snow cover area. That may be another reason to observe large underestimation errors for H10 compared to MODIS in winter months. The narrow band width in the Green and Middle Infrared portion of the electromagnetic spectrum of MODIS may create a possibility to detect more

SCA compared to H10. The overestimation for spring months is due to the high percentage of fractional snow cover due to melting in these months. The algorithm of H10 tends to find more snow over fractional SCAs. Neither the effect of complex topography, nor the shadows were held in the H10 snow mapping algorithm. Therefore the H10 generation algorithm can be modified with the use of a proper Digital Elevation Model (DEM) in order to correct the topography effect. Better snow cover information can be retrieved by using H10, and MODIS snow products together. The cloud-contaminated MODIS snow pixels can be reclassified according to the values observed from the H10 product.

The validation of microwave H13 products at the selected climate stations indicates noticeable underestimation of H13 in comparison to observed snow cover and snow depth observations. Underestimation is more significant in the mountains than in the flatland regions, so more effort is needed to capture representative snow water equivalent at the regional scale. In the future, it is important to account for the sub-grid variability of snow characteristics and to improve the SWE estimation of larger snow packs. Besides the importance of spatial resolution of snow products, a better temporal resolution helps to increase the cloud/snow discrimination, which is very important for the use of satellite snow products in further analysis.

The sensitivity analysis of HBV model parameters were analyzed in Chapter 4. HBV model was calibrated to runoff alone and after finding the optimized values of 15 parameters, 14 were kept at their optimum values and the remaining one was changed within the limits available in the literature. Within the domain of the parameter the model performance was tested by using statistical measures indicating the sensitivity of the parameters to volume error, timing of the discharge series and simulation of peak discharges; percent bias, RMSE, NSE, and correlation coefficient. FDCs segmented into different flow parts were also used to find out the sensitivity of the parameters to hydrological measures. In general L_{PRAT} , FC and BETA as soil parameters and DDF and CSF as snow parameter control the volume error, L_{SUZ} , K_0 , K_1 directly and C_{PERC} and K_2 indirectly control the high flow series and timing of the flow, T_{melt} controls the maximum flow series. L_{SUZ} , K_0 , K_1 , K_2 , and FC control the very low flows. B_{MAX} , C_{ROUTE} , T_{rain} , T_{snow} are found as insensitive for this catchment.

Two approaches were used in the calibration stage. In the first one an optimization method namely SCE-UA algorithm was used for the calibration of 11 parameters to runoff only and to runoff and H10 snow product. The calibrated parameters do not show too much difference between the ones calibrated to runoff only and the ones calibrated to runoff and H10, except DDF, K_0 , K_2 , L_{SUZ} and C_{PERC} . It indicates that including snow product affects the structure of snow routine, very fast storage and slow storage of the model. Though a slight decrease in the statistical measures testing the performance of the model calibration was observed, the most noticeable differences between the calibration to runoff and H10 and calibration to runoff only are the decrease in the snow overestimation. This indicates that constraining the model parameter estimation to runoff and H10 snow cover provides in general more robust parameter sets than parameter optimization based on the runoff data only. During the sensitivity analysis of thresholds ζ_{SCA} and ζ_{SWE} snow simulations are obtained by single-objective calibration to the measured runoff only. $\zeta_{SCA}=25\%$ and $\zeta_{SWE}=0$ were selected for the study. Sensitivity of the runoff model efficiency and snow cover error to the weight w_s indicates 0.9 for w_s as the trade-off between the runoff and snow objectives.

In the second approach the calibration of the model was performed by using hydrological measures. In order to assess different phases of the hydrograph, FDCs were used. They were segmented into five different parts indicating very high, high, middle, low and very low flows. The segmented FDC were used as the hydrological metric to define the performance of the model for low flows, midrange flows and long term water balance. The NSE, PBIAS, and RMSE of the different parts of the flow on FDC were used in the evaluation of the calibration process. Using multiple performance metrics in discharge calibration is a key to accounting for different discharge events. Independent ranking of several performance metrics, followed by a threshold selection, showed characteristic distribution patterns by combining the NSE and PBIAS. NSE and PBIAS metrics indicate the error in high flow simulations and volume error. 20% of the best runs giving high NSE and PBIAS were intersected with the runs give low RMSE for different parts of the FDC. Among the flow parts in the FDC, the highest RMSE values were obtained for the very low flow parts. This is due to the structure of the baseflow part of HBV model.

The conceptual model of low storages in the model and the parameters used to model the low storage are not sufficient to model the real process. The minimum RMSE were obtained for the mid. flow part of the FDC. The very high flow simulations are also comparatively good. These results are matching up with the findings of Pfannerstill et al. (2014). L_{PRAT} , $BETA$, K_0 , K_1 , L_{SUZ} and C_{PERC} do not show too much variation among these best run values, but DDF , T_{melt} , FC , K_2 show variation. The very low flow discharge shows an underestimation, the very high flow and high flow discharge show slight underestimation, the mid flow segment of the flow duration curve shows an overestimation in the part of lower than 50% exceedance probability. When the best run values are compared with the ones obtained by SCE-UA, L_{PRAT} and K_1 values are close to the values obtained by SCE-UA, and the other parameter values show some variation. The precision of the parameters obtained by Shuffle Complex method is higher than the precision of the parameters obtained through joint ranking method. Different parameter sets may result in similar prediction which is known as the phenomenon of equifinality (Beven and Binley,1992). The so-called equifinality showed there is no unique parameter estimation. This may be due to the fact that parameters obtained from calibration were affected by several factors such as correlations amongst parameters, sensitivity or insensitivity in parameters, spatial and temporal scales and statistical features of model residuals (Wagener et al., 2003; Wagener and Kollat, 2007).

The overlay of the selected calibration runs resulted in small discharge band, because all the simulated discharges are similar. All simulation runs tend to over predict high peak events of the hydrograph occurs due to rainfall only. The low flow and recession events are predicted satisfactorily for recession in 2011 and 2012. The hydrograph simulations using SCE-UA also overlay with the best run hydrograph simulations. The early peaks due to snow melting of the hydrograph are simulated better for the best run simulations for the years 2010, 2011 and 2012. During the verification, the model performance is lower than the model performance in the calibration period. The statistical measures for the verification to runoff only and the verification to runoff and H10 are obtained as 0.665 for runoff only and 0.652 for runoff and H10.

During calibration period none of the hydrographs simulated the observed hydrograph well during 19.April.2010 and 17.May.2010. In that period the temperatures were higher than 0 °C at all the elevation zones and the precipitation occurred during this time is in form of rainfall. Therefore rain on snow problem happened during that time period which led to melting of the snow due to rainfall event and the hydrological models still have problems in modelling the rain on snow problem properly.

For 2013, SWE values obtained from the model simulations show early melting and then another snow accumulation in zones B and C. This indicates temperatures are getting higher during winter months and even the elevations 2000 m are affected from the changes in temperature. This finding is very important for water resources management issues. From the ground observations snow on the ground was observed between 10.12.2008 and 29.03.2009 for water year 2009 and average snow depth was observed as 9.11 cm, for water year 2010 it was observed between 01.11.2009 and 31.03.2009 where the average snow depth was observed as 8.07 cm. For water year 2011, the snow season was between 13.12.2010 and 16.04.2011 where the average snow depth was observed as 5.90 cm. For water year 2012 the snow season was observed between 11.11.2011 and 25.03.2012 and the measured average snow depth was 16.50 cm. For water year 2013 the snow season was observed between 05.12.2012 and 22.03.2013 and the average snow depth was measured as 23.38 cm. The observations from ground stations also show that for water year 2013 there was an early melting occurrence in the basin.

CHAPTER 6

CONCLUSIONS AND RECOMMENDATIONS

Satellite snow products are valuable data sources for hydrological studies. The spatial resolution and sub-grid topographical variability for the use of satellite snow cover images in hydrological applications or climatological studies affect the results. Better temporal resolution of satellite data namely MSG-SEVIRI provides an improvement in classification accuracy of the snow products. It can be considered as an alternative for cloud clearance studies. It can be investigated to merge two different satellite imagery source; one having better spatial resolution (MODIS), and the other one having higher temporal resolution (SEVIRI), as a future work.

Including the H10 snow cover data in calibration does not improve the runoff simulations a lot, but improve the snow cover area estimation. The volume error is obtained as 0.84 for the calibration that only use runoff , and 0.76 for calibration that utilized runoff and H10 snow product at the same time. The indirect comparison of model state variable (snow water equivalent) with the snow cover area percentages show that model simulations of SWE coincides well with the snow cover area obtained from H10 snow product.

The simulated hydrographs obtained by using the parameter sets calibrated through joint ranking and SCE-UA methods do not show too much difference. The snow over estimation values obtained from joint ranking method is lower than the one obtained from SCE-UA calibration method.

Only using H10 snow cover data do not give good simulation results and the parameters obtained from this calibration are completely different than the parameters obtained from the calibration to runoff and H10 snow product. The larger frequency of snow cover information, even for coarse resolution, indicates the

potential of H10 for operational assimilation into hydrologic models. The accuracy of the H13 snow product is not sufficient yet to be included in the hydrological models.

Multi-metric evaluation in the calibration stage do not improve the results too much for this basin but it helped to analyze the parameter set giving similar discharge simulations. In addition, it also improved snow cover representation in the model by increasing consistency of snow presence detection. The analysis highlights the concept of equifinality and the need of studies on parameter uncertainty of HBV model in this basin. It could be inferred that the identifiability of an optimal parameter obtained from calibration should also be evaluated. For an already gauged catchment, a virtual study can provide a point of reference for the minimum uncertainty associated with a model application. Monitoring task for several important physical parameters to determine more credible results for watershed management is crucial.

More detailed measurement data and more precipitation stations should be established in the future for hydrological modeling in Karasu Basin. In addition, further studies should be continued in the field of model structure and input to quantify hydrological model uncertainty.

REFERENCES

- Abbott, M.B., Bathurst, J.C., Cunge, J.A., O'Connell, P.E., and Rasmussen, J., (1986a). An introduction to the European Hydrological Systems-Systeme Hydrologique Europeen, 'SHE'. 1. History and philosophy of a physically based distributed modelling system. *Journal of Hydrology* 87:45–59.
- Abbott, M.B., Bathurst, J.C., Cunge, J.A., O'Connell, P.E., and Rasmussen, J., (1986b). An introduction to the European Hydrological Systems-Systeme Hydrologique Europeen, 'SHE'. 2. Structure of a physically based distributed modelling system. *Journal of Hydrology* 87:61–77.
- Abebe A.N., Ogden F.L., and Pradhan N. R., (2010). Sensitivity and uncertainty analysis of the conceptual HBV rainfall-runoff model: Implications for parameter estimation. *Journal of Hydrology*, 389, 301-310.
- Aminou, D.M.A., (2002). MSG's SEVIRI instrument. *ESA Bulletin*(0376-4265), (111), 15-17.
- Andreadis, K.M., and Lettenmaier D.P., (2006). Assimilating remotely sensed snow observations into a macroscale hydrology model, *Advances in Water Resources*, Volume 29, Issue 6, June 2006, Pages 872-886.
- Andreassen, L.M. (2007). Improving runoff modelling using satellite-derived snow covered area. *Nordic Hydrology*, 38(1), 21-32.
- Ault, T.W., Czajkowski, K.P., Coss, B.T., Struble J., Spongberg A., Templin, M., and Gross C., (2006). Validation of the MODIS snow product and cloud mask using student and NWS cooperative station observations in the Lower Great Lakes Region. *Remote Sensing of Environment*, Volume 105, Issue 4, 30 December 2006, Pages 341–353.

Bavera, D., and De Michele, C., (2009). Snow water equivalent estimation in the Mallero basin using snow gauge data and MODIS images and fieldwork validation. *Hydrol. Process.*, 23: 1961–1972.

Beckers, J., and Alila, Y., (2004). A model of rapid preferential hillslope runoff contributions to peak flow generation in a temperate rain forest watershed. *Water Resources Research* 40, W03501.

Bergström, S., (1976). Development and application of a conceptual runoff model for Scandinavian catchments. Ph.D. Thesis. SMHI Reports RHO No. 7, Norrköping.

Bergström, S., (1992). The HBV model - its structure and applications. SMHI Reports RH, No. 4, Norrköping.

Bergström, S., Harlin, J., and Lindström, G., (1992). Spillway design floods in Sweden. I: New guidelines. *Hydrological Sciences Journal*, Vol. 37, No. 5, pp. 505-519.

Bertalanffy, V.L., (1950). The theory of open systems in physics and biology. *Science*, 111(2872), 23-29.

Bertrand, C., Gonzalez, L., Ipe, A., Clerbaux, N., and Dewitte, S., (2008). Improvement in the GERB short wave flux estimations over snow covered surfaces. *Advances in Space Research*, 41(11), 1894-1905.

Beşer, Ö., (2011). PhD Thesis: Determination of Snow Water Equivalent Over Eastern Part of Turkey Using Passive Microwave Data.

Beven, K., (2006). A manifesto for the equifinality thesis. *Journal of hydrology*, 320(1), 18-36.

Beven, K., and Binley, A., (1992). The future of distributed models: model calibration and uncertainty prediction, *Hydrol. Process.*, 6, 279–298.

Beven, K., and Freer, J., (2001). Equifinality, data assimilation, and uncertainty estimation in mechanistic modelling of complex environmental systems using the GLUE methodology. *Journal of hydrology*, 249(1), 11-29.

Blaney, H.F., and Criddle, W.D., (1962). Determining consumptive use and irrigation water requirements. No. 1275. US Department of Agriculture.

Blöschl, G., Gutknecht, D., and Kirnbauer, R., (1991). Distributed snowmelt simulations in an alpine catchment: 2. Parameter study and model predictions. *Water Resources Research*, 27(12), 3181-3188.

Blöschl, G., Kirnbauer, R., and Gutknecht, D., (1991). Distributed snowmelt simulations in an alpine catchment: 1. Model evaluation on the basis of snow cover patterns. *Water Resources Research*, 27(12), 3171-3179.

Brandt, M., Jutman, T., and Alexandersson, H., (1994). Sveriges Vattenbalans. Årsmedelvärden 1961-1990 av nederbörd, avdunstning och avrinning. SMHI Hydrologi, nr 49, Norrköping.

Brasnett, B., (1999). A global analysis of snow depth for numerical weather prediction. *J Appl Meteorol*;38:726-40.

Carroll, T., Cline, D., Fall, G., Nilsson, A., Li, L., and Rost, A., (2001). NOHRSC operations and the simulation of snow cover properties for the coterminous US. In 69th Annual Meeting of the Western Snow Conference, Sun Valley, Idaho (pp. 16-19).

Cermak, J., and Bendix, J., (2008). A novel approach to fog/low stratus detection using Meteosat 8 data. *Atmospheric Research*, 87(3-4), 279-292.

Clark, M.P., Slater, A.G., Barrett, A.P., Hay, L.E., McCabe, G.J., Rajagopalan, B. and Leavesley, G.H., (2006). Assimilation of snow covered area information into hydrologic and land-surface models, *Advances in Water Resources* 29(8), 1209-1221.

Cline, D.W., Bales, R.C., and Dozier, J., (1998). Estimating the spatial distribution of snow in mountain basins using remote sensing and energy balance modeling. *Water Resources Research*, 34 (5), 1275-1285.

Derksen, C.P., Walker, A.E., and Goodison, B.E., (2003). A comparison of 18 winter seasons of in situ and passive microwave-derived snow water equivalent estimates in Western Canada, *Remote Sensing of Environment* 88(3), 271-282.

Doten, C.O., Bowling, L.C., Lanini, J.S., Maurer, E.P., and Lettenmaier, D.P., (2006). A spatially distributed model for the dynamic prediction of sediment erosion and transport in mountainous forested watersheds. *Water Resources Research* 42, W04417.

Dressler, K.A., Leavesley, G.H., Bales, R.C. and Fassnacht, S.R., (2006). Evaluation of gridded snow water equivalent and satellite snow cover products for mountain basins in a hydrologic model, *Hydrological Processes* 20(4), 673– 688.

Driessen, T. L. A., Hurkmans, R. T. W. L., Terink, W., Hazenberg, P., Torfs, P. J. J. F., and Uijlenhoet, R., (2010). The hydrological response of the Ourthe catchment to climate change as modelled by the HBV model. *Hydrology and Earth System Sciences*, 14(4), 651-665.

Duan, Q., Sorooshian, S., and Gupta, V., (1992). Effective and efficient global optimization for conceptual rainfall-runoff models. *Water resources research*, 28(4), 1015-1031.

Duan, Q., Sorooshian, S., and Gupta, V.K., (1994). Optimal use of the SCE-UA global optimization method for calibrating watershed models. *Journal of hydrology*, 158(3), 265-284.

Franz, K.J., and Karsten, L.R., (2013). Calibration of a distributed snow model using MODIS snow covered area data. *Journal of Hydrology*, 494, 160-175.

Gafurov, A., and Bárdossy, A., (2009). Cloud removal methodology from MODIS snow cover product. *Hydrology and Earth System Sciences*, 13(7), 1361-1373.

Georgievsky M.V., (2009). Application of the Snowmelt Runoff model in the Kuban river basin using MODIS satellite images. *Environ. Res. Lett.* 4 045017.

Gupta, H.V., Sorooshian, S., and Yapo, P.O., (1998). Toward improved calibration of hydrological models: multiple and noncommensurable measures of information. *Water Resour. Res.* 34(4), 751-763.

Gupta, H.V., Wagener, T., and Liu, Y., (2008). Reconciling theory with observations: elements of a diagnostic approach to model evaluation. *Hydrol. Process.* 22(18), 3802-3813.

- Hall, D.K., Riggs, G.A., Salomonson, V.V., DiGirolamo, N.E., and Bayr, K.J., (2002). MODIS snow-cover products. *Remote sensing of Environment*, 83(1), 181-194.
- Hall, D.K. and Riggs, G.A., (2007). Accuracy assessment of the MODIS snow-cover products. *Hydrological Processes*, 21, 1534–1547.
- Harrison, A.R., and Lucas, R.M., (1989). Multi-spectral classification of snow using AVHRR imagery. *International Journal of Remote Sensing*, 10 (4–5), 907–916.
- HSAF-PUM, (2013). <http://hsaf.meteoam.it/snow.php> (last visited Jan 28,2015).
- Hornberger, G.M., and Spear, R.C., (1981). An approach to the preliminary analysis of environmental systems. *J. Environ. Manage.*, 12, 7–18.
- Houser, P.R., Shuttleworth, W.J., Famiglietti, J.S., Gupta, H.V., Syed, K.H., Goodrich, D.C., (1998). Integration of soil moisture remote sensing and hydrologic modeling using data assimilation. *Water Resour Research*, 34:3405–20.
- Jutman, T., (1992). Production of a new runoff map of Sweden. *Nordic hydrological Conference, Alta, Norway, NHP report No. 30.* pp 643-651.
- Kolberg, S.A., and Gottschalk, L., (2006). Updating of snow depletion curve with remote sensing data, *Hydrological Processes* 20 (11), 2363–2380.
- Konz, M., Finger, D., Buergi, C., Normand, S., Immerzeel, W.W., Merz, J., and Burlando, P., (2010). Calibration of a distributed hydrological model for simulations of remote glacierised Himalayan catchments using MODIS snow cover data. *Global Change: Facing Risks and Threats to Water Resources*, 465-473.
- Kristensen, K.J., and S.E. Jensen., (1975). A model for estimating actual evapotranspiration from potential transpiration. *Nordic Hydrology*, 6:170–188.
- Lahtinen, P., Erturk, A. G., Pulliainen, J., and Koskinen, J., (2009). Merging flat/forest and mountainous snow products for extended European area. In *Geoscience and Remote Sensing Symposium, 2009 IEEE International, IGARSS (Vol. 2, pp. II-563).* IEEE.

Lindström, G., (1997). A Simple Automatic Calibration Routine for the HBV Model. *Nordic Hydrology*, 28 (3), 153–168.

Liston, G.E., Pielke, R.A., and Greene, E.M. (1999). Improving first-order snow-related deficiencies in a regional climate model. *Journal of Geophysical Research: Atmospheres* (1984–2012), 104(D16), 19559-19567.

López-Burgos, V., Gupta, H.V., and Clark, M. (2013). Reducing cloud obscuration of MODIS snow cover area products by combining spatio-temporal techniques with a probability of snow approach. *Hydrology and Earth System Sciences*, 17(5), 1809-1823.

Madsen, H., Wilson, G., and Ammentorp, H.C., (2002). Comparison of different automated strategies for calibration of rainfall-runoff models. *Journal of Hydrology*. 261 (1), 48-59.

Martinec J., (1975). Snowmelt-runoff model for stream flow forecasts. *Nordic Hydrology* 6(3).

Mayr, E., Hagg, W., Mayer, C., and Braun, L., (2013). Calibrating a spatially distributed conceptual hydrological model using runoff, annual mass balance and winter mass balance, *J. Hydrol.*, 478, 40–49, doi:10.1016/j.jhydrol.2012.11.035.

NWCSAF, (2007). Product User Manual for "Cloud Products", <http://www.nwcsaf.org/HD/MainNS.jsp> , last visited on January 2015.

Nagler, T., Rott, H., Malcher, P., and Müller, F., (2008). Assimilation of meteorological and remote sensing data for snowmelt runoff forecasting. *Remote sensing of environment*, 112(4), 1408-1420.

Nester, T., Kirnbauer, R., Parajka, J., and Blöschl, G., (2012). Evaluating the snow component of a flood forecasting model. *Hydrology Research*, 43(6), 762.

Painter, T.H., Dozier, J., Roberts, D.A., Davis, R.E., and Green, R.O., (2003). Retrieval of subpixel snow-covered area and grain size from imaging spectrometer data. *Remote Sensing of Environment*, 85(1), 64-77.

Parajka, J., and Blöschl, G., (2006). Validation of MODIS snow cover images over Austria. *Hydrology and Earth System Sciences*, 10, 679–689.

Parajka, J., and Blöschl, G., (2008). Spatio-temporal combination of MODIS images-potential for snow cover mapping. *Water Resources Research*, 44, W03406.

Parajka, J., and Blöschl, G., (2012). MODIS-based snow cover products: validation, and hydrologic applications, Chapter 9. In: Ni-Bin Chang, ed. *Multiscale hydrologic remote sensing: perspectives and applications*. Boca Raton, FL: CRC Press.

Parajka, J., Dadson, S., Lafon, T., and Essery, R., (2010). Evaluation of snow cover and depth simulated by a land surface model using detailed regional snow observations from Austria, *J. Geophys. Res.*, 115, D24117, doi:10.1029/2010JD014086.

Pfannerstill, M., Guse, B., and Fohrer, N., (2014). Smart low flow signature metrics for an improved overall performance evaluation of hydrological models. *Journal of Hydrology*, 510, 447-458.

Pulliainen J., and Hallikainen M., (2001) Retrieval of Regional Snow Water Equivalent from Space-Borne Passive Microwave Observations, *Remote Sensing of Environment*, Volume 75, Issue 1, Pages 76-85.

Reichle R.H., Entekhabi D., and McLaughlin D.B., (2001). Downscaling of radiobrightness measurements for soil moisture estimation: a four-dimensional variational data assimilation approach. *Water Resour Res* 2001;37:2353–64.

Rientjes, T.H.M., Haile, A.T., and Fenta, A.A., (2013) Diurnal rainfall variability over the Upper Blue Nile Basin : a remote sensing based approach. In: *International Journal of Applied Earth Observation and Geoinformation : JAG*, 21 (2013) pp. 311-325.

Rodell M., and Houser P. R., (2004). Updating a land surface model with MODIS derived snow cover *Journal of Hydrometeorology*, 5 (6), pp. 1064–1075.

Rodell, M.M., Houser, P.R., Jambor, U.U., Gottschalck, J.J., Mitchell, K.K., Meng, C.J., and Toll, D.D., (2004). The Global Land Data Assimilation System. *Bulletin Of The American Meteorological Society*, 85(3), 381-394.

Roy, V., Goïta K., Royer A., Walker A.E., and Goodison B.E., (2004). Snow water equivalent retrieval in a Canadian boreal environment from microwave measurements using the TKK snow emission model, *IEEE Transaction .Geoscience RemoteSensing.*, 42(9), pp. 1850–1859.

Sawicz, K., Wagener, T., Sivapalan, M., Troch, P.A., and Carrillo, G., (2011). Catchment classification: empirical analysis of hydrologic similarity based on catchment function in the eastern USA. *Hydrology and Earth System Sciences*, 15(9), 2895-2911.

Schmugge, T.J., Kustas, W.P., Ritchie, J.C., Jackson, T.J., and Rango, A., (2002). Remote sensing in hydrology. *Advances in water resources*, 25(8), 1367-1385.

Siljamo, N., and Hyvärinen, O., (2011). New geostationary satellite-based snow-cover algorithm. *Journal of Applied Meteorology and Climatology*, 50.6, 1275-1290.

Skaugen, T., and Onof, C., (2014). A rainfall-runoff model parameterized from GIS and runoff data, *Hydrological Processes*, Wiley Online Library.

Skøien, J.O., Merz, R., and Blöschl, G., (2006). Top-kriging - geostatistics on stream networks, *Hydrology and Earth System Sciences*, 10, 277–287, doi:10.5194/hess-10-277-2006.

Şorman, A.A., Şensoy, A., Tekeli, A.E., Şorman, A.Ü., and Akyürek, Z., (2009). Modelling and forecasting snowmelt runoff process using the HBV model in the eastern part of Turkey. *Hydrological processes*, 23(7), 1031-1040.

Su, H., Yang, Z.-L., Niu, G.Y., and Dickinson, R.E., (2008) Enhancing the estimation of continentalscale snow water equivalent by assimilating MODIS snow cover with the ensemble Kalman filter, *J. Geophys. Res.*, 113, doi:10.1029/2007JD009232,. 1331, 1333, 1338.

Sun, C., Walker J.P., and Houser P.R., (2004). A methodology for snow data assimilation in a land surface model. *J Geophys Res*;109:D08108.

Surer, S., and Akyurek, Z., (2012). Evaluating the utility of the EUMETSAT HSAF snow recognition product over mountainous areas of eastern Turkey, *Hydrological Sciences Journal*, 57:8, 1684-1694.

Surer, S., Parajka, J., and Akyurek, Z., (2014). Validation of the operational MSG-SEVIRI snow cover product over Austria. *Hydrology and Earth System Sciences Discussions*, 10(10), 12153-12185.

Tampellini, M.L., Brivio, P.A., Carrara, P., Fantoni, D., Gnocchi, S., Ober, G., Strozzi, T., (2003). Monitoring snow cover in alpine regions through the integration of MERIS and AATSR ENVISAT satellite observations. In *Proceedings of MERIS User Workshop*, Frascati, Italy (pp. 10-13).

Tang, Q., and Lettenmaier, D.P., (2010). Use of satellite snow-cover data for streamflow prediction in the Feather River Basin, California. *International Journal of Remote Sensing*, 31(14), 3745-3762.

Tekeli, A.E., (2005). PhD Thesis: Operational Hydrological Forecasting of Snowmelt Runoff by Remote Sensing and Geographic Information systems Integration.

Tekeli, A.E., Akyürek Z., Şorman A.A., Şorman A.Ş., and Şorman A.Ü., (2005). Using MODIS snow cover maps in modeling snowmelt runoff process in the eastern part of Turkey, *Remote Sensing of Environment*, Volume 97, Issue 2, 30 July 2005, Pages 216-230.

Tekeli, Y., and Tekeli, A., (2011). A technique for improving MODIS standard snow products for snow cover monitoring over eastern Turkey. *Arabian Journal of Geosciences*, 5 (2), 353–363, doi:10.1007/s12517-010-0274-3.

Thirel, G., Salamon, P., Burek, P., and Kalas, M., (2011). Assimilation of MODIS snow cover area data in a distributed hydrological model. *Hydrology and Earth System Sciences Discussions*, 8(1), 1329-1364.

Thirel, G., Notarnicola, C., Kalas, M., Zebisch, M., Schellenberger, T., Tetzlaff, A., and de Roo, A., (2012). Assessing the quality of a real-time snow cover area product for hydrological applications. *Remote Sensing of Environment*, 127, 271-287.

Thyer, M., Beckers, J., Spittlehouse, D., Alila, Y., and Winkler, R., (2004). Diagnosing a distributed hydrologic model for two high-elevation forested

catchments based on detailed stand- and basin-scale data, *Water Resources Research* 40, W01103.

Tian Y., Yue-Ping Xu, and Xu-Jie Zhang, (2013). Assessment of Climate Change Impacts on River High Flows through Comparative Use of GR4J, HBV and Xinanjiang Models, *Water Resources Management*, 27:2871–2888 DOI 10.1007/s11269-013-0321-4.

Van Griensven, A., Meixner, T., Grunwald, S., Bishop T., Diluzio, M., and Srinivasan, R., (2006). A global sensitivity analysis tool for the parameters of multi-variable catchment models. *Journal of Hydrology*. 324 (1), 10-23.

Wagener, T., and Kollat, J., (2007). Visual and numerical evaluation of hydrologic and environmental models using the Monte Carlo Analysis Toolbox (MCAT), *Environ. Modell. Softw.*, 22, 1021–1033.

Waganer, T., and Gupta, H.V., (2005). Model identification for hydrological forecasting under uncertainty. *Stochast. Environ. Res. Risk.Assess.* 19(6), 378-387.

Wagener, T., McIntyre, N., Lees, M. J., Wheater, H. S., and Gupta, H. V., (2003). Towards reduced uncertainty in conceptual rainfall-runoff modeling: dynamic identifiability analysis, *Hydrol. Process.*, 17, 455–476.

Whitaker, A., Alila, Y., Beckers, J., and D. Toews., (2003). Application of the distributed hydrology soil vegetation model to Redfish Creek, British Columbia: Model evaluation using internal catchment data. *Hydrological Processes* 17:199–224.

Wigmosta, M.S., Nijssen, B., and Storck, P., (2002). The distributed hydrology soil vegetation model. In *mathematical models of small watershed hydrology and applications* V. P. Singh and D. K. Frevert (editors) Water Resources Publications Highlands Ranch, CO.

Wigmosta, M.S., Vail, L.W., and Lettenmaier, D.P., (1994). A distributed hydrology-vegetation model for complex terrain. *Water Resources Research* 30(6):1665–1679.

Wriedt, G., and Rode, M., (2006). Investigation of parameter uncertainty and identifiability of the hydrological model WaSIM-ETH. *Adv. Geosci.* 9, 145-150.

Yang, D., Robinson, D., Zhao, Y., Estilow, T. and Ye, B., (2003). Streamflow response to seasonal snow cover extent changes in large Siberian watersheds, *Journal of Geophysical Research D: Atmospheres* 108(D18), 4578 ACL-7 1-14.

Yilmaz, K.K., Gupta, H.V., and Wagener, T., (2008). A process-based diagnostic approach to model evaluation: Application to the NWS distributed hydrologic model. *Water Resources Research*, 44(9).

Yilmaz, K.K., Vrugt, J.A., Gupta, H.V., and Sorooshian, S., (2010). Model calibration in watershed hydrology. *Advances in data-based approaches for hydrologic modeling and forecasting*. World Scientific Publishing Company, Singapore, 53-105.

Zaitchik, B.F., Rodell, M., and Reichle, R.H., (2008). Assimilation of GRACE Terrestrial Water Storage Data into a Land Surface Model: Results for the Mississippi River Basin. *Journal Of Hydrometeorology*, 9(3), 535-548.

APPENDICES

Appendix A: PUBLICATION-1

Evaluating the utility of the EUMETSAT HSAF snow recognition product over mountainous areas of eastern Turkey

Serdar Surer¹ and Zuhul Akyurek²

¹*Geodetic and Geographic Information Technologies, Middle East Technical University, Ankara, Turkey*
serdarsurer@gmail.com

²*Civil Engineering Department, Middle East Technical University, Ankara, Turkey*
zakyurek@metu.edu.tr

Received 17 September 2011; accepted 26 March 2012; open for discussion until 1 May 2013

Editor Z.W. Kundzewicz

Citation Surer, S. and Akyurek, Z., 2012. Evaluating the utility of the EUMETSAT HSAF snow recognition product over mountainous areas of eastern Turkey. *Hydrological Sciences Journal*, 57 (8), 1–11.

Abstract Monitoring snow parameters (e.g. snow-cover area, snow water equivalent) is challenging work. Because of its natural physical properties, snow strongly affects the evolution of weather on a daily basis and climate on a longer time scale. In this paper, the snow recognition product generated from the MSG-SEVIRI images within the framework of the Hydrological Satellite Facility (HSAF) Project of EUMETSAT is presented. Validation of the snow recognition product H10 was done for the snow season (from 1 January to 31 March) of the water year 2009. The MOD10A1 and MOD10C2 snow products were also used in the validation studies. Ground truth of the products was obtained by using 1890 snow depth observations from 20 meteorological stations, which are mainly located in mountainous areas and are distributed across the eastern part of Turkey. The possibility of 37% cloud cover reduction was obtained by merging 15-min observations from MSG-SEVIRI as opposed to using only one daily observation from MODIS. The coarse spatial resolution of the H10 product gave higher commission errors compared to the MOD10A1 product. Snow depletion curves obtained from the HSAF snow recognition product were compared with those derived from the MODIS 8-day snow cover product. The preliminary results show that the HSAF snow recognition product, taking advantage of using high temporal frequency measurement with spectral information required for snow mapping, significantly improves the mapping of regional snow-cover extent over mountainous areas.

Key words MSG-SEVIRI; mountains; HSAF; snow cover

Evaluation de l'utilité du produit EUMETSAT HSAF de reconnaissance de la neige sur les régions montagneuses de Turquie orientale

Résumé Le suivi des variables nivales (par exemple la superficie de la couverture nivale ou l'équivalent en eau de la neige) est un travail difficile. En raison de ses propriétés physiques naturelles, la neige affecte fortement l'évolution quotidienne des conditions météorologiques, et celle du climat sur une échelle de temps plus longue. Dans cet article, on présente le produit de reconnaissance de la neige généré à partir des images MSG-SEVIRI dans le cadre du projet Dispositif satellitaire hydrologique (Hydrological Satellite Facility HSAF) d'EUMETSAT. La validation du produit de reconnaissance de la neige a été réalisée pour la saison neigeuse de l'année hydrologique 2009, qui couvre la période allant du 1er janvier au 31 mars 2009. Les produits d'enneigement MOD10A1 et MOD10C2 ont également été utilisés dans les études de validation. La vérité terrain pour ces produits a été obtenue en utilisant 1890 observations de hauteur de neige de 20 stations météorologiques, principalement situées dans les zones montagneuses et réparties dans la partie orientale de la Turquie. L'éventualité d'une réduction de 37% de la couverture nuageuse a été envisagée en fusionnant les observations issues de MSG-SEVIRI au pas de temps de 15 minutes, par rapport à l'utilisation d'une seule observation quotidienne issue de MODIS. La résolution spatiale grossière du produit H10 a donné davantage de faux positifs que le produit MOD10A1. Les courbes de tarissement nival obtenues à partir du produit HSAF de reconnaissance de la neige ont été comparées avec celles déduites du produit de couverture nivale MODIS sur huit jours. Les résultats préliminaires montrent que le produit HSAF de reconnaissance de la neige, en bénéficiant de l'utilisation de mesures de haute fréquence temporelle

avec l'information spectrale requise pour la cartographie de la neige, améliore significativement la cartographie de l'étendue régionale de la couverture nivale des zones montagneuses.

Mots clefs MSG-SEVIRI; montagnes; HSAF; couverture nivale

1 INTRODUCTION

Snow is one of the major water resources in many regions of the world; therefore monitoring and estimating the snow parameters play an important role in predicting discharges during melting seasons. Snow-covered area information is one of the inputs for distributed snow models. For mountainous regions, satellite imagery is the most convenient way for keeping track of snow-cover extent considering the inaccessibility due to the difficulties of rough terrain and high elevations.

Remote sensing data have been used for better comprehension of information on snow-cover extent (Cline *et al.* 1998, Painter *et al.* 2003). Several satellite sensors have been used for snow-cover mapping, such as: AVHRR, MODIS and MERIS (Harrison and Lucas 1989, Hall *et al.* 2002, Tampellini *et al.* 2004). MODIS has good temporal and spatial resolutions for snow-cover monitoring; therefore, it has been utilized in numerous studies (Parajka and Blöschl 2012). Various studies have been done on the validation of MODIS snow-cover products under a variety of snow- and land-cover conditions. Most studies show an overall "clear sky" accuracy of 94% compared with ground measurements (Parajka and Blöschl 2006, 2012, Hall and Riggs 2007). Lower accuracies are typically obtained in the autumn and spring, under thin-snow conditions and in densely-forested areas. Also, a significant source of error in the MODIS snow products is due to the cloud-masking algorithm, which is embedded in the snow algorithm. In Tekeli *et al.* (2005), comparison of MODIS snow maps with *in situ* measurements over the snow season showed good agreement, with overall accuracies ranging between 62 and 82% considering the shift in the days of comparison. In that study, the main reasons for disagreement between MODIS and *in situ* data are given as the high cloud cover frequency in the area and the current version of the MODIS cloud mask that appears to frequently map edges of snow-covered areas and land surfaces (Tekeli *et al.* 2005). Parajka and Blöschl (2008) presented an evaluation of simple mapping methods that reduce cloud coverage by using information from neighbouring non-cloud-covered pixels in time and space, and by combining MODIS data from

the Terra and Aqua satellites. Tekeli and Tekeli (2011) performed a similar approach for improving MODIS standard snow-cover products for snow-cover monitoring over eastern Turkey. Ault *et al.* (2006) performed a validation of the MODIS snow product (MOD10_L2) and cloud mask (MOD35) in the Lower Great Lake region, USA. They found that when cloud cover does not obscure the ground, the MOD10_L2 snow product provides an accurate and reliable record of snow and ice extent. However, when cloud cover is prevalent in an image, the MOD10_L2 snow product can sometimes misinterpret the cloud cover as either ice or snow (Ault *et al.* 2006). Cloud cover discrimination is the most challenging problem in retrieving snow-cover information from the satellite images acquired in the optical portion of the spectrum. The Spinning Enhanced Visible and Infrared Imager (SEVIRI) instrument on board the MSG (METEOSAT Second Generation) satellite, a geostationary satellite scanning the whole hemisphere, requires the inclusion of visible, near-infrared and thermal parts of the spectrum, at the same time as the essential spectral content for adequate snow-cover extent monitoring. The high temporal resolution (15-min) and wide aerial coverage of SEVIRI imagery make it a good choice for observing rapidly changing phenomena, such as for fog monitoring, tracking cloud movements or snow-cover mapping (Bertrand *et al.* 2008, Cermak and Bendix 2008).

The use of snow products retrieved from satellite images in hydrological applications and observation of the impact of such products in hydrological models are key issues in the Hydrological Satellite Facility (HSAF) Project, which is financially supported by the European Organization for the Exploitation of Meteorological Satellites (EUMETSAT). Turkey takes part in the HSAF Project in the development of satellite-derived snow products (snow recognition, effective snow cover and snow water equivalent) for mountainous areas, calibration/validation of satellite-derived snow products and impact studies with hydrological modelling in the 21 selected test basins of Europe.

In this study, the daily snow recognition product (referred to as H10 herein) generated from MSG-SEVIRI data is described, and the validation analysis

performed with observations from ground measurements at synoptic weather observation stations and with another satellite-derived snow product, MOD10C2, for the melting period (1 January to 31 March) of water year 2009, is presented and the results are discussed.

2 DATA

2.1 Satellite data

2.1.1 MSG-SEVIRI Data Meteosat-9, also named Meteosat Second Generation, or MSG-2, was launched in December 2005 with significantly improved services and products of Meteosat satellites. The MSG-2 provides imagery with 15-min temporal resolution and 3-km spatial resolution (at nadir) through 12 spectral channels for the whole hemisphere of the Earth. Further information about the instrument can be found at: <http://www.eumetsat.int/Home/Main/Satellites/MeteosatSecondGeneration/Instruments/index.htm>.

The Turkish State Meteorological Service (TSMS) has been receiving MSG-2 data of the SEVIRI sensor for more than three years in level 1.5 high rate image transmission (HRIT) data format. The HRIT data are converted to hierarchical data

Table 1 SEVIRI channels used in the snow recognition algorithm.

Channel no.	Central wavelength (μm)	Description
1	0.635	Visible (VIS0.6)
3	1.64	Near infrared (NIR1.6)
4	3.90	Shortwave infrared (IR3.9)
9	10.80	Infrared (IR10.8)

format (HDF) and used in the product generation chain at the TSMS. Of the 12 spectral channels, four have been used mainly in the snow recognition algorithm development. The central wavelengths and channel numbers of these bands are given in Table 1.

The H10 product is produced covering the predefined spatial domain that is the area between longitude 25°W – 45°E and latitude 25° – 75°N , as shown in Fig. 1. The mountain mask applied in the product generation algorithm is also depicted in Fig. 1. Snow cover over mountainous areas and over flat/forest areas shows completely different physical properties; thus, the use of two separate algorithms makes it possible to get better results compared to using a generic algorithm (Dorothy Hall, personal communication). A mountain mask is required for development of the algorithm that is only applicable or suitable on mountainous (rough) terrains; by using a mountain mask,

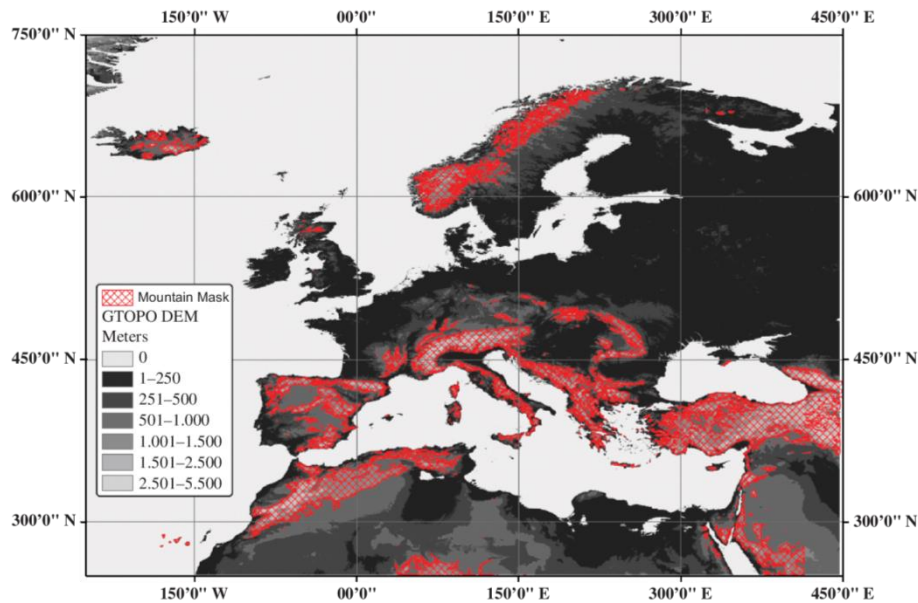


Fig. 1 HSAF domain shown with mountain mask.

the areas that might be classified as flat land are discarded. In order to generate this mountain mask, a 1-km spatial resolution GTOPO digital elevation map (DEM) was used. After building a $0.05^\circ \times 0.05^\circ$ interval mesh, an algorithm for binary mountain mask creation was run inside each individual mesh interval, in which mainly the elevation and the slope of the terrain are considered. All the statistics are searched in the given mesh interval and the points satisfying the given rules are selected as mountain pixels. The algorithm for mountain mask generation is as follows:

$$(\mu \geq 1000 \text{ m}) \text{ OR } (\sigma \geq 2\% \text{ AND } \mu \geq 700 \text{ m})$$

$$\text{OR } (\tau \geq 800 \text{ m AND } \mu \geq 500 \text{ m})$$

where μ is mean elevation, σ is standard deviation and τ is range, which is the difference between maximum and minimum elevation in the mesh.

2.1.2 Terra-MODIS snow products MODIS data have been used since early 2000 to produce daily, global snow maps in an automated environment. These maps have been validated, are available at a variety of spatial resolutions (500 m, 0.05° and 0.25°), and provide snow extent and fractional snow cover (FSC), as well as snow albedo (Klein and Stroeve 2002, Hall and Riggs 2007). Inputs to the products include the MODIS cloud mask (Ackerman *et al.* 1998, Platnick *et al.* 2003), the land/water mask, the geolocation product, radiance products, and the surface-reflectance product (for snow albedo), and land cover. In this study, the MOD10A1 product is used in the comparison with ground data. The MOD10A1 MODIS/Terra daily snow cover Level 3, 500-m resolution product is in the sinusoidal map

projection (Hall *et al.* 2000). In developing the MOD10C1 product, the snow-cover extent is mapped by processing the MOD10A1 (500-m) product for a day in the climate modelling grid (CMG) projection used in the MOD10C1. In order to derive the snow depletion curves, the MOD10C2 product is used. The MOD10C2 is the 8-day CMG snow cover data product, and the snow-cover extent is expressed as an areal percentage of coverage of the input data at 500-m resolution in a 5-km cell of the CMG. Details of the product can be found in the study by Riggs *et al.* (2006).

2.2 Ground data

Snow depth measurements from synoptic weather observation stations and climatic stations were used for the validation of the H10 product generated from MSG-SEVIRI. The data from those meteorological observation stations are mainly composed of periodically-measured snow depth information reported on a daily basis. The validation analyses using the ground observations were performed for the snow season of water year 2009 (January–March 2009). A total of 1890 observations from 20 stations operated by TSMS were used. The elevation of the stations ranges between 808 and 2500 m a.s.l. The land-cover information was obtained from the COoRdinate INformation on the Environment (CORINE) land database, a pan-European land-cover/land-use map for non-commercial use provided by the European Environmental Agency (EEA). The land cover in the study area is not complex and is composed of bare ground, pasture and cultivated land. The distribution of stations over Turkey is shown in Fig. 2. For comparisons of cloud coverage and regional snow depletion curves, a test basin, the

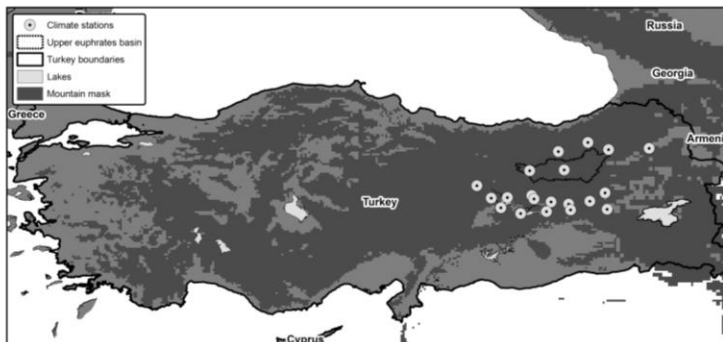


Fig. 2 Distribution of the stations used in the validation analysis.

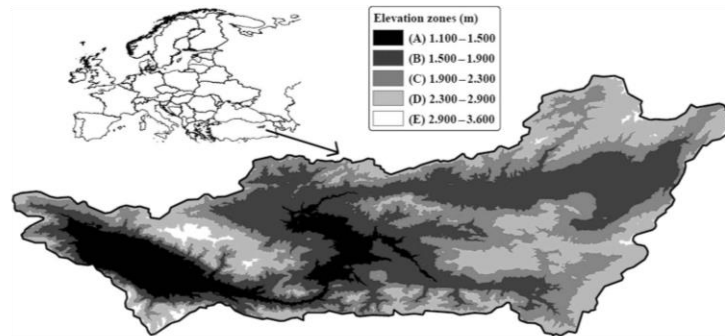


Fig. 3 The five elevation zones of Upper Euphrates basin.

Upper Euphrates basin, located in the eastern part of Turkey, was used (Fig. 3).

3 METHODOLOGY

3.1 Algorithm for the generation of H10 product

The derivation of snow products over mountainous regions is considered very challenging. This can be done by periodic and precise mapping of the snow cover. However, inaccessibility and the scarcity of ground observations limit snow-cover mapping in mountainous areas. Nowadays, it is carried out operationally by means of optical satellite imagery. Retrieving the snow-cover area from satellite images faces the problem of topographical variations within the footprint of satellite sensors, and the spatial and temporal variation of snow characteristics in mountainous areas. Most global and regional operational snow products use generic algorithms for both flat and mountainous areas. However, the non-uniformity of the snow characteristics needs to be modelled with different algorithms for mountains and flat areas. In this study, the algorithm developed for mountainous areas is presented; the algorithm used for flat areas is given in Siljamo *et al.* (2008). The final snow recognition product is obtained after merging the products developed for flat areas and mountainous areas, which was done at the Finnish Meteorological Institute (FMI)—detailed information on the algorithms can be found in Siljamo *et al.* (2008) and Surer (2008).

For the snow recognition algorithm for mountainous areas, spectral thresholding methods were applied on sub-pixel-scale MSG-SEVIRI images. The different spectral characteristics of cloud, snow and land determined the structure of the algorithm,

and these characteristics were obtained from subjective classification of known snow-cover features in the MSG/SEVIRI images. Discrimination between snow and cloud is the most challenging part of the snow recognition algorithm development. Before carrying out further investigation of snow pixels, discrimination of cloud was done; thereafter, only cloud-free pixels were considered for snow and land discrimination. In order to get rid of cloud-covered pixels, Cloud Mask (CMA) and Cloud Type (CT) products of the Nowcasting Satellite Application Facility (NWCSAF 2007) were used. After detailed analysis of the CMA and CT products, they were combined, in order to integrate them into the proposed snow recognition algorithm, as the cloud recognition part has been generated.

Snow cover maps using MSG-SEVIRI data were produced for each 15-min cycle between 08:00 and 15:45 GMT, making 32 individual images per day. All individual 15-min images acquired during a day were subjected to a series of thresholding tests. A threshold for the sun zenith angle is also considered to eliminate the dark pixels due to the location of the sun. First, the high visible reflectance of snow was considered and pixels having reflectance values higher than 0.35 were collected. Then, a spectral indexing method similar to Dozier's method was used: Dozier (1989) used snow index (SI) by dividing the bands NIR1.6 to VIS0.6. The pixels having NIR1.6/VIS0.6 values lower than a fixed threshold value of 0.6 were collected. Normalized difference snow index (NDSI) is another well-known snow index used in snow product generation from MODIS data. The NDSI takes advantage of the fact that snow reflectance is high in the visible (0.5–0.7 μm) wavelengths and low in the shortwave infrared (1.0–4.0 μm) wavelengths (Hall *et al.* 2001, 2002). The NDSI and SI values

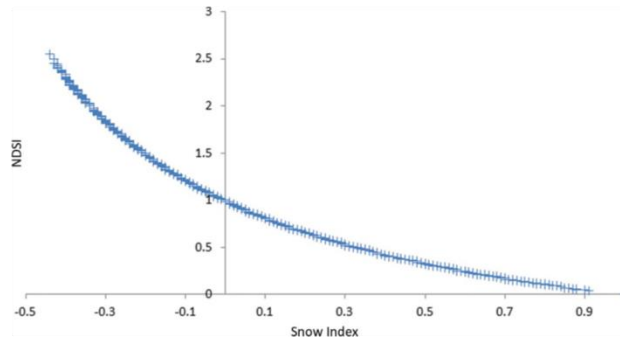


Fig. 4 Relationship of NDSI vs SI derived from MSG-SEVIRI data.

were compared for several clear-sky MSG-SEVIRI images for the study area (Fig. 4), and those for the snow-cover areas show a good relationship. The selected threshold value of 0.6 for the snow-cover area retrieval corresponds to the NDSI value of 0.2. The NDSI value for 50% snow-covered areas is taken as 0.4 (Dozier 1989, Hall *et al.* 2002). By selecting $SI = 0.6$ as the threshold for full snow coverage, it is aimed to include the partial snow-covered areas in the retrieval of the H10 product.

Next, pixels having low sun zenith angle (sza) were discarded by a filter accepting pixels only higher than 5° . A final test for covering all cold pixels below freezing point was applied and pixels with temperature lower than 288K on channel-9 (IR10.8) were accepted, given that the temperature of snow cannot exceed the freezing point (Romanov *et al.* 2003). After obtaining snow-cover maps for each individual 15-min image, a daily snow-cover map was generated by accepting pixels having at least three snow hits among the 32 daily images. Finally, a daily thematic map of 5-km spatial resolution was produced that

consists of four different classes: snow, cloud, bare ground and water, a sample of which is given in Fig. 5. Due to the coarse spatial resolution of MSG-SEVIRI data, the retrieval of fractional snow-cover area from MSG-SEVIRI data was not considered; therefore, the proposed thresholds are used to retrieve the full snow cover in mountainous areas.

3.2.1 Validation with ground data In order to test the performance and accuracy of the H10 product, a set of comparison tests were applied with the ground observations of snow depths for eastern Turkey, which is mostly mountainous. The daily ground measurements (snow or no snow) were compared to the collocated pixel information in the snow-cover map by making contingency tables (snow, no snow) on a monthly basis (Table 2). For the validation, the most common forecasting metrics, such as probability of detection (POD), hit rate (HR), omission error (snow missing rate, SMR) and commission error (false alarm rate, FAR) were

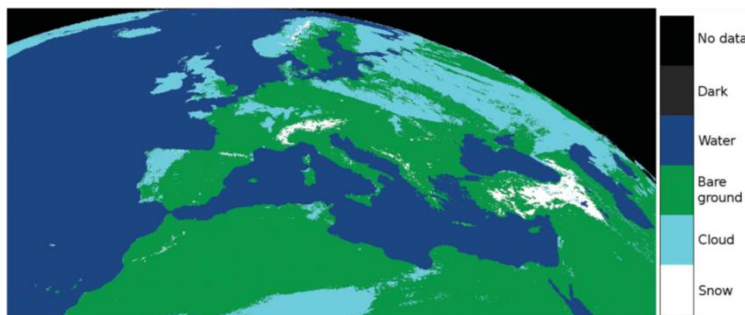


Fig. 5 Sample snow recognition product for 9 February 2011.

Table 2 Metric values.

		Ground observation	
		Snow presence	No snow
Snow cover product	Snow presence	<i>a</i>	<i>b</i>
	No snow	<i>c</i>	<i>d</i>

Table 3 Calculation of metrics.

POD	FAR	HR	SMR
$\frac{a}{(a+c)}$	$\frac{b}{(a+b)}$	$\frac{(a+d)}{(a+b+c+d)}$	$\frac{c}{(a+b+c+d)}$

Note: POD: probability of detection; FAR: false alarm rate; HR: hit rate; SMR: snow missing rate.

used. These were calculated using the metric values described in Table 3. Similar validation analysis was performed for the MOD10A1 snow product. In order to give similar spatial resolution, the MOD10A1 snow product was resampled to 5-km resolution with the nearest-neighbourhood resampling method. The same metric values were also computed for the resampled MOD10A1 product. The frequency of cloud pixels for the months January–March 2009 in the Upper Euphrates basin was also evaluated for the H10 and resampled MOD10A1 snow products. The percentage of cloud coverage was calculated by dividing the total basin area by the cloud-covered area on a daily basis.

3.2.2 Validation with MOD10C2 The H10 product is developed for hydrological impact studies within the HSAF Project. Snow-depletion curves are among the inputs to hydrological models in which snow melting is modelled. Therefore, in addition to validation with ground measurements, a comparison of the snow-depletion curves derived from the H10 product and the 8-day snow-cover product of the Terra-MODIS (MOD10C2) product was performed. The latter was selected, as it has the same spatial resolution as the HSAF snow product. As stated by Zhou *et al.* (2005), the MODIS 8-day

product has a better correlation with streamflow and a lower percentage of spurious snowmelt events in winter than the MODIS daily product. The relationship between the SCA derived from MOD10C2 snow products and the runoff during the spring was analysed for the period 2004–2009 in the Upper Euphrates basin (Akyurek *et al.* 2011).

The basin is divided into five elevation zones in order to observe the behaviour of snow melting at different elevations, as shown in Fig. 3. The areal coverage distribution of the zones for the full basin is: Zone A: 11%, Zone B: 34%, Zone C: 34%, Zone D: 20% and Zone E: 1%. Because Zone E is much smaller than the other zones, and only three pixels of the H10 product fall into this area, it was not taken into account for the analyses.

Cloud coverage percentages were also obtained for the basin. The snow-cover percentage was obtained by considering the ratio of snow classified pixels in a given elevation zone to the total area of the zone. Days when the cloud coverage was over 25% were discarded from the depletion curve derivation. In the previous hydrological studies in the basin, snow products having cloud coverage lower than 20–30% were found suitable for deriving snow depletion curves for modelling the snowmelt runoff (Marim 2008).

4 RESULTS AND DISCUSSION

4.1 Results from validation with ground data

The validation of H10 and MOD10A1 snow products for January, February and March 2009 was performed. Since the H10 product is intended to map the snow extent for mountainous areas, the ground observations located in the mountainous areas were used. Early results show good general agreement between H10 product and *in situ* data, as was observed in a previous study (Surer *et al.* 2009) with a rather smaller data set. The metrics obtained from the analysis are depicted in Table 4. The highest overall

Table 4 Results obtained from validation analysis for the snow season in 2009.

	January		February		March	
	H10	MOD10A1	H10	MOD10A1	H10	MOD10A1
HR (%)	81.32	89.74	68.63	85.92	78.45	96.59
POD (%)	95.56	92.45	82.72	76.47	85.33	79.31
SMR (%)	3.08	5.13	5.49	5.63	3.16	3.41
FAR (%)	15.60	7.55	25.88	31.58	18.39	0.00
Cloud (%)	30.11	79.33	56.63	89.09	46.54	77.89

accuracy was obtained for January for H10 and March for MOD10A1. The probability of detection values obtained for H10 was larger than that obtained for MOD10A1. However, the overall accuracies obtained for H10 are lower than those obtained for MOD10A1. This is because of the large commission errors of the H10 product. The commission error, indicating snow on the ground where no snow occurred on the ground, is low in January, but comparatively high in February and March. It is very well known that, as melting starts, the evaluation of satellite mapping accuracy is difficult when snow cover becomes patchy. However, the omission error is low for the whole winter period. This error indicates that the algorithm does not find snow where snow occurs on the ground. Since the algorithm uses visible channels in discriminating snow, the strength of visible channels in identifying fresh snow on the ground can be seen in the computed metrics. The coarse spatial resolution of the MSG-SEVIRI data leads to high commission errors for the H10 product. The effect of spatial resolution can be seen in Fig. 6, in which the MOD10A1 snow product, the resampled MOD10A1 product (5-km resolution with nearest-neighbourhood method), and the H10 snow product are presented.

The other reason for the lower overall accuracy for February is the high cloud coverage that occurred in this month. The limitation of optical bands on cloudy days is very well known. Using

a geostationary satellite for mapping snow extent improved the results due to the higher temporal resolution (15-min), but the coarse spatial resolution brings a disadvantage to mapping shallow snow and fractional snow in the melting season.

The cloud coverage percentage values for January–March 2009 are presented in Fig. 7. The mean cloud coverage for the three months was 82.10% and 44.42% for the resampled MOD10A1 and H10 snow products, respectively. This indicates a possibility of 37.68% cloud cover reduction by merging 15-min observations from MSG-SEVIRI, compared to using only one daily observation from MODIS.

4.2 Results from validation with MOD10C2

The depletion curves derived from H10 and MOD10C2 snow products are presented in Fig. 8(a) and (b), together with the cloud percentages. A good agreement is seen between the two curves. The main disagreement is observed where there is high cloud coverage on 25 January 2009. The MOD10C2 product, having a low confidence index, indicates high cloud coverage for 8 days. From the ground observations, it was observed that snow was recorded on this date at the ground stations within the basin. Due to the high cloud coverage, it may not be possible to identify the snow-covered area from the MOD10C2 products.

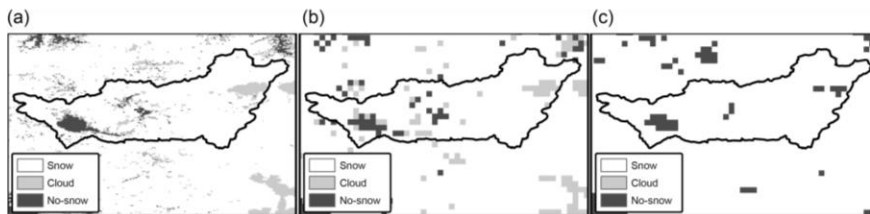


Fig. 6 For 22 January 2009: (a) MOD10A1 product, (b) MOD10A1 product resampled to 5 km, and (c) H10 product.

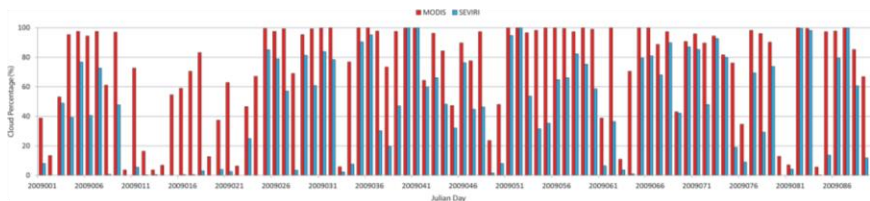


Fig. 7 Cloud coverage (%) obtained from H10 (SEVIRI) and resampled MOD10A1 (MODIS) for January, February and March 2009.

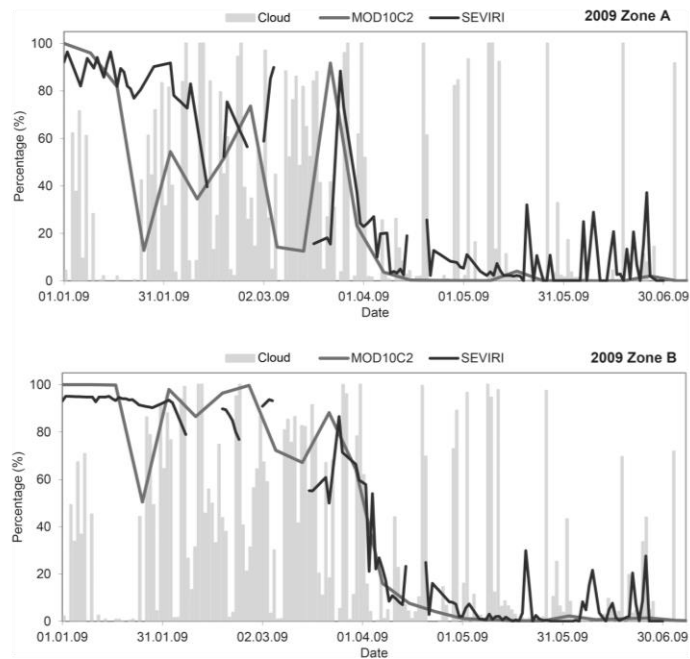


Fig. 8(a) Snow depletion curves for zones A and B of the Upper Euphrates basin with H10 and MOD10C2 products.

During the melting stage of the snow cover, after 17 May 2009, snow depletion curves derived from the H10 product show abrupt changes. During this period, the snow recognition algorithm misclassifies the ice crystals in the high opaque clouds as snow. In optical remote sensing, some types of ice clouds can be erroneously identified as snow, because they show similar reflectance and temperature values. Parajka and Blöschl (2006) stated that, during the assessment of MODIS snow product over Austria for the period 2000–2005, almost all MODIS overestimation errors in the summer months were caused by the misclassification of cirrus clouds as snow. The abrupt changes in the SCA depletion curves, which are not recommended in the SRM manual (Rango and Martinec 1979), may lead to overestimation in runoff predictions. This indicates the need for post-processing analysis for the end of the depletion curves by using the surface temperature values in the basin.

The consistency of the snow products can be seen for zones B and C. For zone D there is an over-estimation in the snow depletion curve obtained from MOD10C2 compared to that obtained from the H10 product. Both snow products have 5-km spatial resolution and this coarse resolution leads to a mixed-pixel problem, which may be more important

for regional studies than for global hydrological studies.

5 CONCLUSIONS

The most important contribution to the success of the snow recognition algorithm is to have observations from geostationary satellite imagery SEVIRI, which provides a high temporal frequency measurement with spectral information required for snow mapping. This high temporal frequency helps to improve the snow mapping despite the cloud coverage problem during the day if the clouds are moving. The possibility of 37% cloud cover reduction by merging 15-min observations from MSG-SEVIRI compared to using only one daily observation from MODIS was obtained. The high percentage of cloud coverage removal ability makes this snow product suitable for hydrological applications.

Early results show good general agreement between the H10 product and *in situ* data. They also indicate the suitability of the H10 product for use in hydrological studies. This work will be continued with more validation studies: the algorithm will be tuned to improve the snow extent mapping on the forest-covered areas. Variable thresholds

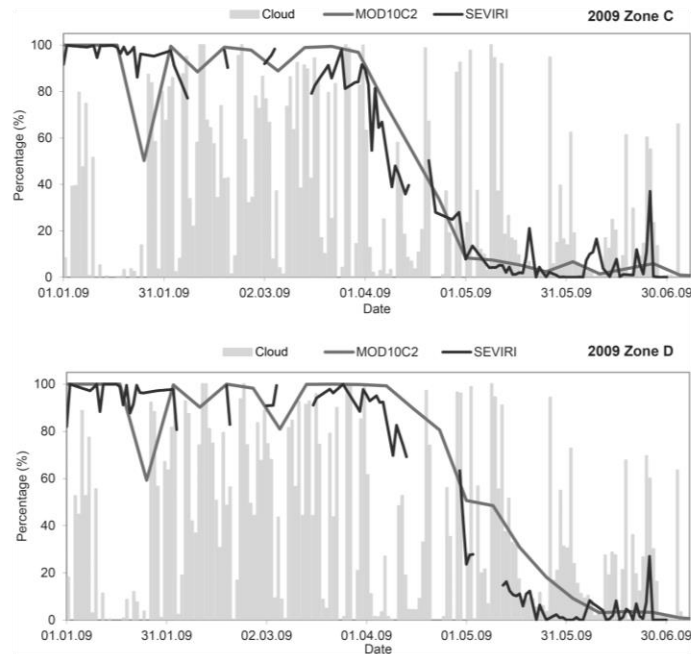


Fig. 8(b) Snow depletion curves for zones C and D of the Upper Euphrates basin with H10 and MOD10C2 products.

depending on season can also be included in the algorithm.

Acknowledgements This study was prepared within the framework of HSAF project funded by EUMETSAT. We kindly thank the Remote Sensing Division of the Turkish State Meteorological Service, especially Mr Aydın G. Ertürk and Dr İbrahim Sönmez for their support. Thanks to Kenan Bolat for his technical support. Thanks are also due to the referees for providing valuable comments on earlier drafts of the manuscript.

REFERENCES

- Ackerman, S.A., *et al.* 1998. Discriminating clear sky from clouds with MODIS. *Journal of Geophysical Research*, 103, D24, 32141–32157.
- Akyurek, Z., Surer, S., and Beser, Ö., 2011. Investigation of the snow-cover dynamics in the Upper Euphrates basin of Turkey using remotely sensed snow-cover products and hydrometeorological data. *Hydrological Processes*, 25, 3637–3648, doi: 10.1002/hyp.8090.
- Ault, T.W., *et al.*, 2006. Validation of the MODIS snow product and cloud mask using student and NWS cooperative station observations in the Lower Great Lakes Region. *Remote Sensing of Environment*, 105, 341–353.
- Bertrand, C., *et al.*, 2008. Improvement in the GERB short wave flux estimations over snow covered surfaces. *Advances in Space Research*, 41 (11), 1894–1905, doi:10.1016/j.asr.2006.12.016.
- Cermak, J. and Bendix, J., 2008. A novel approach to fog/low stratus detection using Meteosat 8 data. *Atmospheric Research*, 87 (3–4), 279–292.
- Cline, D.W., Bales, R.C., and Dozier, J., 1998. Estimating the spatial distribution of snow in mountain basins using remote sensing and energy balance modeling. *Water Resources Research*, 34 (5), 1275–1285.
- Dozier, J., 1989. Spectral signature of alpine snow cover from Landsat Thematic Mapper. *Remote Sensing of Environment*, 28, 9–22.
- Hall, D.K. and Riggs, G.A., 2007. Accuracy assessment of the MODIS snow-cover products. *Hydrological Processes*, 21, 1534–1547.
- Hall, D.K., Riggs, G.A., and Salomonson, V.V., 2000. *Updated daily MODIS/Terra Snow Cover Daily L3 Global 500m Grid V004, January to March 2003*. Boulder, CO: National Snow and Ice Data Center.
- Hall, D.K., *et al.*, 2002. MODIS snow-cover products. *Remote Sensing of Environment*, 83 (1), 181–194.
- Harrison, A.R. and Lucas, R.M., 1989. Multi-spectral classification of snow using AVHRR imagery. *International Journal of Remote Sensing*, 10 (4–5), 907–916.
- Klein, A.G. and Stroeve, J., 2002. Development and validation of a snow albedo algorithm for the MODIS instrument. *Annals of Glaciology*, 34 (1), 45–52.
- Marim, G., 2008. *Temporal evaluation of snow depletion curves derived for Upper Euphrates basin and applications of snowmelt runoff model (SRM)*. Thesis (Masters), Middle East Technical University, Turkey. <http://etd.lib.metu.edu.tr/upload/3/12609938/index.pdf> [Accessed 12 January 2012].

- NWCSAF (Nowcasting Satellite Application Facility), 2007. *User manual for the Cloud Products of the Nowcasting Satellite Application Facilities*. <http://www.nwcsaf.org/HD/MainNS.jsp> [Accessed 12 January 2012].
- Painter, T.H., *et al.*, 2003. Retrieval of subpixel snow-covered area and grain size from imaging spectrometer data. *Remote Sensing of Environment*, 85, 64–77.
- Parajka, J. and Blöschl, G., 2006. Validation of MODIS snow cover images over Austria. *Hydrology and Earth System Sciences*, 10, 679–689, doi:10.5194/hess-10-679-2006.
- Parajka, J. and Blöschl, G., 2008. Spatio-temporal combination of MODIS images-potential for snow cover mapping. *Water Resources Research*, 44, W03406, doi:10.1029/2007WR006204.
- Parajka, J. and Blöschl, G., 2012. MODIS-based snow cover products: validation, and hydrologic applications, Chapter 9. In: Ni-Bin Chang, ed. *Multiscale hydrologic remote sensing: perspectives and applications*. Boca Raton, FL: CRC Press.
- Platnick, S., *et al.*, 2003. The MODIS cloud products: algorithms and examples from Terra. *IEEE Transactions on Geoscience and Remote Sensing*, 41, 459–473.
- Rango, A. and Martinec, J., 1979. Application of a snowmelt runoff model using Landsat data. *Nordic Hydrology*, 10 (4), 225–238.
- Riggs, G.A., Hall, D.K., and Salomonson, V.V., 2006. *MODIS Snow products user guide collection 5*. http://nsidc.org/data/docs/daac/modis_v5/dorothy_snow_doc.pdf [Accessed 12 January 2012].
- Romanov P., *et al.*, 2003. Mapping and monitoring of the snow cover fraction over North America. *Journal of Geophysical Research*, 108 (D16), 8619, doi:10.1029/2002JD003142.
- Siljamo, N., Hyvarinen, O., and Koskinen, J., 2008. Operational snow cover mapping using MSG/SEVIRI data. In: *IEEE International geoscience and remote sensing symposium*. 7–11 July 2008, 45–48, doi:10.1109/IGARSS.2008.4780023.
- Surer, S., 2008. *Real-time snow cover mapping over mountainous areas of Europe using MSG-SEVIRI imagery*. Thesis (Masters), Middle East Technical University, Turkey. <http://etd.lib.metu.edu.tr/upload/12609911/index.pdf> [Accessed 12 January 2012].
- Surer, S., *et al.*, 2009. Real time snow recognition from MSG satellite for mountainous areas. In: *Remote sensing for a changing Europe*. Proceedings of the 28th European Association of Remote Sensing Laboratories, Turkey, 2–5 June 2008. Lansdale PA: IOS Press, 86–93. doi:10.3233/978-1-58603-986-8-86.
- Tampellini, M.L., *et al.*, 2004. Monitoring snow cover in Alpine regions through the integration of MERIS and AATSR ENVISAT satellite observations. In: *Proceedings of MERIS User Workshop* (Frascati, Italy, May 2004), ESA SP-549, 10–13 [online]. http://envisat.esa.int/workshops/meris03/participants/219/paper_38_tampellini.pdf [Accessed 12 January 2012].
- Tekeli, A.E., *et al.*, 2005. Using MODIS snow cover maps in modeling snowmelt runoff process in the eastern part of Turkey. *Remote Sensing of Environment*, 97 (2), 216–230.
- Tekeli, Y. and Tekeli, A., 2011. A technique for improving MODIS standard snow products for snow cover monitoring over eastern Turkey. *Arabian Journal of Geosciences*, 5 (2), 353–363, doi:10.1007/s12517-010-0274-3.
- Zhou, X., Xie, H., and Hendrick, J.M.H., 2005. Statistical evaluation of remotely sensed snow-cover products with constraints from streamflow and SNOTEL measurements. *Remote Sensing of Environment*, 94, 214–231.

Appendix B: PUBLICATION-2

Hydrol. Earth Syst. Sci., 18, 763–774, 2014
www.hydrol-earth-syst-sci.net/18/763/2014/
doi:10.5194/hess-18-763-2014
© Author(s) 2014. CC Attribution 3.0 License.



Hydrology and
Earth System
Sciences



Validation of the operational MSG-SEVIRI snow cover product over Austria

S. Surer¹, J. Parajka^{2,*}, and Z. Akyurek³

¹Geodetic and Geographic Information Technologies, Middle East Technical University, Ankara, Turkey

²Institute of Hydraulic Engineering and Water Resources Management, Vienna University of Technology, Vienna, Austria

³Civil Eng. Dept., Middle East Technical University, Ankara, Turkey

*on leave from: Institute of Hydrology, Slovak Academy of Sciences, Liptovský Mikuláš, Slovakia

Correspondence to: S. Surer (serdarsurer@gmail.com)

Received: 12 September 2013 – Published in Hydrol. Earth Syst. Sci. Discuss.: 7 October 2013

Revised: 8 January 2014 – Accepted: 25 January 2014 – Published: 24 February 2014

Abstract. The objective of this study is to evaluate the mapping accuracy of the MSG-SEVIRI operational snow cover product over Austria. The SEVIRI instrument is aboard the geostationary Meteosat Second Generation (MSG) satellite. The snow cover product provides 32 images per day, with a relatively low spatial resolution of 5 km over Austria. The mapping accuracy is examined at 178 stations with daily snow depth observations and compared with the daily MODIS-combined (Terra + Aqua) snow cover product for the period April 2008–June 2012.

The results show that the 15 min temporal sampling allows a significant reduction of clouds in the snow cover product. The mean annual cloud coverage is less than 30 % in Austria, as compared to 52 % for the combined MODIS product. The mapping accuracy for cloud-free days is 89 % as compared to 94 % for MODIS. The largest mapping errors are found in regions with large topographical variability. The errors are noticeably larger at stations with elevations that differ greatly from those of the mean MSG-SEVIRI pixel elevations. The median of mapping accuracy for stations with absolute elevation difference less than 50 m and more than 500 m is 98.9 and 78.2 %, respectively. A comparison between the MSG-SEVIRI and MODIS products indicates an 83 % overall agreement. The largest disagreements are found in Alpine valleys and flatland areas in the spring and winter months, respectively.

1 Introduction

Monitoring and modeling of snow characteristics is important for many hydrological applications, including snowmelt runoff forecasting and water resources assessment using a range of techniques (e.g., Blöschl and Kirnbauer, 1991; Blöschl et al., 1991; Nester et al., 2012). The large spatial variability of snow cover, particularly in mountains, limits the use of ground-based snow observations. Satellite imagery is thus an attractive alternative, as the resolution and availability does not depend much on the terrain characteristics (Parajka and Blöschl, 2008).

Recently, operational satellite products have become available that provide snow cover information at different spatial and temporal resolutions (Table 1). Table 1 indicates that most of the current products provide daily snow cover information at spatial resolutions ranging from 500 m to 5 km. The numerous validation studies indicate that the satellite products have large snow mapping accuracy with respect to ground snow observations for cloud-free conditions, which varies between 69 and 94 % in the winter seasons. The main limitation of existing optical platforms operating at a daily timescale is cloud coverage, which significantly reduces the availability of snow cover information. There are different approaches for cloud reduction, including space–time filtering (e.g., Parajka and Blöschl, 2008; Gafurov and Bárdossy, 2009; Hall et al., 2010, among others), but clouds are real and the accuracy of such approaches decreases with their efficiency to reduce clouds.

Published by Copernicus Publications on behalf of the European Geosciences Union.

Table 1. Summary of some existing operational satellite snow cover products.

Snow cover product	Sensor	Available since	Spatial resolution	Temporal resolution	Mapping accuracy
NOHRSC/ +GOES	NOAA/AVHRR	1986	1 km	Daily Barnett, 2003)	76 % (Klein and
NOAA/NESDIS (IMS)	GOES+SSM/I	1998	4 km	Daily, weekly	85 % (Romanov et al., 2000); < 20 % (October), ~ 60 % (November), ~ 95 % (December), ~ 70 % (March) (Brubaker et al., 2005)
MOD10A1, MYD10A1, MOD10A2, MYD10A2, MOD10C1, MYD10C1, MOD10CM, MYD10CM	MODIS- Terra/Aqua	2000/2002	500 m –0.05°	Daily, 8-day, monthly	~ 94 % summary in Parajka and Riggs, 2007 or (see e.g., Hall and Blöschl, 2012)
HSAF (EUMETSAT)	MSG-SEVIRI	2008	5 km	Daily	80 % compared to IMS (Siljamo and Hyvärinen, 2011); 69–81 % in winter months (Surer and Akyurek, 2012)

An alternative to the space–time filtering of daily products is to merge satellite images obtained at higher temporal resolution. The new generation of MSG-SEVIRI product provides snow cover information at 15 min temporal resolution for the whole Northern Hemisphere. The preliminary assessment of data from one snow season over eastern Turkey (Surer and Akyurek, 2012) indicates that the merging of 32 consecutive images per day enables a 37 % reduction of clouds in comparison to the MODIS daily product, and improves the mapping of regional snow-cover extent over mountainous areas.

The main objective of this study is to assess the accuracy of the new MSG-SEVIRI snow cover product over Austria for the period 2008–2012. The spatial and temporal variability in mapping accuracy is examined for a large number of meteorological stations observing snow depth and is evaluated against combined MODIS snow cover product. Austria is an ideal test bed for such an assessment, as it allows evaluating the mapping accuracy in different altitudinal zones ranging from the lowlands to the high Alpine environment. The MSG SEVIRI snow product has been produced operationally within the HSAF project funded by EUMETSAT. The validation studies composed of ground observation comparisons with satellite snow product have been performed on mountainous areas of Europe (HSAF, 2011). The idea in this study is to extend the test sites in order to evaluate the MSG SEVIRI snow product and perform detailed validation studies.

2 MSG-SEVIRI snow cover product

The Spinning Enhanced Visible and Infrared Imager (SEVIRI) is an optical imaging radiometer mounted aboard the geostationary Meteorol Second Generation (MSG) satellite operated by EUMETSAT. MSG-SEVIRI provides continuous imaging of the earth in 12 spectral channels with a repeat cycle of 15 min. The imaging spatial resolution is 3 km at sub-satellite point (Aminou, 2002) and degrades to 5 km over Europe.

The snow cover mapping is based on a multi-channel retrieval algorithm. It exploits the high reflectivity of snow in the visible spectrum and the low reflectivity at shorter wavelengths. The snow cover retrieval algorithm differs for flat and mountainous regions. Considering the different characteristics of snow for mountainous and flat areas, two different algorithms are used in producing the snow products for flat and mountainous areas, and then the products are merged to have a single snow product. In flat regions, the algorithm utilizes the top-of-atmosphere radiance of six SEVIRI channels (0.6, 0.8, 1.6, 3.9, 10.8 and 12.0 μm) and brightness temperatures of three channels (3.9, 10.8, and 12.0 μm). The snow recognition is based on the snow cover classification (Siljamo and Hyvärinen, 2011). The cloud–snow discrimination for flatlands relies on the cloud mask (CMA) provided by the Nowcasting and Very Short Range Forecasting Project (NWCSAF, 2007). In this product clouds are classified only into two classes (cloud contaminated and cloud filled).

In the mountains, the snow recognition algorithm uses the snow index (SI), which relates 0.6 μm (0.56–0.71 μm) and

Table 2. Number of meteorological stations in different elevation zones.

Elevation zone (m a.s.l.)	0–500	500–1000	1000–1500	1500–2000	2000–2500	2500–3109
Number of stations	59	78	29	6	4	2

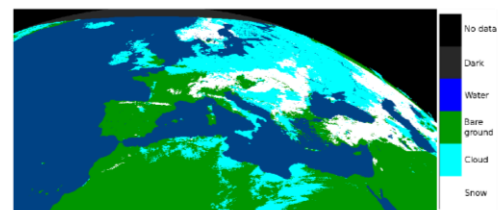
1.6 μm (1.5–1.78 μm) SEVIRI channels. The used snow index is obtained by dividing the bands NIR1.6 to VIS0.6. The pixels having NIR1.6/VIS0.6 values lower than a fixed threshold value of 0.6 were collected. The cloud–snow discrimination is based on the CMA and cloud type (CT) product of the NWCSAF. The CT product has 15 different cloud types, which allow more robust cloud recognition (Surer, 2008). Both algorithms use sun zenith angle for discarding the low-illuminated areas, and land surface temperature values for covering all cold pixels below freezing point (Romanov et al., 2003). The main difference in the algorithms is the location of the samples collected for developing the thresholding method, and the cloud–snow discrimination applied in the retrieval. A detailed description of the MSG-SEVIRI snow algorithm is presented in the Algorithm Theoretical Basis Document (HSAF, 2010).

The definition of the mountainous areas is based on the mean altitude and standard deviation of the slope within 5 km \times 5 km pixels (Lahtinen et al., 2009). The area is defined to be mountainous if the mean altitude in the particular mesh exceeds 1000 m or the mean altitude in the mesh exceeds 700 m, and the standard deviation of the slope is greater than 2° or the mean altitude variation (the difference between the maximum and minimum altitude in the particular mesh) exceeds 800 m and the mean altitude exceeds 500 m.

Daily snow cover maps are derived from 32 images per day, blending data from 08:00–15:45 UTC + 2. Snow cover is mapped when there are at least 4 hits of snow recognition in a day. The final snow cover product, which is merged at Finnish Meteorological Institute, has snow, land, cloud, water and unclassified classes. An example map for Europe is presented in Fig. 1.

3 Study area and snow cover data

This paper evaluates the accuracy of snow cover images over Austria. Austria is located in the temperate climate zone, where the Alps act as a dominant barrier between continental climate in the north and the meridional circulation from the Adriatic Sea in the south. Elevations range from 115 m in the flatlands to more than 3700 m in the mountains (Fig. 2). Mean annual precipitation varies between 400 mm in the eastern flatlands and almost 3000 mm in the western part of the Alps. The mountainous parts of Austria are covered by snow for several months a year (Parajka and Blöschl, 2006), while the flatlands are characterized by warm and dry summers and cold winters without significant snowfall. Land

**Fig. 1.** Example of a MSG-SEVIRI snow cover map for 21 February 2012.

use is mainly agricultural in the lowlands and forest in the medium elevation ranges. Alpine vegetation and rocks prevail in the highest catchments.

Snow cover data used for MSG-SEVIRI evaluation include ground snow depth measurements at 178 meteorological stations (Fig. 2) and daily MODIS satellite snow cover images from April 2008 to June 2012. The snow depth readings are taken from permanent staff gauges and represent point measurements performed daily at 07:00 UTC + 1 with 1 cm reading precision (Parajka and Blöschl, 2006). Table 2 summarizes the number of stations in different elevation zones and indicates that most of the stations are located in elevation zones between 500 and 1000 m. In the mountains, the stations tend to be located at lower elevations, typically in the valleys, which suggest a slight bias of the validation statistics towards lower elevations.

The satellite snow cover images have been acquired by the MODIS instrument mounted on Terra and Aqua satellites of the NASA Earth Observation System. The daily Terra (MOD10A1, V005) and Aqua (MYD10A1, V005) snow products are available through the Distributed Active Archive Center located at the National Snow and Ice Data Center (NSIDC, <http://www.nsidc.org>). The spatial resolution of the products is 500 m. Normalized difference snow index (NDSI) is a well-known snow index used in snow product generation from MODIS data. The NDSI takes advantage of the fact that snow reflectance is high in the visible (0.545–0.565 μm) wavelengths and low in the shortwave infrared (1.628–1.652 μm) wavelengths (Hall et al., 2006; Hall and Riggs, 2007). For the validation, the snow cover product obtained from the Terra satellite and a combined product of the Terra and Aqua satellites are used. The two products are combined to reduce cloud coverage in the mountains (Parajka and Blöschl, 2008). In the combined product, the

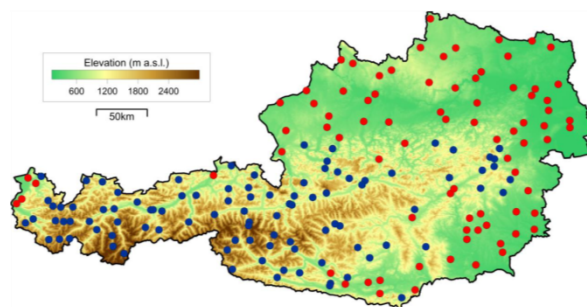


Fig. 2. Topography of Austria and location of 178 stations with daily snow depth measurements for the period April 2008–June 2012. Red and blue colors respectively represent meteorological stations located in the flatland (81 stations) and mountain (97 stations) regions according to the MSG-SEVIRI mountain mask.

pixels classified as clouds in the Terra images are updated by the Aqua pixel value of the same location if the Aqua pixel is snow or land. This approach combines satellite observations on the same day, shifted by several hours.

4 Methodology of MSG-SEVIRI evaluation over Austria

Evaluation of the MSG-SEVIRI snow cover accuracy is performed in two steps. In the first step, the accuracy of MSG-SEVIRI is evaluated at meteorological stations by using daily snow depth observations. Snow depth observations at the stations are considered as ground truth for each MSG-SEVIRI pixel that is closest to each station. The ground is considered as snow covered if the snow depth measurement exceeds 1 cm. In the second step, MSG-SEVIRI images are compared with daily MODIS snow cover maps. In this case, the frequency of MODIS snow, no snow and cloud classes is estimated and compared within each MSG-SEVIRI pixel.

The snow cover mapping accuracy with respect to snow depth observations is quantified by three variants of the accuracy index: k_A , k_M and k_C . The overall accuracy index k_A is estimated at each meteorological station and it is used to compare the sum of all correctly classified days where snow and no snow have been observed to the number of all cloud-free days at each meteorological station (station days) in the selected period. The seasonal accuracy index k_M is defined in a similar way, but relates the sum of all correctly classified station days (snow-snow, no snow-no snow) at different meteorological stations to the number of all cloud-free station days at those stations in a particular month. The k_M index is estimated separately for all stations located in the mountain and flatland areas as defined by the MSG-SEVIRI mountain mask (Fig. 2), respectively. The all-days accuracy index k_C relates the correctly classified station days to the total number of station days in the selected period, including

days with cloud cover. It is also estimated for each month and two groups of stations (mountain and flatland).

Additional to the three accuracy indices, two types of mapping errors are quantified with respect to the ground snow depth observations: the MSG-SEVIRI misclassification of land as snow (termed here the MSG-SEVIRI overestimation error (k_O)) and the misclassification of snow as land (termed the MSG-SEVIRI underestimation error (k_U)). Both types of errors relate the sum of misclassified station days to the total number of station days in each particular month and mask region.

The agreement between MSG-SEVIRI and MODIS snow cover products is quantified by the index of overall m_A and seasonal agreement m_M . These indices are defined in a similar way as the k_A and k_M , but instead of using snow depth observations at meteorological stations, the aggregated frequencies of MODIS snow, land and cloud classes within each MSG-SEVIRI pixel are used. The comparison is performed at the coarser spatial resolution of the MSG-SEVIRI and for those MSG-SEVIRI pixel-days where the fraction of MODIS pixels classified as clouds is less than 60%. Our test simulations (not shown here) indicate that the results are insensitive to the selection of this threshold between 40 and 70%. In the m_A and m_M evaluation, the ground is considered as snow covered if the fraction of MODIS snow pixels within the MSG-SEVIRI pixel is at least 50% of the sum of MODIS pixels classified as snow and land. The presence of no snow (land class) is considered in the same way; that is, the fraction of MODIS pixels classified as land is larger than the sum of snow and land pixels. The presence of no snow (land class) is considered in the same way, i.e., the frequency of MODIS pixels classified as land is larger than the sum of snow and land pixels.

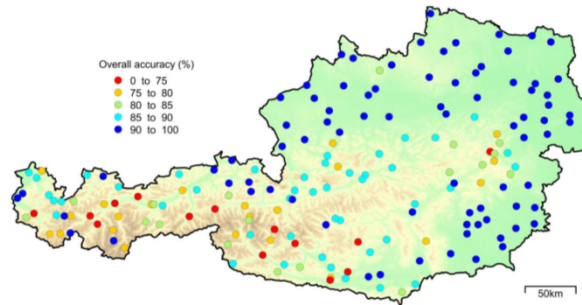


Fig. 3. MSG-SEVIRI snow product overall accuracy k_A (%) at 178 meteorological stations for the period April 2008–June 2012.

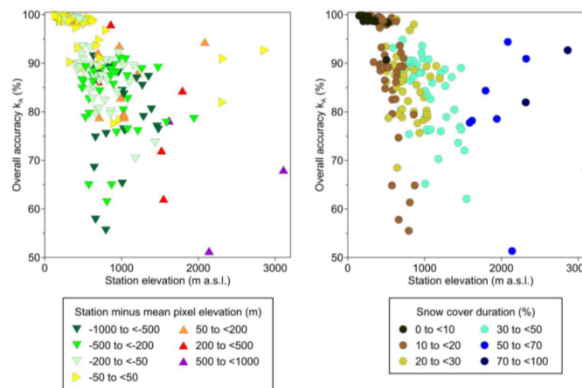


Fig. 4. Relationship between MSG-SEVIRI snow mapping accuracy (k_A) and elevation of the meteorological stations. Color of the triangles in the left panel indicates the difference between elevation of the meteorological stations and mean elevation of the respective MSG-SEVIRI pixels (as derived from a 25 m digital elevation model). Color of the symbols in the right panel shows relative snow cover duration observed at the meteorological stations for the period April 2008–June 2012.

5 Results

5.1 Validation of MSG-SEVIRI against ground snow depth measurements

The snow cover accuracy (k_A) of MSG-SEVIRI estimated for cloud-free days at the meteorological stations is presented in Fig. 3 and summarized in Table 3. The k_A varies between 51.3 % at the Villacher Alpe (2140 m a.s.l.) in the Eastern Alps (Carinthia) and almost 100 % in Gross-Enzersdorf (154 m a.s.l.) near Vienna. Table 3 indicates that the MSG-SEVIRI accuracy is larger in the flatland than in the mountain regions, i.e., the median of k_A is 98.8 and 84.3 % in the flatland and mountain regions, respectively. Figure 4 shows a clear decrease of snow mapping accuracy with increasing elevation of the meteorological stations. The results indicate that this tendency is caused mainly by increasing sub-grid

Table 3. Overall accuracy k_A (%) of the MSG-SEVIRI snow cover product for cloud-free days at the meteorological stations. Stations in flatland and mountains are stratified according to the mountain mask used for the MSG-SEVIRI product (Fig. 2).

Statistics	All stations	Stations in mountains	Stations in flatland
Count	178	97	81
Minimum k_A	51.3	51.3	78.9
25 % percentile k_A	82.6	78.2	93.9
50 % percentile k_A	89.3	84.3	98.8
75 % percentile k_A	98.7	88.4	99.4
Maximum k_A	99.9	94.4	99.9

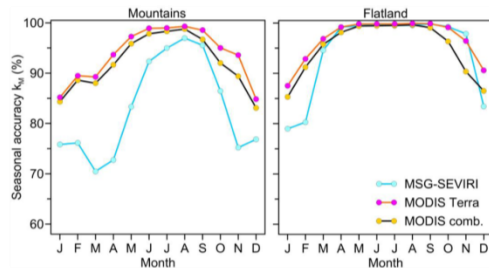


Fig. 5. Seasonal frequency of snow mapping accuracy k_M for the MSG-SEVIRI, MODIS-Terra and MODIS-combined products estimated for cloud-free days for the period April 2008–June 2012. Left and right panels show the results for meteorological stations in the mountain (97 stations) and flatland (81 stations) regions, respectively.

topographical variability in the mountains. Meteorological stations are often situated at different elevations than the mean elevation of MSG-SEVIRI pixels, which causes biases between station and satellite snow cover observations. As is indicated in the left panel of Fig. 4, the mapping accuracy is larger for stations with smaller elevation difference. For example, the median of k_A for stations with absolute elevation difference less than 50 m and more than 500 m is 98.9 and 78.2 %, respectively. For the station with the largest mapping errors (Villacher Alpe), the elevation difference is larger than 960 m. The stations located significantly below or above the pixel mean may have noticeably different snow cover observations (right panel of Fig. 4). The snow cover observations at meteorological stations in Austria show a clear linear relationship ($R^2 = 88$ %) between snow cover duration and the altitude, indicating an increase of snow cover duration by 2.8 %/100 m (not shown here). An elevation difference of 500 m can therefore be easily transferred in about 14 % difference in snow cover duration and thus different snow cover mapping accuracy. Interestingly, the MSG-SEVIRI mapping accuracy is larger than 90 % for two stations situated above 2000 m a.s.l. (Ischgl-Idalpe and Pitztaler Gletscher), but located approximately at the mean elevation of the MSG-SEVIRI pixel. This finding indicates the importance of the spatial resolution and sub-grid topographical variability for the assimilation of satellite snow cover images in operational hydrological applications.

The seasonal frequencies of MSG-SEVIRI snow mapping accuracy (k_M) are presented in Fig. 5. The results show that, in the mountains, the k_M accuracy varies between 70 and 77 % in the winter and between 92 and 97 % in the summer months. The flatland region typically has much shorter snow coverage, which most likely results in larger k_M accuracy between April and October, but larger mapping errors (k_M between 79 and 83 %) in the winter months. As compared to k_M

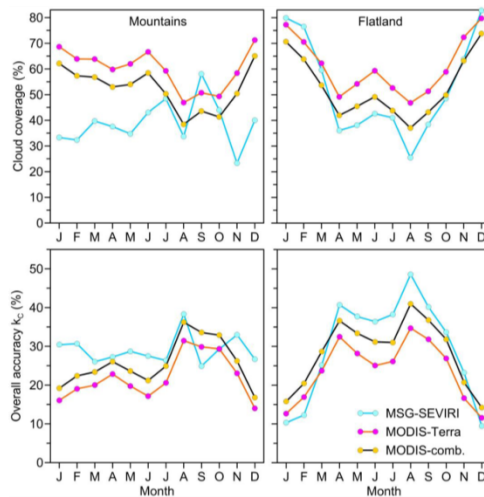


Fig. 6. Seasonal frequency of the clouds (top panels) and snow mapping accuracy k_C for the MSG-SEVIRI, MODIS-Terra and MODIS-combined products estimated for all days for the period April 2008–June 2012. Left and right panels show the results for meteorological stations in the mountain (97 stations) and flatland (81 stations) regions, respectively.

obtained for the MODIS/Terra and MODIS/combined snow cover products, the MSG-SEVIRI mapping accuracy is 10–13 % lower in the mountains and 3–11 % lower in the flatland area in the winter months. However, the MSG-SEVIRI product contains significantly less pixels classified as clouds than MODIS, particularly in the mountains (Fig. 6, top panels). Here, the merging of 32 MSG-SEVIRI images per day reduces cloud coverage between 15 and 29 % for the period November–June as compared to the MODIS-combined product. The cloud reduction is even about 7 % larger when compared to the MODIS-Terra product. For the period July–October, the cloud coverage of MSG-SEVIRI is similar to that of MODIS in the mountains. Interestingly, in the flatland areas a decrease in cloud coverage is observed only for the period April and September. In the winter months, MSG-SEVIRI indicates cloud coverage larger than 75 %, which is similar to or even slightly larger than indicated by the MODIS products. This is probably caused by the use of different cloud masking algorithms.

The reduction in clouds, particularly in the mountains, then translates into an improvement of all-days mapping accuracy k_C (Fig. 6, bottom panels). The k_C accuracy assumes clouds as a mapping error, and it varies for MSG-SEVIRI between 26 and 31 % (mountains) and between 9 and 25 % (flatland areas) in the winter and spring periods. In the mountains, this is about 3–14 % larger than the k_C obtained for the

Table 4. Seasonal frequency of overestimation (k_O) and underestimation (k_U) mapping errors (%) estimated for the MSG-SEVIRI, MODIS-Terra and MODIS-combined snow cover products for the period April 2008–June 2012. The mapping errors are estimated at 97 and 81 meteorological stations in the mountain (Mnt) and flatland (Flat) areas, respectively.

Season	MSG- SEVIRI	MSG- SEVIRI	MODIS- Terra	MODIS- Terra	MODIS- comb.	MODIS- comb.
	overest. k_O (Mnt/Flat)	underst. k_U (Mnt/Flat)	overest. k_O (Mnt/Flat)	underst. k_U (Mnt/Flat)	overest. k_O (Mnt/Flat)	underst. k_U (Mnt/Flat)
January	4.6/0.4	6.3/2.4	1.0/ 1.0	1.8/0.8	1.4/1.6	2.2/1.2
February	4.3/0.4	6.8/2.6	0.7/0.7	1.5/0.6	1.1/1.2	1.8/0.8
March	6.1/0.3	5.7/1.1	1.1/0.3	1.3/0.4	1.5/0.7	1.7/0.6
April	8.8/0.1	2.5/0.2	0.8/0.1	0.7/0.2	1.4/0.5	1.0/0.2
May	5.5/0.2	1.1/0.0	0.3/0.1	0.3/0.0	0.7/0.2	0.3/0.0
June	2.2/0.1	0.4/0.0	0.1/0.0	0.1/0.0	0.3/0.2	0.1/0.0
July	1.3/0.2	0.2/0.0	0.1/0.0	0.1/0.0	0.3/0.2	0.1/0.0
August	0.9/0.2	0.4/0.0	0.1/0.0	0.1/0.0	0.3/0.1	0.2/0.0
September	1.0/0.1	0.3/0.0	0.3/0.0	0.1/0.0	1.0/0.3	0.1/0.0
October	4.0/0.2	1.1/0.0	1.2/0.2	0.3/0.0	2.4/1.2	0.4/0.0
November	6.1/0.2	7.9/0.4	1.1/0.4	0.5/0.2	2.4/2.0	0.7/0.3
December	5.1/ 0.5	4.6/1.5	0.9/0.7	1.6/0.5	1.4/1.6	2.0/0.6

The largest mapping error for each product and mask area is marked by bold print.

MODIS data set. In the flatland areas, the large cloud coverage in winter does not enable an increase in k_C as compared to MODIS products. The evaluation of k_C clearly indicates the tradeoff between increased cloud reduction due to higher temporal sampling (32 images per day) and higher mapping error due to coarser spatial resolution (particularly in the mountains) of the MSG-SEVIRI snow product.

The seasonal frequency of MSG-SEVIRI mapping errors is summarized in Table 4. Table 4 compares the overestimation (k_O) and underestimation (k_U) errors of MSG-SEVIRI, MODIS-Terra and MODIS-combined data sets as observed at meteorological stations. The general distribution of MSG-SEVIRI errors shows a typical seasonal pattern of larger errors in winter and spring and smaller errors in summer. In comparison to MODIS products, the MSG-SEVIRI mapping errors are significantly larger during the snowmelt season in the mountains (4–9%) and somewhat larger during the winter months in the flatlands (1–3%). A detailed analysis of k_O and k_U errors (Fig. 7) indicates that the MSG-SEVIRI mapping errors are much larger at stations that are located at different elevations than the mean elevation of the closest MSG-SEVIRI pixel. The largest k_O , i.e., more than 25% in April or 15% in November, is estimated at stations that are located more than 500 m lower than the pixel mean. Similarly, the largest k_U errors are found at stations located more than 500 m above the pixel mean. The evaluation of MSG-SEVIRI mapping errors at stations that are located at approximately the same elevation (yellow triangles in Fig. 7) indicates that the MSG-SEVIRI tends to more frequently underestimate snow cover in winter than overestimating it. The largest k_O errors are less than 0.5%, but k_U errors exceed 3% in the winter months.

Table 5. Overall agreement m_A (%) between MSG-SEVIRI and MODIS-combined snow cover products for MSG-SEVIRI pixels with less than 60% MODIS cloud coverage. The agreement m_A accuracy is evaluated for all MSG-SEVIRI pixels, flatland and mountain mask areas in Austria.

Statistics	All pixels	Pixels in mountains	Pixels in flatland
Count	2635	1403	1232
Minimum m_A	57.3	57.3	64.4
25% percentile m_A	78.4	77.4	81.1
50% percentile m_A	82.5	81.6	82.9
75% percentile m_A	84.3	85.2	84.1
Maximum m_A	92.7	92.7	86.0

5.2 Comparison between MSG-SEVIRI and MODIS snow cover data

The overall agreement between the MSG-SEVIRI and MODIS-combined maps (m_A) is summarized in Table 5. The m_A vary between 57.3 and 92.7%, with a median of 82.5%. The difference in medians between the flatland (82.9%) and mountain (81.6%) regions is not large. The spatial patterns indicate (Fig. 8) that m_A is between 80 and 90% in the flatland, with an exception in the hilly region at the border between Upper and Lower Austria (Waldviertel), where m_A is less than 75%. In the mountains, the m_A variability tends to be larger. The m_A agreement is over 90% in the high mountain locations, but smaller than 65% in the Alpine valleys in western Austria. It is also less than 70% in the southeastern part of the mountain mask region (Styria) (Lahtinen et al., 2009). The relationship between m_A and altitude is plotted

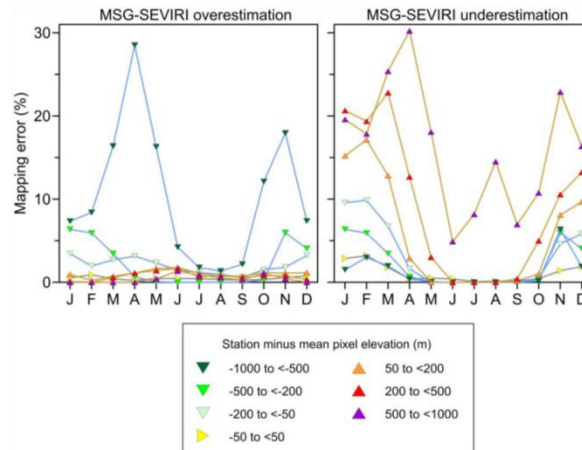


Fig. 7. Seasonal frequency of MSG-SEVIRI overestimation (k_O , left panel) and underestimation (k_U , right panel) errors summarized for stations with different elevation difference between meteorological station and respective MSG-SEVIRI pixel mean. The elevation difference is estimated as station elevation minus mean pixel elevation (as derived from a 25 m digital elevation model).

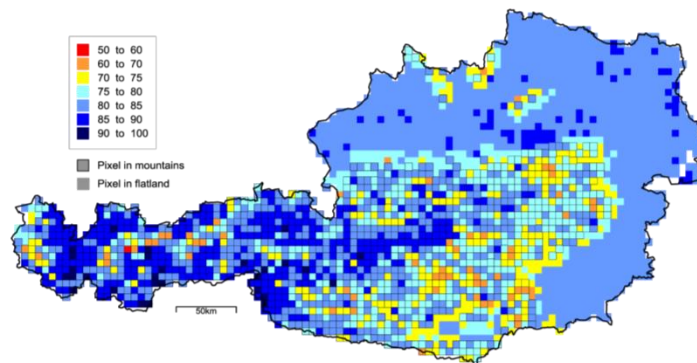


Fig. 8. Overall accuracy k_A of MSG-SEVIRI with respect to the MODIS-combined product for the period April 2008–June 2012. k_A is estimated for the MSG-SEVIRI pixels where MODIS cloud coverage is less than 60 %. Pixels with black outline indicate the MSG-SEVIRI mountain mask.

in Fig. 9. While in the flatlands m_A tends to decrease with elevation; in the mountains there is a tendency of increasing m_A with altitude. The results show that the largest m_A variability in Austria is in the regions with altitudes between 700 and 1500 m.

The seasonal variability (m_M) in the agreement between MSG-SEVIRI and MODIS is presented in Fig. 10. In the flatland areas (red line), m_M is the largest in April and July and less than 70 % in the winter months. The m_M amplitude is smaller in the mountains (blue line), ranging from more than 85 % in May, June and August to 70 % in September.

A more detailed evaluation of the spatio-temporal patterns of the agreement between MSG-SEVIRI and MODIS is presented in Figs. 11 and 12. Figure 11 compares the spatial patterns of the frequencies of three MSG-SEVIRI and MODIS mapping classes – clouds, snow, and no snow. It is clear that the agreement between the snow cover products is the largest for mapping the clouds, for mapping the land in the flatland and snow in the high alpine areas. These cases occur in more than 25 % of days in the selected period, in most of the MSG-SEVIRI pixels. The MSG-SEVIRI maps snow, while the MODIS-combined product indicates clouds in 10–15 %

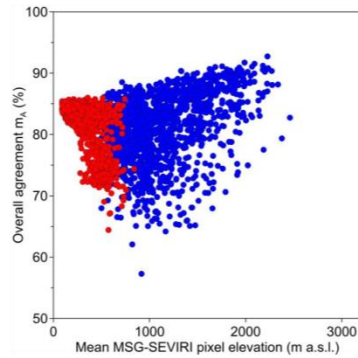


Fig. 9. Relationship between mean MSG-SEVIRI pixel elevation and the overall agreement (m_A) between the MSG-SEVIRI and MODIS-combined products. Red and blue points represent MSG-SEVIRI pixels in the flatland and mountain mask areas, respectively.

of days in the Alps. Interestingly, in the flatland, there are only a few days when both MSG-SEVIRI and MODIS indicate snow. The spatial patterns of the disagreement between the products (i.e., MSG-SEVIRI maps no presence of snow (land), but MODIS indicates snow) show that most of the cases are in Upper Austria, Styria and the mountain valleys. An opposite case occurs quite frequently in the mountain valleys of western Austria, where MSG-SEVIRI and MODIS map snow and land in 10–15 % of days, respectively. Figure 12 shows that MSG-SEVIRI overestimates snow in comparison to MODIS (middle panels) mainly in the summer for both mountain and flatland areas. The bottom panel (Fig. 12) indicates that the opposite case (i.e., MSG-SEVIRI underestimates snow in the winter) is less frequent (up to 10 %). There is quite a large frequency of days where MSG-SEVIRI maps land and MODIS indicates clouds. These cases occur in more than 20 % of the days of each month in the flatland area. In the mountains, the reduction of clouds is noticeable in the winter months, where MODIS indicates clouds, but MSG-SEVIRI maps snow in more than 15 % of the days.

6 Discussion and conclusions

This study evaluates the snow cover mapping accuracy of the MSG-SEVIRI operational product. This product is based on blending 32 consecutive images per day, which is foreseen as an alternative to different filtering methods used for cloud reduction in optical remote sensing products. The limitation of the product is a coarser spatial resolution of about 5 km. Our results indicate that the blending of multiple observations during the day allows a significant cloud reduction in Austria. The mean annual cloud coverage of the MSG-SEVIRI

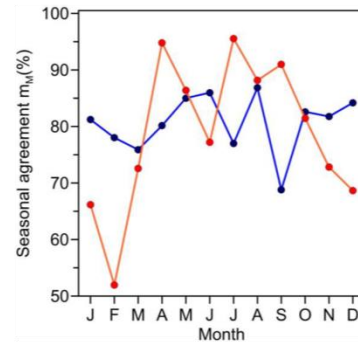


Fig. 10. Seasonal agreement m_M between the MSG-SEVIRI and MODIS-combined products for MODIS cloud-free pixels for the period April 2008–June 2012. Red and blue lines represent mountain and flatland areas, respectively.

product is less than 30 %, which is 23 and 30 % lower than obtained by the MODIS-combined and MODIS-Terra snow cover products, respectively. Such cloud reduction is similar to that obtained by 1-day temporal filter performed on the MODIS-combined product (Parajka and Blöschl, 2008). The results are consistent with the preliminary MSG-SEVIRI assessment study (Surer and Akyurek, 2012), which indicates a 31–49 % cloud reduction in mountainous parts of Turkey in the winter season. Despite the coarser spatial resolution of MSG-SEVIRI, the overall mapping accuracy is large. The average accuracy for cloud-free days is 89 %, which is 5 % lower than obtained by the MODIS-combined product, but similar to that obtained by land-surface (JULES) model simulations driven by a regional climate model HadRM3-P (Parajka et al., 2010). The overall accuracy also relates well with the hit rate measure of Surer and Akyurek (2012), which is in between 68 and 81 % in winter. The accuracy with respect to all weather conditions (in all weather conditions assessments the pixels with clouds are considered as mapping errors) is, however, about 3–4 % larger than obtained by the MODIS product. The larger frequency of snow cover information, even for coarse resolution, indicates the potential of MSG-SEVIRI for operational assimilation into hydrologic models.

The analysis of mapping errors indicates that MSG-SEVIRI tends to underestimate snow cover, particularly in flatland areas. Large errors are also found in the Alpine region characterized by large topographical and snow cover variability. The errors are noticeably larger at stations that are located at different elevations than the mean of the MSG-SEVIRI pixels. The differences in mapping accuracy clearly indicate the limits of using meteorological stations for validating coarse satellite products. In order to account for scaling relationships between point measurement and pixel size

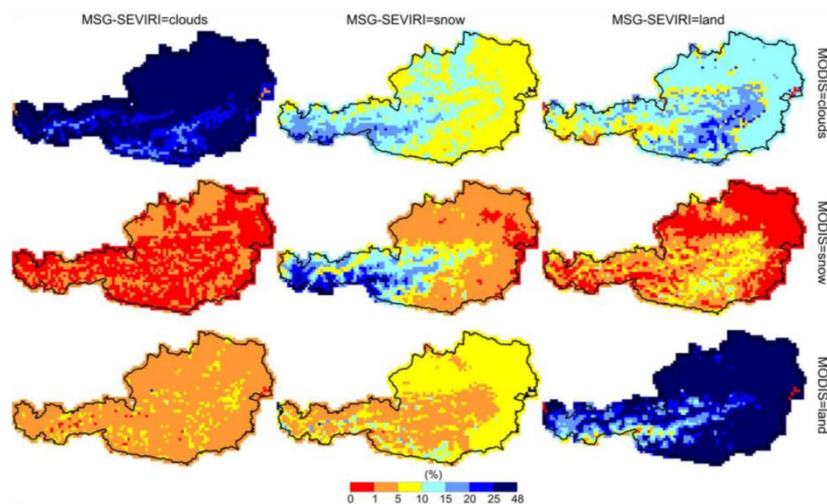


Fig. 11. Relative frequency of days with agreement and disagreement between the MSG-SEVIRI and MODIS-combined snow cover products for the period April 2008–June 2012.

(Blöschl and Kirnbauer, 1992; Blöschl, 1999; Skøien et al., 2003) some studies used different thresholds for considering ground as snow covered. For example, Simic et al. (2004) examined the sensitivity of the mapping accuracy to the reference threshold of 1 and 3 cm and found that the difference is small, ranging approximately between -2 and 4 %. In this study, a 1 cm threshold is used in order to be consistent and comparable with other studies performed in Austria. In the future, the sensitivity of results to this reference threshold should be investigated in more detail.

The comparison between MSG-SEVIRI and MODIS snow cover products shows a good overall agreement. The use of the MSG-SEVIRI snow product in hydrological modeling is under study, but calibration of a conceptual hydrological model by using MSG-SEVIRI snow cover product has been performed. It is observed that the multi-objective calibration, in which MSG-SEVIRI snow cover data is used beside the runoff data, improved the snow cover estimation of the hydrological model (Akyurek et al., 2013).

The snow retrieval algorithms for MSG-SEVIRI and MODIS snow products are more or less the same. The comparison between the normalized difference snow index (NDSI), used as the retrieval algorithm for MODIS product, and SI, used as the retrieval algorithm for MSG-SEVIRI product, shows a good relationship for several clear-sky MSG-SEVIRI images (Surer and Akyurek, 2012). The selected SI threshold value of 0.6 for the snow-cover area retrieval corresponds to 0.2 for the NDSI value. For the MODIS products the NDSI value for 50% snow-covered areas is taken as 0.4 (Dozier, 1989; Hall et al., 2002). The aim

of selecting SI as 0.6 is to include the partial snow-covered areas in the retrieval of MSG-SEVIRI snow product. The differences are because of coarse spatial resolution of MSG-SEVIRI. The finding in this study indicates the importance of spatial resolution and sub-grid topographical variability for the use of satellite snow cover images in operational hydrological applications or climatological studies.

The comparison between MSG-SEVIRI and MODIS snow cover products shows a good overall agreement. The overestimation and underestimation errors of MSG-SEVIRI snow product is larger compared to the MODIS-Terra snow product. In both of the products underestimation error is observed in the winter months and overestimation error is observed in the spring and summer months. The overestimation and underestimation are more pronounced for mountainous areas compared to flat lands for MSG-SEVIRI snow product. Besides the spatial resolution affecting the snow mapping accuracy, the difference in the viewing geometries of two sensors may have an effect on the snow mapping. The view geometry may be one of the major error sources in snow mapping algorithms. The influence of the varying MODIS view zenith angles on snow mapping algorithm must be investigated in detail. As view zenith angle increases, it is known that NDSI decreases (Xin et al., 2012). Since MODIS observes the surfaces at a much smaller view zenith angle (VZA) than the SEVIRI, it detects more snow cover area. That may be the reason to observe large underestimation errors for SEVIRI compared to MODIS in winter months. The narrow band width in the Green and Mid. Infrared portion of the spectrum for MODIS creates the possibility to map more snow

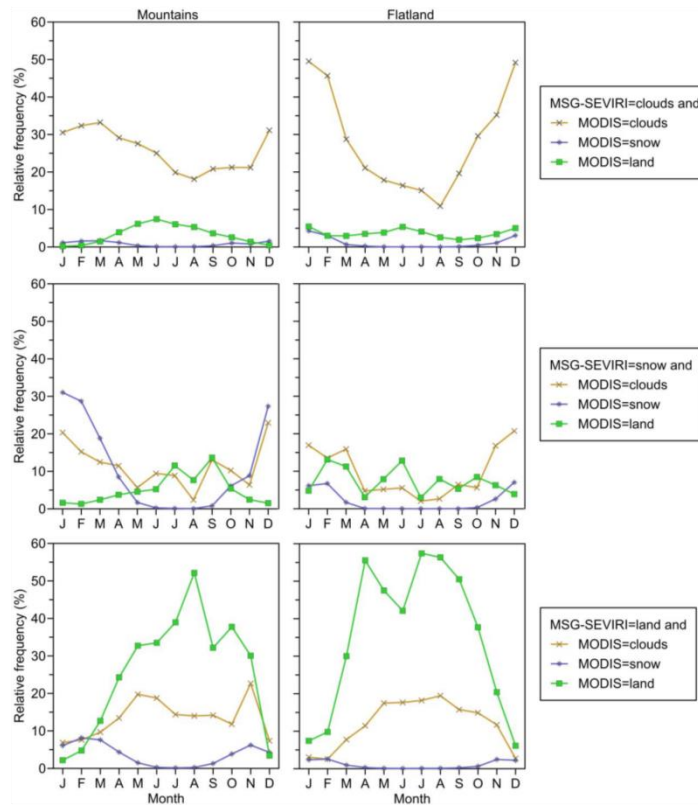


Fig. 12. Mean seasonal frequency of days with agreement and disagreement between the MSG-SEVIRI and MODIS-combined snow cover products in each month for the period April 2008–June 2012.

compared to SEVIRI. The overestimation for spring months is due to the high percentage of fractional snow cover due to melting in these months. The MSG-SEVIRI algorithm tends to map more snow for fractional snow-covered areas. Neither the effect of complex topography, nor the shadows were held in the MSG-SEVIRI snow mapping algorithm. Therefore the MSG-SEVIRI algorithm can be modified with the use of a proper DEM in order to correct the topography effect.

Better snow cover information can be retrieved by using MSG-SEVIRI and MODIS snow products together. The cloud-contaminated MODIS snow pixels can be reclassified according to the values observed from the MSG-SEVIRI snow product. The merging of snow products having comparatively better spatial resolution (MODIS) and temporal resolution (MSG-SEVIRI) can be studied as a future work.

Besides the importance of spatial resolution of snow products, a better temporal resolution helps to increase the

cloud/snow discrimination, which is very important for the use of satellite snow products in further analysis. The new sensors and satellite missions to be used for hydrological and climatological studies can be designed according to an optimum spatial and temporal resolution.

Acknowledgements. This study was prepared within the framework of HSAF project funded by EUMETSAT. The second author was supported by EUMETSAT as a visiting scientist at METU within the H-SAF project. Thanks to Kenan Bolat for his technical support. The authors would like to thank the Central Institute for Meteorology and Geodynamics (ZAMG) for providing the snow depth data.

Edited by: A. Loew

References

- Akyurek, Z., Surer, S., and Parajka, J.: Calibration of a Conceptual Hydrological Model Using EUMETSAT Snow Covered Area Product, AGU Fall Meeting, San Francisco, USA, 2013.
- Aminou, D. M. A.: MSG's SEVIRI Instrument, ESA Bull., 111, 15–17, 2002.
- Blöschl, G.: Scaling issues in snow hydrology, *Hydrol. Process.*, 13, 2149–2175, 1999.
- Blöschl, G. and Kirnbauer, R.: Point snowmelt models with different degrees of complexity – internal processes, *J. Hydrol.*, 129, 127–147, 1991.
- Blöschl, G. and Kirnbauer, R.: An analysis of snow cover patterns in a small Alpine catchment, *Hydrol. Process.*, 6, 99–109, 1992.
- Blöschl, G., Gutknecht, D., and Kirnbauer, R.: Distributed snowmelt simulations in an Alpine catchment, 2. Parameter study and model predictions, *Water Resour. Res.*, 27, 3181–3188, 1991.
- Brubaker, K. L., Pinker, R. T., and Deviatova, E.: Evaluation and comparison of MODIS and IMS snow-cover estimates for the continental United States using station data, *J. Hydrometeorol.*, 6, 1002–1017, 2005.
- Dozier, J.: Spectral signature of alpine snow cover from Landsat Thematic Mapper, *Remote Sens. Environ.*, 28, 9–22, 1989.
- Gafurov, A. and Bárdossy, A.: Cloud removal methodology from MODIS snow cover product, *Hydrol. Earth Syst. Sci.*, 13, 1361–1373, doi:10.5194/hess-13-1361-2009, 2009.
- Hall, D. K. and Riggs, G. A.: Accuracy assessment of the MODIS snow products, *Hydrol. Process.*, 21, 1534–1547, 2007.
- Hall, D. K., Riggs, G. A., Salomonson, V. V., DiGiromamo, N., and Bayr, K. J.: MODIS Snow-Cover Products, *Remote Sens. Environ.*, 83, 181–194, 2002.
- Hall, D. K., Riggs, G. A., and Salomonson, V. V.: MODIS/Terra Snow Cover Daily L3 Global 500 m Grid V005, USA, Digital media, updated daily, National Snow and Ice Data Center, Boulder, Colorado, 2006.
- Hall, D. K., Riggs, G. A., Foster, J. L., and Kumar, S. V.: Development and Evaluation of a Cloud-Gap-Filled Modis Daily Snow-Cover Product, *Remote Sens. Environ.*, 114, 496–503, 2010.
- HSAF: Algorithms Theoretical Baseline Document for product H10 – SN-OBS-1, available at: <http://hsaf.meteoam.it/ATDD-sn.php> (last access: 7 October 2013), 2010.
- HSAF: Product Validation Report for product H10-SN-OBS-1, available at: <http://hsaf.meteoam.it/PVR-sn.php> (last access: 7 October 2013), 2011.
- Klein, A. and Barnett, A. C.: Validation of daily MODIS snow cover maps of the Upper Rio Grande River Basin for the 2000–2001 snow year, *Remote Sens. Environ.*, 86, 162–176, 2003.
- Lahtinen, P., Erturk, A. G., Pulliainen, J., and Koskinen, J.: Merging flat/forest and mountainous snow products for extended European area, in: *Geoscience and Remote Sensing Symposium, 2009 IEEE International, IGARSS 2009*, Cape Town, 2009.
- Nester, T., Kirnbauer, R., Parajka, J., and Blöschl, G.: Evaluating the snow component of a flood forecasting model, *Hydrol. Res.*, 43, 762–779, 2012.
- NWCSAF – Nowcasting Satellite Application Facility: Usermanual for the Cloud Products of the Nowcasting Satellite Application Facilities, <http://www.nwcsaf.org/HD/MainNS.jsp> (last access: 7 October 2013), 2007.
- Parajka, J. and Blöschl, G.: Validation of MODIS snow cover images over Austria, *Hydrol. Earth Syst. Sci.*, 10, 679–689, doi:10.5194/hess-10-679-2006, 2006.
- Parajka, J. and Blöschl, G.: Spatio-temporal combination of MODIS images – potential for snow cover mapping, *Water Resour. Res.*, 44, W03406, doi:10.1029/2007WR006204, 2008.
- Parajka, J. and Blöschl, G.: MODIS-based Snow Cover Products, Validation, and Hydrologic Applications, in: *Multiscale Hydrologic Remote Sensing Perspectives and Applications*, edited by: Chang, Y. and Ni-Bin, H., CRC Press, 185–212, 2012.
- Parajka, J., Dadson, S., Lafon, T., and Essery, R.: Evaluation of snow cover and depth simulated by a land surface model using detailed regional snow observations from Austria, *J. Geophys. Res.*, 115, D24117, doi:10.1029/2010JD014086, 2010.
- Romanov, P., Gutman, G., and Csiszar, I.: Automated monitoring of snow cover over North America with multispectral satellite data, *J. Appl. Meteorol.*, 39, 1866–1880, 2000.
- Romanov, P., Tarpley, D., Gutman, G., and Carroll, T.: Mapping and monitoring of the snow cover fraction over North America, *J. Geophys. Res.*, 108, 8619, doi:10.1029/2002JD003142, 2003.
- Siljamo, N. and Hyvärinen, O.: New geostationary satellite-based snow-cover algorithm, *J. Appl. Meteorol. Clim.*, 50.6, 1275–1290, doi:10.1175/2010JAMC2568.1, 2011.
- Simic, A., Fernandes, R., Brown, R., Romanov, P., and Park, W.: Validation of VEGETATION, MODIS, and GOES+SSM/I snow cover products over Canada based on surface snow depth observations, *Hydrol. Process.*, 18, 1089–1104, 2004.
- Skøien, J. O., Blöschl, G., and Western, A. W.: Characteristic space scales and timescales in hydrology, *Water Resour. Res.*, 39, 1304, doi:10.1029/2002WR001736, 2003.
- Surer, S.: Real-time snow cover mapping over mountainous areas of Europe using MSG-SEVIRI imagery, Thesis (Masters), Middle East Technical University, Turkey, <http://etd.lib.metu.edu.tr/upload/12609911/index.pdf> (last access: 12 September 2013), 2008.
- Surer, S. and Akyurek, Z.: Evaluating the utility of the EUMETSAT HSAF snow recognition product over mountainous areas of eastern Turkey, *Hydrolog. Sci. J.*, 57, 1684–1694, 2012.
- Xin, Q., Woodcock, C. E., Liu, J., Tan, B., Melloh, R. A., and Davis, R. A.: View angle effects on MODIS snow mapping in forests, *Remote Sens. Environ.*, 118, 50–59, 2012.

CURRICULUM VITAE

PERSONAL INFORMATION

Surname, Name: Sürer, Serdar
Nationality: Turkish (TC)
Date and Place of Birth: 25 January 1981, Konya
Marital Status: Single
Phone: +90 537 573 53 17
email: serdarsurer@gmail.com

EDUCATION

Degree	Institution	Year of Graduation
PhD METU	GGIT	2015
MSc METU	GGIT	2008
BSc METU	Environmental Engineering	2006
High School	SDAL High School, Ankara	1999

WORK EXPERIENCE

Year	Place	Enrollment
2014-Present	DHI Turkey	Managing Director
2011-2014	Hidrosaf Software	Director
2012-2014	Geopylon Software	Founder/Director
2008-2010	Beray Engineering	RS/GIS Expert
2006-2013	EUMETSAT HSAF Project	Research Assistant

FOREIGN LANGUAGES

Advanced English, Basic French

PUBLICATIONS

Surer, S., and Akyurek, Z., (2012). Evaluating the utility of the EUMETSAT HSAF snow recognition product over mountainous areas of eastern Turkey, *Hydrological Sciences Journal*, 57:8, 1684-1694.

Surer, S., Parajka, J., and Akyurek, Z., (2014). Validation of the operational MSG-SEVIRI snow cover product over Austria. *Hydrology and Earth System Sciences Discussions*, 10(10), 12153-12185.

HOBBIES

Model building, observing clouds, sports, comic books.